Queen Mary College
University of London

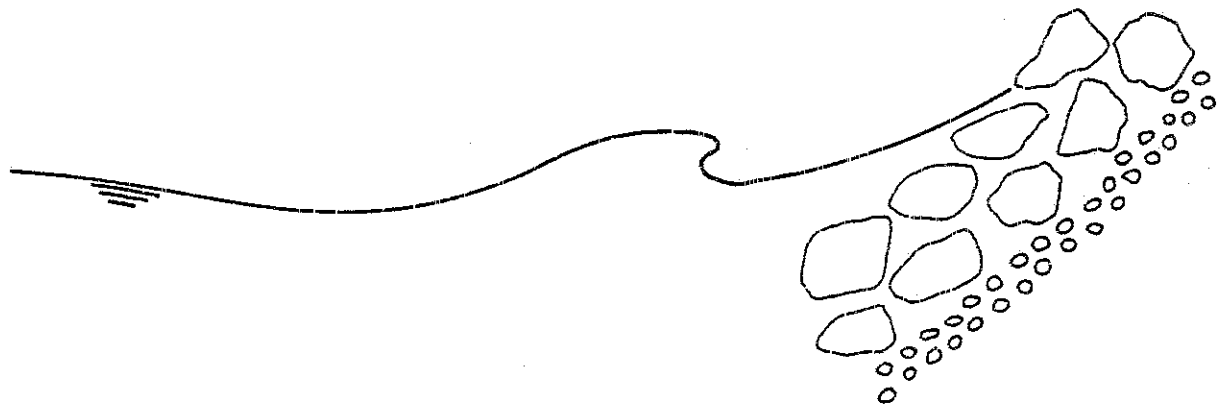

THE INFLUENCE OF ARMOURSTONE SHAPE AND ROUNDING ON THE STABILITY OF BREAKWATER ARMOUR LAYERS

Latham, J-P., Mannion, M.B., Poole, A.B.,
Bradbury*, A.P. & Allsop*, N.W.H.

September 1988

* Hydraulics Research

Coastal Engineering Research Group : Report 1

The influence of armourstone shape and rounding on the stability of breakwater armour layers

Latham J-P., Mannion M.B., Poole A.B., Bradbury A.P.*. & Allsop N.W.H.*

Coastal Engineering Research Group, Queen Mary College, University of London
Research Report 1, September 1988

*Hydraulics Research, Wallingford

Abstract

This is the second of two reports relating to a collaborative programme of random wave flume tests to quantify the effect of rock shape on stability. The first report, SR150, by Hydraulics Research, Wallingford, gives a summary of recent advances in design methods for rock armoured coastal structures and presents a detailed description of the test programme with an early interpretation of the results.

This second report is a collation of the recent results from several parallel research studies carried out at Queen Mary College, the principal subject being armourstone shape and rounding.

Practical and theoretical developments in image analysis techniques are given for gross shape and surface texture measurement of prototype and model armour blocks. The five shape classes of armour used in the flume tests, namely tabular (including elongate), equant (cubic), fresh (angular), semi-round and very round were described using the new techniques. Samples of test material used in the development of Van der Meer's design equations were also subjected to the shape analysis techniques.

A detailed discussion of Van der Meer's formulae is given in relation to the new flume test results and an indication of the relationships between rounding and instability is deduced, using a new shape parameter. For the impermeable core conditions tested, stability is more sensitive to shape under surging wave than under plunging wave conditions.

Long-term degradation resulting in rounding of prototype armourstone is considered within a quantitative framework for different environmental conditions, initial block sizes, rock types and with reference to limited field data.

THE INFLUENCE OF ARMOURSTONE SHAPE AND ROUNDING ON THE STABILITY OF BREAKWATER ARMOUR LAYERS

Abstract

1 INTRODUCTION 1
- 1.1 Background
- 1.2 Outline of this report

2 SHAPE OF ROCK ARMOURSTONE 4
- 2.1 Background
- 2.2 Fourier and Fractal shape analysis
  - 2.2.1 Automated imaging system and key analysis references
  - 2.2.2 Fourier shape descriptors
  - 2.2.3 Fractal shape descriptors
- 2.3 Measurements on prototype structures
  - 2.3.1 Photography guidelines
  - 2.3.2 Outline tracing
  - 2.3.3 Video data capture
  - 2.3.4 Scale equilization and definitions
  - 2.3.5 Particle size estimates from image analysis
  - 2.3.6 Choice of video camera magnification
- 2.4 Measurements on model armour
  - 2.4.1 Positioning of blocks on the light table
  - 2.4.2 Choice of camera magnification
  - 2.4.3 Grain scale effects

3 REVIEW OF EVIDENCE OF SHAPE EFFECTS ON STABILITY 16

4 FLUME TEST PROGRAMME 19
- 4.1 Conceptual framework
- 4.2 Summary

5 GEOMETRIC CHARACTERISTICS OF MODEL ARMOUR IN FLUME TESTS 20
- 5.1 Preparation of materials
  - 5.1.1 Preparation of armour
  - 5.1.2 Preparation of rounded rock
  - 5.1.3 Sizing of armour
  - 5.1.4 Preparation of filter
- 5.2 Shape of subsamples
  - 5.2.1 Sampling
  - 5.2.2 Gross shape and size from XYZ axial dimensions
  - 5.2.3 Image analysis results
- 5.3 Layer thickness and fictitious porosity
  - 5.3.1 Flume tests
  - 5.3.2 Static model tests
- 5.4 Topographic roughness parameters from 'along slope' profiles on static models
- 5.5 Downslope profiling in the flume tests
- 5.6 Shape of Van der Meers' test material
- 5.7 Summary

6 TEST RESULTS 34
- 6.1 Qualitative discussion of armour behaviour
- 6.2 Calculation of damage
- 6.3 Analysis of damage data

7 ANALYSIS OF TEST RESULTS 37
7.1 Comparison of flume results with Van der Meer's stability equations
7.1.1 Choice of stability equation - discussion
7.1.2 Plunging wave condition
7.1.3 Surging wave condition
7.1.4 Validity of a comparison with Van der Meer's equations
7.2 Synthesis of Van der Meer's shape data with the flume test results

8 MEASUREMENTS OF PROTOTYPE ROUNDING AND WEIGHT LOSS 49
8.1 Large scale testing and field observations from North Carolina (Allison & Savage, 1976)
8.2 Theoretical considerations using field observations of Portland limestone from West Bay, Dorset (Clark, 1988)
8.3 Rounding observations using image analysis of Whin Sill dolerite from Buckhaven, Scotland
8.4 Rounding observations using image analysis of Scandinavian granite from Herne Bay, Kent
8.5 Summary

9 CONCLUSIONS AND RECOMMENDATIONS 56
9.1 Image analysis of armour shape
9.2 Hydraulic stability
9.3 Rates of armourstone wear

10 REFERENCES

11 ACKNOWLEDGEMENTS

12 APPENDICES
Appendix A - Details of projected block outlines and shape analysis results of the five subsamples used in the flume tests
Appendix B - Details of projected block outlines and shape analysis results from four batches of armour tested at Delft Hydraulics
Appendix C - Details of projected block outlines and shape analysis results from photographs of prototype armourstones at Buckhaven, Scotland and Herne Bay

TABLES

Table 4.1 Test condition
Table 5.1 Weight characteristics of armourstone batches used in the tests
Table 5.2 Subsample gross shape characteristics based on XYZ axial dimensions
Table 5.3 Summary of Fourier and Fractal shape descriptors and size estimates from image analysis of the five shape classes
Table 5.4 Summary of geometric characteristics of armour layers from static models
Table 5.5 Topographic roughness and damage from downslope profiles in flume tests
Table 5.6 Summary of Fourier and Fractal shape descriptors and size estimates from image analysis of Delft Hydraulics Laboratory samples
Table 5.7 Shape characteristics of armour layers - summary
Table 6.1 Damage analysis
Table 8.1 Correlation of Portland limestone wear rates from mill abrasion test with prototype wear near 'block A' at West Bay, Dorset
Table 8.2 Equivalent wear factors for different block sizes and environmental site conditions in the intertidal zone of a breakwater

FIGURES

Figure 2.1 Harmonic contributions to shape, after Ehrlich & Weinberg (1970). The thin line represents the digitized coordinates; (a) and (b) show the contribution of the second and third harmonics respectively. In (c), their combined contributions are shown and (d) which includes the first 10 harmonics gives quite a good approximation.
Figure 2.2 Mendelbrot-Richardson plot for two block outlines from Herne Bay. The Fractal coefficient F is calculated using the Schwarz & Exner (1980) algorithm for step lengths between 3 and 10 pixels.
Figure 2.3 Calculation of the corrected Fractal coefficient F_{40} for a video image equivalent particle radius S_i of about 40 pixels. (The correction curves were developed in Latham, 1987).
Figure 2.4 Digitization and Fourier reconstructed normalised outline with explanation of size parameters. See also Appendix C.
Figure 2.5 Relationship between the number of pixels in the outline, N and the video image equivalent particle radius, Si. Example data from Buckhaven (U - upper, L - lower), see Appendix C.
Figure 2.6 Illustration of procedure for obtaining random projections of blocks on light table using plasticene to obtain random orientations from inside plastic bag.
Figure 4.1 Cross-section through the model test section.
Figure 4.2 Plan of deep random wave flume.
Figure 5.1 The 10 tonne pile of 40 to 75mm sized aggregate from which the five armourstone batches were prepared.
Figure 5.2 Material preparation and sizing of armourstone batches.
Figure 5.3 X/Z ratio percentage exceedance curves for the subsamples representing the five shape classes.
Figure 5.4 The Fourier shape contribution factor P_C percentage exceedance curves for both the random projections of the five shape classes.
Figure 5.5 The Fourier asperity roughness factor P_R percentage exceedance curves for both the random projections of the five shape classes.
Figure 7.1 Regression analysis plot for Van der Meer's plunging wave equation with P = 0.1, for TABULAR.
Figure 7.2 Regression analysis plot for Van der Meer's plunging wave equation with P = 0.1, for FRESH.
Figure 7.3 Regression analysis plot for Van der Meer's plunging wave equation with P = 0.1, for EQUANT.
Figure 7.4 Regression analysis plot for Van der Meer's plunging wave equation with P = 0.1, for SEMIROUND.
Figure 7.5 Regression analysis plot for Van der Meer's plunging wave equation with P = 0.1, for VERY ROUND.
Figure 7.6 Regression analysis plot for Van der Meer's plunging wave equation with P = 0.1, for all shape classes.
Figure 7.7 Summary of regression analysis results for plunging wave equation with P = 0.1.
Figure 7.8 Regression analysis plot for Van der Meer's surging wave equation with P = 0.1, for TABULAR.
Figure 7.9 Regression analysis plot for Van der Meer's surging wave equation with P = 0.1, for FRESH.
Figure 7.10 Regression analysis plot for Van der Meer's surging wave equation with P = 0.1, for EQUANT.

Figure 7.11 Regression analysis plot for Van der Meer's surging wave equation with P = 0.1, for SEMIROUND.
Figure 7.12 Regression analysis plot for Van der Meer's surging wave equation with P = 0.1, for VERY ROUND.
Figure 7.13 Regression analysis plot for Van der Meer's surging wave equation with P = 0.1, for all shape classes.
Figure 7.14 Effect of shape on stability in relation to shape analysis results of Van der Meer's flume test material (circled points). Crosses are plunging condition (P) and points are surging condition (S). Left axis is surging formula coefficient C_{su} and right axis is plunging formula coefficient C_{pl}. P = 0.1 is assumed.
Figure 7.15 Effect of shape on stability in relation to shape analysis results of Van der Meer's flume test material (circled points). Crosses are plunging condition (P) and points are surging condition (S). Left axis is surging formula coefficient C_{su} and right axis is plunging formula coefficient C_{pl}. P = 0.05 is assumed.
Figure 7.16 Regression analysis plot for Van der Meer's plunging wave equation with P = 0.05, for all shape classes.
Figure 7.17 Regression analysis plot for Van der Meer's surging wave equation with P = 0.05, for all shape classes.
Figure 8.1 Correlation of wear in Portland limestone from laboratory mill abrasion test with wear on prototype blocks at West Bay near 'block A' (see Clark, 1988) assuming various prototype abrasion models and initial block sizes.
Figure 8.2 Abraded 15 tonne blocks of Portland limestone near 'block A' at West Bay, Dorset.
Figure 8.3 The slope protection works at Buckhaven, Scotland.

NOTATION

A_e erosion area in a cross section

A_n phase angle

C empirical constant

C_n amplitude coefficient of the nth harmonic

C_{pl} coefficient describing the shape effect for plunging waves

C_{su} coefficient describing the shape effect for surging waves

Circ Fourier circularity ($= 2\pi/L_n$)

D Fractal dimension

D_{eq} Fourier equivalent particle diameter (derived from a random projection Fourier analysis)

D_{ef} Fourier effective diameter

D_n nominal block diameter = $(W_n/\rho_a)^{1/3}$

D_{n50} nominal diameter, $(W_{50}/\rho_a)^{1/3}$

D_{50} sieve diameter, diameter of stone which exceeds the 50% value of sieve curve

D_{85} 85% value of sieve curve

D_{15} 15% value of sieve curve

D_{85}/D_{15} armour grading

F Fractal coefficient (= D-1) for a given range of step lengths

F_m Fractal coefficient value for an image with equivalent particle radius S_i of m pixels

F_{40} Fractal coefficient corrected to equivalent value for $S_i = 40$

H_s significant wave height, average of the highest one-third of waves

$H_s/\Delta D_{n50}$ dimensionless wave height parameter

K_Δ layer thickness coefficient

K_D stability coefficient in Hudson formula

K_{1c} fracture toughness

L wave length, $gT^2/2\pi$

L_n dimensionless perimeter of the Fourier reconstructed image

L_{pn} video image perimeter length L_p (subscript n = number of pixels in step)

N number of waves

N' number of pixels in video image outline

N_Δ damage level defined in Thomson & Shuttler (1975)

P permeability coefficient

P_f fictitious porosity ($= 100(1-(\rho_a/\rho_b))$)

P_n Fourier noncircularity, based on the harmonic amplitudes from 1to ∞

P_S Fourier shape factor based on the 1st to 10th harmonic amplitudes

P_R Fourier asperity roughness based on the 11th to 20th harmonic amplitudes

P_C Fourier shape contribution factor ($= 10P_n$)

Q	sum of the amplitude coefficients for a chosen range of harmonics
R_a	centre-line-average roughness of a surface from topographic profile data
S	damage level, A_e/D_{n50}^2
S_{md}	damage level, mean of damage S calculated separately for each profile line
$S/\sqrt{N}$	dimensionless damage level
S_i	Video image equivalent particle radius (= N/L_n = N*Circ/2π)
T	Fourier total roughness factor (= $C/(L/P_n)$)
T_C	Fourier surface texture contribution factor (= $T-P_C$)
T_m	average wave period of a time signal
T_s	average period belonging to the highest one-third of waves
W_n	nominal block weight
W_0	original weight of armour block
X	maximum dimension of the armour block shape
Y	intermediate dimension of the armour block shape
Z	minimum dimension of the armour block shape
f	video image scale factor (= length on particle or block represented by one pixel)
g	acceleration of gravity
m_p	photograph scale ratio (= length on prototype block/equivalent length on print of armour block)
n	harmonic order
r	radius vector
r_i	object to video image length scale (= length on photographic print represented by one pixel)
s_m	fictitious wave steepness, $2\pi H_s/gT_m^2$
t	number of revolutions, in thousands, in mill abrasion test of Latham & Poole (1988)
t(armour), t(filter)	armour, filter layer thickness
w_p	bed profiler probe width
x	equivalent wear factor
α	angle of seaward slope of structure
Δ	relative mass density, $(\rho_a-\rho)/\rho$
Δx	horizontal separation between profile points
Δy	vertical separation between profile points
ξ	surf similarity parameter, $\tan\alpha/\sqrt{H/L}$
ξ_m	surf similarity parameter using T_m, $\tan\alpha/\sqrt{(2\pi H_s/gT_m^2)}$
ρ	mass density of water
ρ_a	mass density of the armour
ρ_b	bulk density of material as laid on slope
σ	root-mean-square roughness of a surface from topographic profile data
θ	polar angle measured from an arbitrary reference line

1. INTRODUCTION

1.1 Background

Rock armouring is used extensively in the design of rubble mound breakwaters, sea walls and revetments. Using current rock quality specifications and lowest initial cost criteria, it has been a relatively simple task to make the choice (not necessarily the best choice in the long term) between a number of geologically contrasting sources of rock armour for a particular breakwater or revetment project. More recently, particularly with the introduction of the dynamically stable design concept, it has been recognized that in the future the scientific framework for economic optimization on a project would require a greater appreciation of the long-term performance of different rocks. Research at Queen Mary College has been concerned with several parallel studies to help provide this framework. The principal ones are :

(i) To assess rock durability in the marine environment using laboratory tests (Fookes & Poole 1981, Dibb et al 1983a,b, Poole et al 1984, Fookes & Thomas 1986, Latham & Poole 1987b and see also Allsop et al 1985 for a summary).

(ii) To develop techniques for describing hydraulically sensitive geometric features of armour layers :

(a) roughness of armour layer profile topography (Latham & Poole 1986 and Latham et al 1988)

(b) shape and texture of individual blocks from armour layers (Latham & Poole 1987a).

(iii) To develop approaches for the prediction of rates of wear on prototype structures (Allsop & Latham 1987, Latham & Poole 1988).

(iv) To assess the influence of shape and surface texture on hydraulic stability and its possible relevance to design equations.

The techniques in (ii) were a prerequisite for the flume tests required in (iv). Only with reliable measures of texture is it possible to test the suggestion that rounded rock has a lower stability than angular or cubic rock and to begin to quantify the relationship.

The flume study undertaken jointly between Queen Mary College and Hydraulics Research at Wallingford was performed by A.Bradbury and M.Mannion. Hydraulics Research has close contact with practising coastal engineers and long-standing interests in rock armouring of coastal structures under random wave attack (since Thompson & Shuttler 1975). This background has helped facilitate effective collaboration of which this series of flume tests is the latest example. The test programme was designed for the systematic investigation of surface texture within the context of Van der Meer's design formulae (1984,1988), while retaining aspects of direct practical value. For example, the decision was made to investigate gross shape including extremely tabular armour, as this is often the only type of armour that a quarry manager can produce economically, due to geological constraints. The five shape classes tested were tabular, fresh (angular), equant (cubic), semiround and very round.

1.2 Outline of the report

This report is the second of two reports relating to the programme of flume tests to quantify the effect of rock shape on stability. The first report (Bradbury et al 1988) will be referred to as SR150 throughout this second report.

SR150 outlines recent advances in rock and riprap design methods before describing the model studies in detail. At the time of preparation of SR150 a full examination of the significance of the results was not possible as details of the shape analysis were not available. Scatter in the results appeared to mask any significant effects of rounding on stability but clear indications that tabular shaped material was more stable than the other shapes tested were emphasised. The importance of placement techniques and resulting layer porosities were the subject of much discussion. Conclusions were directed towards design practise and recommendations that differences in layer porosity should be investigated together with shape effects were made.

This second report contains important additional data following a shape analysis at Queen Mary College of some of the test material that was used by Van der Meer (1988) in his extensive flume study (which led to his design formulae). It includes a synthesis of the experimental data relating to the shape effect on hydraulic stability and attempts to show how the results may be fitted into the recently recommended design formulae of Van der Meer. This report may be considered to be a collation of recent research relating to techniques and experimental studies in (ii) and (iv) of Section1.1 (with less detailed accounts of studies in (i) and (iii)), the principal subject being that of armourstone shape and rounding.

Section 2 of the report gives practical and theoretical details behind the development of the new image analysis techniques for gross shape and surface texture measurement for both prototype and model armour blocks. Section 3 reviews the evidence for shape effects, highlighting some of the results of Van der Meer's study which also suggested a likely effect of rounding of model armourstone on stability. A brief outline of the flume test programme is given for completeness in Section 4.

In Section 5, all the geometric information on the test sections is given. Using both axial measurement and image analysis, the gross shape and surface texture of each armourstone shape class used in the model tests together with some of Van der Meer's material is examined. Details of armourstone weight, fictitious porosity and armour layer thickness together with a small sample of topographic roughness data from downslope profiles were also discussed. Results of the tests are given in Section 6 and analysed in Section 7. Much discussion is devoted to Van der Meer's design formulae and an indication of the relationship between rounding and instability can be deduced. Section 8 gives a first insight into how rapidly prototype armour might be wearing under different environmental conditions for different initial block sizes and rock types so that together with the findings of Section 7, the effect on stability of long-term degradation and rounding can eventually be tackled.

Finally, Section 9 draws together conclusions and recommendations on image analysis, armour shape, hydraulic stability and armourstone wear. Further details of image analysis are included in the appendices.

2. SHAPE MEASUREMENT OF ROCK ARMOURSTONE

2.1 Background

In this report, shape is taken to be the general term which includes all aspects of external morphology of a particle and incorporates gross shape, roundness, smoothness, angularity and surface texture within a heirarchy of increasingly magnified detail (Barrett, 1980). The quarrying and in-service controls of shape of natural armourstone were discussed by Fookes & Poole (1980) and Dibb et al (1983a).

The traditional measure of gross shape relevant to armourstone specification has been the X/Z ratio, where X, Y and Z are the maximum, intermediate and minimum dimensions of the enclosing cuboid. Thomson & Shuttler (1975) presented their model armour shape data in a series of X/Y versus Z/Y scatter plots and also on a percentage exceedance graph to show the distribution of X/Z ratios (from the three samples of different size model riprap that they investigated). For reasons of poor structural and handling performance, armourstones with X/Z greater than 2 or sometimes 2.5 are often designated as outside specification. To match these prototype requirements, most model studies of stability have therefore used crushed rock which has been selected (usually by eye) to be equant. The 50 percent exceedance value for the X/Z ratio was between 1.6 and 1.8 in both the Thomson & Shuttler (1975) and the Van der Meer (1988) investigations. However, shape was not a controlled variable in either of these test programmes on static stability.

Hudson (1959) developed details of the layer thicknesses and packing density relationship for 7 different shape classes of stone ranging from X/Z = 1.5 to X/Z = 3.3. However, the authors are unaware of any associated laboratory results relating these shape classes to stability.

It could be argued that X/Z is not the best parameter to evaluate the gross shape effect on stability as there is a growing need to develop parameters that can be automatically measured from two dimensional images.

To study the effect of wear and rounding on stability, some success was achieved in earlier studies based on the Wadell-Krumbein measure of roundness which is the ratio of the average radius of curvature of the several corners or edges to the radius of curvature of the maximum inscribed circle; see, for example, Dibb et al (1983a) and Fookes & Thomas (1986). To provide an appropriate field and laboratory parameter of block roundness or roughness, a new set of automated and objective descriptors had to be introduced since Wadell-Krumbein roundness gives

unacceptable operator variability for more angular material and is not amenable to automated techniques of analysis.

The problem of obtaining shape and roughness parameters, intended to represent 3-dimensional block geometry, from 2-dimensional images can be overcome if the disposition of the many blocks sampled can be assumed to be random (Section 2.4.1).

2.2 Fourier and Fractal shape descriptors

2.2.1 Automated imaging system & key analysis references

The key references to the techniques of obtaining descriptor values from a series of outline (x,y) co-ordinates are Schwarcz & Shane (1969), Ehrlich & Weinberg (1970), Czernecka & Gillott (1977) and Clark (1981) for Fourier, and Mandelbrot (1982), Schwarz & Exner (1980) and Orford & Whalley (1983) for Fractal. The technical implementation for model studies on aggregate size rock fragments was described in Latham & Poole (1987, 1988) and for prototype armourstone, in Latham (1987). The methods of Fourier and Fractal analysis of the shapes of model armourstone in the flume study of this report remain essentially the same and are summarized in the following sections.

The particle boundary co-ordinates are obtained from video captured images. The video image is manipulated using the VIP image analysis unit (made by Sight Systems, Newbury, Berks, UK) linked to a BBC microcomputer and the boundary pixel locations are recorded onto data files for Fourier and Fractal analysis on a mainframe computer.

2.2.2 Fourier shape descriptors

The particle outline as given by a series of (x,y) co-ordinates can be described by a series of independent uncorrelated harmonics of the form:

$$C_n \cos(n\theta - A_n)$$

where C_n is the amplitude coefficient of the nth harmonic, n is the harmonic order, θ is the polar angle measured from an arbitrary reference line, and A_n is the phase angle. This is the (r,θ) Fourier method for which the centre of gravity is calculated and taken as the origin for the radius vector r but for which any re-entrant outlines cannot be represented - though this is not a problem for armourstones.

Figure 2.1 illustrates how each harmonic represents a specific geometric contribution to total particle shape. Gross shape, for example elongation, is measured at lower harmonic orders and increasingly fine scale texture is represented at higher orders. By the time the tenth harmonic has been added in, the Fourier representation will be quite good but generally smoother than rough outlines with surface texture. To describe a rough irregular outline, the 11th to 20th harmonics will be required. The coefficient Q provides a flexible quantitative index which can be computed over all or a chosen range of harmonics and is defined as:

$$Q = (0.5 \Sigma C_n^2)^{0.5}$$

where the following names were proposed (Latham & Poole, 1988) for the most generally accepted specification of Q:

Symbol	Range of n	Name
P_n	1 to ∞	Fourier noncircularity
P_S	1 to 10	Fourier shape factor
P_R	11 to 20	Fourier asperity roughness factor

The 0th harmonic is set to be the circle of unit radius and thus the Fourier descriptors are unaffected by differences in particle size (provided that outlines contain at least 300 pixels, see Latham (1987) for a discussion of size corrections. In this report, P_n is calculated using an upper limit of n = 30 although results for n = 10 and n = 20 are practically identical because amplitudes fall off rapidly as harmonic order increases (as illustrated in Latham & Poole, 1987a). Given a sample with many particles, an approach often used now in sedimentology is to compute the 'shape frequency histogram' for each harmonic (Ehrlich et al, 1980). Comparisons of shape frequency histograms from samples abraded to differing degrees will show the histogram being skewed towards the lower amplitudes for the most abraded.

Czarnecka & Gillott (1977) found that P_R did not distinguish well between smooth and jagged squares, rectangles and angular polygons so they defined the following shape descriptors which proved more suitable to their application of concrete aggregates:

$T = C((L_n-2\pi)/P_n)$	Fourier total roughness
$P_C = 10\ P_n$	Fourier shape contribution factor
$T_C = T - P_C$	Fourier surface texture contribution

Here, L_n is the length of the perimeter of the normalized outline and C is an empirical constant value which they established experimentally. Thus, they attempted to obtain a coefficient of total roughness which did not over represent the roughness of smooth surfaced elongate particles and with which the separate contributions of shape and surface texture could be determined. Note that P_C carries practically the same information as P_S but is scaled by a factor of 10 for compatability with T and T_C. In studies using wear simulation (Latham & Poole, 1988), P_R has given a more reliable average measure of surface roughness than either T or T_C for random projection views of the sample of particles. However, T and T_C values will be given together with P_C and P_R in Appendix A as they may be of interest in future applications.

2.2.3 Fractal shape desciptors

Another shape descriptor is the Fractal coefficient F which quantifies the crinckledness or convolutedness of a particle. Particle shape categorization using the concepts of Fractal geometry (Mandelbrot, 1982) is based on the Mandelbrot-Richardson plot. This can be simply defined as the log perimeter length estimate versus log resolution of the measuring instrument used to make the estimate. For example, if a pair of dividers were used, the perimeter length estimated by stepping around the outline is calculated with divider legs at a fixed separation (i.e. step length = resolution). This is repeated for many different step lengths and the dependance of the length estimate is displayed on the Mandelbrot-Richardson log-log plot. For rock fragment outlines this plot is in fact nonlinear. However, the local slope (= -F) may be determined by a least squares regression over a chosen range of step lengths. The fractal dimension D for that regression range is equal to 1 minus the slope, and the Fractal coefficient F (= D-1) is the absolute value of the slope. Two examples of this kind of plot are shown in Figure 2.2 where the Schwarz & Exner (1980) algorithm has been used to compute step lengths (as throughout this report) and F has been calculated over the fixed regression range of 3 to 10 pixel widths for two equal sized armourstones where the scale of roughness being measured is from 15 to 50 mm.

Two difficulties with using the Fractal coefficient measure of roughness were investigated in Latham (1987). The problems were essentially that:

(i) Regression step length limits chosen to calculate the slope F must be defined because of the nonlinearity of the M-R plot.

(ii) Regression step lengths are most conveniently set up in terms of pixel widths and therefore F will be to a certain degree correlated with size. Any one outline viewed at different magnifications will give different values of F for a fixed range of step lengths, although it is the same image - a size effect.

To these problems, the following solutions were found:

(i) The recommended regression range for sensitive roughness discrimination is from 3 to 10 pixels, because the first two pixels introduce the spurious effect of the artificial rectilinear form imposed at the limits of resolution (see Figure 2.2), and because values higher than 10 will tend to introduce higher variability within populations that include gross shape variability but no real differences in roughness.

(ii) The Fractal coefficient value F_m as determined from an image with equivalent particle radius S_i (see definition in section 2.3.4) of m pixels can be corrected to its F_{40} value for an S_i of 40 pixels using a series of correction curves developed in Latham (1987) and presented in Figure 2.3. The value $S_i = 40$ is chosen because the Fourier shape descriptors are independent of image size for S_i greater than 40 pixels.

2.3 Measurements on prototype structures

2.3.1 Photography guidelines

1. Each photograph should be taken featuring one individual block's outline projection.

2. Each photograph should show a 1m or 0.5m scale bar on or adjacent to the block and as near to the camera axis perpendicular as possible. (Ideally the scale bar and the centre of the block should be at the same distance from the camera but this will invariably be impractical if not impossible. The usual positioning of the scale bar on top of the block will result in a slight underestimate of block size).

3. It is better to shoot photographs at the same object scale (i.e. the scale bar occupies a constant proportion of the field of view), and thereby achieve scale equilization, than to adjust so that each picture is just filled by each block. The use of a zoom lens is highly recommended but not essential.

4. The number and location of the sample of armourstones is to be adhered to as strictly as possible and selected at random. In practice, most blocks are unsuitably disposed for photography due to overlap or awkwardness in position, but

it is reasonable to suggest that this effect on sampling, as well as projection angle, should not affect the assumed randomness of the photographed sample. Care should be taken not to rephotograph the same block twice. The sample to be analysed should contain at least 30 blocks, and therefore choosing 35 to 40 blocks will allow rejection of those where the full block projection cannot be picked out. A sample of about 35 blocks will take about one hour to photograph.

5. Colour printing allows clearer definition of block outlines than black and white. The UK standard format (150 by 100 mm) postcard-sized print is the smallest size of working print acceptable since printed block diameters of 100 mm or greater are generally required to minimize the inaccuracies that could be introduced in the next stage of outline drawing. The suggestion that the latest generation of imaging systems incorporating filters might be able to define the edges of blocks automatically is encouraging but seems unrealistic when confronted with typical examples of such photographs with problems of shadows and very low contrasts between neighbours. The simplicity of black and white photography gives greater flexibility, in that scale equilization which may not have been achieved during initial photography on site, can be introduced at the print enlargement stage

2.3.2 Outline tracing

Use a fine (i.e. approximately 0.3 mm) black ink pen to reproduce faithfully the outline of each block on a separate piece of transparent drawing film. Use a thick pen and fill inwards from the outline with a suitably opaque ink to give a border of at least 5 mm (for the purpose of enabling a boundary following routine to operate on a thresholded margin of at least 2 pixels thickness). The outer ink line should be precisely maintained. If scale equilization is to be introduced during a later process using the video camera lens, then the scale bar length on each photograph must be transferred accurately to a position next to the traced outline of each block. The tracing of outlines is the single most time-consuming stage of the analysis procedure and to prepare 30 outlines for the video camera will take one person about 4 hours.

2.3.3 Video data capture

The image analysis system operating at Queen Mary College since 1986 has a 512 by 512 pixel screen image arranged into four quadrants of 256 by 256 pixels. Using menu and cursor-driven software, the traced outlines seen by the video camera can be precisely thresholded relative to a white background (e.g. a light table) and a boundary following routine used to strip co-ordinates from sucessive outlines

provided these outlines do not cross the quadrant boundaries. The stored data files may contain many outlines. The 256 by 256 dimensions impose an upper limit of around 700 for the number of pixels on a typical outline from an armour block or piece of model armour. The software allows for a grid to be superimposed on the screen image at an operator selected x and y spacing so that zoom adjustment by matching of grid and scale bar may be made prior to co-ordinate stripping. However, these adjustments are slow to implement for every image captured, and therefore such scale equilization is encouraged at earlier stages in the image processing, ideally at source when taking the photographs.

To obtain the pixel co-ordinates from 30 traced outlines and have them stored on disc presently takes up to 2 hours. File transfer to mainframe computer and file manipulation typically takes up to one hour at Queen Mary College but times will be dependant on facilities available. The analysis itself yields tabulated results within minutes. The whole analysis sytem could no doubt be mounted most efficiently on the latest generation of powerful microcomputers set to run the Fortran analysis program.

2.3.4 Scale equilization and definitions

In the shape analysis study of limestone fragments (26.5 to 31.5 mm sieve size), Latham and Poole (1987) reported that blocks were placed on a light table and imaged directly at one camera setting for magnification (one pixel = 0.5 mm). The need for photography in the study of prototypes introduces further sets of scale variables which call for the complete set of definitions given below and a more in depth study of the sensitivity of shape descriptors to image size, (see Latham, 1987).

Photograph scale ratio (m_p) = length on prototype block/equivalent length on print of block

Object to video image length scale (r_i) = length on photographic print represented by one pixel.

Video image scale factor (f) = length on particle or block represented by one pixel.

These scale variables are related by the equation:

$$f = m_p * r_i$$

For the purpose of investigating the effects of image size on the constancy of different shape descriptors and for comparing rates of rounding of small particles and large blocks, it is also necesary to standardize, relative to the particle image size the amount of boundary detail to be used in representing the particle outline.

Although the number of pixels in the particle outline N' gives a general measure of this detail, since it is an un-normalized approximation for the perimeter length, it will also be apparent that N' is not a shape independent measure of the size of the pixel video image. The area enclosed by the outline, which can be determined for example by a pixel count from an infilled block outline, gives an obvious measure of size. However, a more rapid and convenient though computationally more complex area or size measure can be obtained from the mainframe analysis of the boundary co-ordinates. Variations in the size determination resulting from lighting conditions leading to unreproducible edge detection can be disregarded for all but the smallest of images.

In the Fourier analysis methods described earlier (Latham & Poole 1987a), the dimensionless perimeter length of the normalized Fourier reconstructed particle outline, L_n, was used to calculate a number of descriptors (the Fourier Total Roughness T and a Fourier derived measure of circularity, Circ = $2\pi/L_n$). It may be useful at this point to recall that the reconstructed normalized outline uses a 30 term Fourier Series and L_n is the sum of the distances between the N'/4 equi-distributed reconstructed boundary points (see Fig.2.4, note for one quarter of the particle, only N'/16 lines are shown). Together, L_n and N' provide a simple measure of the video image particle size in pixel units. Dividing N' by L_n gives the Video Image Equivalent Particle Radius, S_i, where

$$S_i = N'/L_n = N' * Circ/2\pi$$

This equation has been investigated in graphical form (Fig.2.5) where some prototype data of well rounded and virtually unabraded blocks from Buckhaven coastal protection works, in Scotland, are included to give a realistic range of the influence of the Fourier circularity parameter, Circ.

The shape independence of S_i can then be used to examine the influence of pixel image size on different descriptors. When comparing shape descriptors of samples from different sizes, for example, prototype armour blocks and laboratory abraded aggregate, the analysis is most meaningful if the typical values of S_i do not differ too greatly between the two samples. (How much difference can be tolerated and the effects resulting from such differences were considered in Latham, 1987).

2.3.5 Particle size estimates from image analysis

The decision was taken to include this section because of its potential for development as a means of quality control on sizes. However, it is acknowledged that the problem of constraining this degree of scale misrepresentation during photography of blocks, may not be easy to solve.

From the computer evaluation of S_i, it is simple to back calculate a measure of size in the original particle or prototype block. The Fourier Equivalent Diameter D_{eq} of a particle (derived from a random projection Fourier analysis) is given by the equation:

$$D_{eq} = 2 S_i * f$$

However, D_{eq} has the disadvantage as a size parameter because of its use of N' to determine perimeter length. Several other terms of potentially greater practical value which also relate to size are now considered. Recall from the Fourier analysis that the normalized reconstructed outline, by definition, contains the same area as the unit circle. By comparing the perimeter lengths of the video image outline with the normalized outline (see Fig.2.4), it is easy to find the diameter of the circle which occupies the same area as the video image outline. It is a Fractal algorithm (that given by Schwarz & Exner (1980) is preferred for the present analyis) which yields the perimeter length estimates. For the resolutions of N' = 300 to 500 used in this study, probably the best estimate of perimeter length for natural prototype block or rock aggregate outlines (L_{p3}) is that obtained by summing distances between every third pixel centre, tracking round the block 3 times and averaging. Taking the number of pixels N' will underestimate the perimeter length by about 10% because both the diagonals and straights are represented by one, and taking L_{p1}, the summed distance between every adjacent pixel centre, will overestimate because of the rectilinear pixel form (see Figs. 2.2 and 2.4) which sums lengths of either 1 or 2. Therefore to find the diameter D_i of the circle containing the same area as the video image outline of the block, a combination of both Fourier and Fractal computations is used. The new terms are defined below.

Video Image Effective Diameter D_i = diameter of circle with area equal to video image

Video Image Perimeter Length L_{p3} (based on every third pixel) = perimeter length estimate based on Schwarz & Exner (1980) algorithm using every third pixel and cycling around the outline three times.

The defining equation is thus:

$$D_i = L_{p3}/L_n$$

which leads to an equation for the Effective Fourier Diameter of the block:

$$D_{ef} = D_i * f$$

Assume now that the block has the same weight as a sphere of diameter D_{n50} which is not unreasonable for a completely random outline projection, then the ratio of the nominal to the effective block diameter D_n/D_{ef} is $(\pi/6)$ or

$$D_n = 0.806\ D_{ef}$$

where

$$D_n = (W_n/\rho_a)^{1/3}$$

and W_n and ρ_a are the nominal block weight and rock density.

The above development shows how size estimates could be derived. However, the effect of scale distortions due to unsystematic positioning of scale bars in relation to the block centre of gravity will lead to inaccuracies which have yet to be evaluated.

2.3.6 Choice of video camera magnification

In order that video image size effects can be treated as negligible, an average value of S_i of at least 40 pixels is required for the Fourier descriptors and the size effect on the Fractal coefficient can be reliably corrected at this image size. Taking $S_i = 40$ as desirable, since $D_{eq} = 2\ S_i * f$ and D_{ef} is approximately 10% greater than D_{eq}, the recommended setting for the video image scale factor f is given by the inequality

$$f \leq D_{ef}/\ 100$$

This would ensure that most of the smaller blocks in natural samples including a fair degree of size gradation would satisfy the condition $S_i > 35$. For prototype sizes of armour of 0.5 and 1.5 m, a setting of f to 5 mm and 15 mm respectively would be appropriate.

2.4 Measurements on model armour

2.4.1 Positioning of blocks on the light table

The placement of model armour blocks directly on the surface of a light table presents the video camera with a silhouette projection of the block which can be directly thresholded and processed to give the outline co-ordinates without the need for photography and outline drawing.

Natural stability while positioning the blocks will result in the Z dimension of the block lying near to the vertical. Thus, with a little operator judgement the 'maximum projections' can be viewed. To give an overall indicator of the three dimensional aspects of the particle shape, it is possible to examine randomly selected projections of the blocks. Although it may not be of critical importance, no simple distinction can be made between disc, blade and prolate gross shape features of the sample obtained by this type of analysis. Any divergence from equant will however be accurately represented by the Fourier shape analysis.

To obtain 'random projections', the armour blocks were placed in a plastic bag. Each block was then carefully taken from the bag and erected on the light table (using plasticene), with its vertical axis corresponding with that which it had assumed inside the bag (see Fig.2.6).

2.4.2 Choice of camera magnification

As with the prototype analysis, the inequality $f \leq D_{ef}/100$ sets the appropriate f values. For example, with nominal block weights of $W_n = 300$ g and density of 2.7×10^3 kg.m^{-3}, D_n is approximately 48 mm, D_{ef} is approximately 60 mm and therefore a setting giving $f = 0.6$ mm is appropriate.

The inequality if only for rough guidance as the magnification based on a scale bar placed on the light table surface will overestimate the size of the blocks compared with that given by positioning the scale bar at a level approximating the centre of gravity of the block. Note, the reverse is true of prototype blocks where the scale bar has been laid on top of the block, i.e. nearer the camera, and the block size is generally underestimated.

2.4.3 Grain scale effects

It is reasonable to expect very fine scale roughness to be present at the mineral or fossil grain scale of the rock. At a certain length scale on the model armour, the roughness as detected by an image analyser may no longer resemble a scaled down version of roughness on prototype blocks since grain scale roughness on the prototype blocks is unlikely to be resolvable in the traced outlines from photographs while it may show up clearly on model armour if the grain size is large. For this reason, the use of fine-grained rock for model armour material and related abrasion studies is to be recommended. The rock aggregate used for model studies should have a grain size less than that represented by 2 or 3 pixels.

If, however, the scale of roughness of interest is that which is contributed to by irregularities on the grain scale of the rock, literally the surface texture, then the size represented by one pixel will have to be smaller, perhaps by one fifth, than the mean grain size of the rock with the smallest grain size being compared. (Such a study would be of great interest to concrete and road aggregate research). With the present video imaging arrangement at Queen Mary College, the upper limit for D_i is around 220 pixels. A rock of grain size of 1mm, for example, will only yield particle shape descriptors which reflect grain scale roughness if the block/particle (imaged directly on a light table) has effective diameter D_{ef} of less than 45 mm (assuming an f setting of 0.2 mm) to ensure a complete outline fits within the screen, and greater than 20 mm to ensure $S_i > 40$ and thus no size effects on the Fourier descriptors.

3. REVIEW OF EVIDENCE OF SHAPE EFFECTS ON STABILITY

Jensen (1984) presented two sets of results from random wave tests carried out at the Danish Hydraulics Institute, one for stability of quarrystone and one for rounded 'seastones'. A comparison of these results which generally indicated greater stability for the quarrystones, was considered in the companion report SR150. However, the profile sections and core permeabilities of the two sets of test conditions appear to be different making it difficult to evaluate the significance of the poorer stability observed with the rounded stone.

Bergh (1984) investigated the effect of slope on stability using regular waves, an impermeable core and composite profile of 1:1.5 (deepest) and 1:2.5 where the break of slope was at 135mm below still water level. In 18 tests, 4 shape classes were examined : flat slate (X/Z average ≈ 3.4), cubic slate (X/Z average ≈ 1.9), cubic granite (X/Z average ≈ 1.6) and well rounded glacial boulders (X/Z average ≈ 1.5). For the start of damage, the non-dimensional significant wave height $H_s/\Delta D_{n50}$ for rounded material was only 50% of its value for cubic granite. This represents a factor of 8 in stone mass to achieve the same stability factor. For the failure criterion, the $H_s/\Delta D_{n50}$ was 77% of its value for cubic granite (a factor of 2.2 in stone mass). For zero damage, the $H_s/\Delta D_{n50}$ for flat slate was 78% of its value for cubic slate suggesting that flat material is less stable than cubic. Significant differences in the surf similarity parameter at the condition for zero damage of each shape class and the small number of tests cast doubt on the general applicability of the results.

Van der Meer (1988) did not consider gross shape and roundness as test variables in his static stability programme. Nevertheless, significant abrasive rounding of test material during the extensive programme, which involved 400 tests and painting of the stones in a cement mixer, seems to be the likeliest explanation of some of the stability results. Three pieces of evidence point towards a potentially significant influence of roundness or surface texture on stability :

(i) For one repeat test with identical wave conditions, but using relatively worn and rounded material compared with its more angular condition at the start of testing, the observed damage S for 1000 and 3000 waves was as follows

test 32 original state

$S(1000) = 4.43$; $S(3000) = 8.70$

test 189 well worn after painting in cement mixer

$S(1000) = 11.43$; $S(3000) = 20.65$

The damage S was therefore approximately 2.5 times higher in the second case.

(ii) Tests to investigate the influence of spectral width showed that differences between narrow and wide spectra were insignificant provided average and not peak period is used. Data from more angular riprap material that had been used in a total of 21 to 40 tests gave more stable results than the same material after it had become increasingly worn through handling and usage in 115 to 150 tests and which had a second painting in the cement mixer. The differences in stability could not be explained by differences in wave spectra associated with the different sets of results and therefore the reduction in armour interlock due to rounding was suggested. For the surging wave condition with surf similarity $\xi_m > 3$ to 4, where rundown has a major influence on stability, the abraded test material gave $H_s/\Delta D_{n50}$ values typically 65% of those obtained for the less abraded material used nearer the start of the test programme. The effect was noticeable but less marked for plunging waves. It is interesting to note from Van der Meer's thesis that the stability results of the abraded test material (shown in his Figure 3.20) for the cot $\alpha = 3$ conditions are virtually identical to those predicted for the cot $\alpha = 2$ condition (his Figure 3.16) and that the effect of having more rounded material is similar to that of steepening the slope angle.

(iii) During the tests to investigate the influence of relative mass density of the rock type, a systematic effect apparently uncorrelated to rock density was noted. For permeable core test conditions, and taking into account the different densities, broken brick produced greatest stability. Crushed basalt gave $H_s/\Delta D_{n50}$ values typically 95 to 90% of that for bricks and the normal limestone test material, about 85 to 80% of that for bricks. These results were thought to be due to differences in roundness and/or surface texture between the three types of test material.

The Shore Protection Manual (1984, Table 7-8) summarizes the results from a great many model investigations, principally those of Hudson at the Waterways Experimental Station, Vicksburg. For breaking and surging waves, it recommends

different values of K_D for smooth rounded and rough angular quarrystone. For breaking waves and zero damage $K_D = 2.0$ and 1.2 for rough and smooth respectively, which implies $H_s/\Delta D_{n50}$ for smooth is 84% of its value for rough. Table 7-8 of the SPM refers to a study by Markle & Davidson (1979). It suggests that $H_s/\Delta D_{n50}$ for long slab-like stone (parrallelpipedic) with axial ratio X/Z of about 3 can be 1.5 to 2.15 times higher than for rough quarrystone but requires special placement to achieve these high stabilities. In fact, for special placement of rough quarrystone with the largest axes perpendicular to the slope, the value of $K_D = 5.8$ suggests a 1.43 times higher value of $H_s/\Delta D_{n50}$ compared with random placement.

The above evidence suggests that both gross shape and roundness together with placement technique, will have an important effect on stability but the results do not give clear guidance to the designer on these influences.

4. FLUME TEST PROGRAMME

4.1 Conceptual framework

The purpose of the model tests was to quantify the effect of armour shape and roughnesson the stability of breakwater armour layers under random wave attack and to compare the results with Van der Meer's (1988) recent stability equation. Five contrasting shapes of rock were chosen and each tested under random waves for five different wave conditions. Damage was measured at 1000 and 3000 waves, to identify the influence of storm (test) duration. Wave height and period were varied to cover the full range of damage, but the following parameters were not varied for two reasons, (i) to allow a clearer picture to form of any dependance of damage on the shape of rock for a range of wave conditions due to resource constraints, (ii) limited flume time available. The fixed parameters were :

- armour weight W_{50} = 323g ≈ 2%
- relative mass density of rock ρ_a = 1.73
- permeability = impermeable core
- armour slope (cot α = 2)
- armour grading (D_{85}/D_{15} = 1.25)
- spectral shape = JONSWAP
- approach beach slope = 1/52
- filter size D_{50} = 11mm
- construction method, crest level & angle of wave attack
- water depth = 0.5m at the toe of the structure

4.2 Summary

In all, 59 tests were carried out in a joint research project at Hydraulics Research Ltd., Wallingford over the winter of 1987/88. The conditions selected for model testing are given in Table 4.1; Figure 4.1 shows a cross section through the model test section and Figure 4.2 shows the deep random wave flume used for the model test programme. The wave generator was driven by microcomputer and calibrated to produce the desired wave spectrum significant wave height and mean period. A more detailed coverage of the flume tests is given in SR150.

5. GEOMETRIC CHARACTERISTICS OF MODEL ARMOUR IN FLUME TESTS

5.1 Preparation of materials

5.1.1 Preparation of armour

Carboniferous limestone from the ARC Tytherington quarry was used. This rock had a saturated and surface dried relative density of 2.73. Five batches of armour of single size and consistent W_{50} were prepared, each batch having different shape characteristics. The 10 tonne load of 40 to 75mm quarrystone supplied (see Fig.5.1) was split into five shapes - FRESH, TABULAR, EQUANT, SEMIROUND and VERY ROUND. The selection criteria were

TABULAR : The max/min dimension was greater than two. Flat and elongate was included. Selection was by eye.

EQUANT : The max/min dimension was less than two and there were at least two parallel faces. Selection was by eye.

FRESH : The angular material left after the tabular and equant rock had been removed.

SEMI ROUND : Fresh material was rounded to achieve 5 to 10% weight loss.

VERY ROUND : Fresh material was rounded to achieve 20 to 25% weight loss.

5.1.2 Preparation of rounded rock

Preliminary tests were used to determine the rate of weight loss of the quarrystone resulting from rounding the stones in a cement mixer. The time periods required for the desired weight losses were 1.5 and 6.5 hours for the SEMIROUND and VERY ROUND stones, yielding weight losses of 7.7% and 23.3% respectively. The procedure was as follows :

(i) Remove chippings with 23mm sieve and weigh out sufficient quarrystone to half fill the cement mixer.

(ii) Place weighed stone in cement mixer.

(iii) Set mixer at correct angle to achieve tumbling action.

(iv) Add water.

(v) Start mixer and run for required time.

(vi) Wash the stone and again remove chippings with a 23mm sieve.

(vii) Weigh stone and calculate % weight loss.

(viii) Repeat until sufficient stone to form a test section has been rounded.

5.1.3 Sizing of armour

Each batch of the five shape classes was prepared with a W_{50} of 323g ± 2% and D_{85}/D_{15} of 1.25 ± 0.05. To achieve this, the stones of each shape were individually weighed, placed in order and their weights logged on a microcomputer. The arrangemenet for material preparation and sizing is shown in Fig.5.2. The target W_{50} was 325g ± 5%. To help achieve this, a preliminary test was used to set upper and lower limits of 470 and 170 grammes and all stones outside these limits were rejected. The W_{50} and armour grading (D_{85}/D_{15} ratio) were calculated and where necessary, adjusted by adding or removing stones from their logged positions and recalculating the new W_{50} until the target had been satisfied. The exact number of stones used in the flume tests and their individual and sum weight were recorded for each shape class.

Thus the five batches were prepared and Table 5.1 shows the weight statistics of the armourstone batches together with the exact number of stones used in the flume tests.

5.1.4 Preparation of filter

To obtain compatibility with the flume tests of Thompson & Shuttler and Van der Meer, the armour/filter/core configuration chosen was that given by Figure 3.25a of Van der Meer (1988) (first referred to in Van der Meer, 1984) for which the permeability P can be assumed to take a value of 0.1. It was noted that the sizes used in these previous studies were given as sieve size D_{50} not nominal diameter D_{n50} as printed in Figure 3.25a. Provided nominal or sieve sizes are used consistently when preparing armour/filter/core combinations, the permeability coefficient P will be unaffected unless (i) the shape factors relating D_{50} to D_{n50} are different for armour and filter, or (ii) the coefficient P is very sensitive to the size and thickness of the filter.

From Figure 3.25a for which P = 0.1

Filter size, $D_{n50}(\text{filter}) = D_{n50}(\text{armour})/4.5$

Layer normal thickness, $t(\text{filter}) = 0.5\ D_{n50}(\text{armour})$

Armour grading $D_{85}/D_{15} = 2.25$

Given D_{n50}(armour) = 49.1mm, the target values were t(filter) = 24.6mm and D_{n50}(filter) = 10.9mm. The filter thickness of 25mm was achieved. However, a misunderstanding resulted in a mix design giving sieve size D_{50} of 11mm instead of D_{n50} of 11mm. Therefore, D_{n50}(filter) = 9.4mm (assuming a shape factor of 0.85). Carboniferous limestone was also used for the filter mix which was

30%	14 to 20mm sieve size
30%	10 to 14mm sieve size
40%	6 to 10mm sieve size

giving a reasonably linear percentage exceedance versus logarithmic size plot with D_{85}/D_{15}(filter) of about 2.25.

100kg of filter mix was spread evenly over the test slope and toe sections (see Figure 4.2) to achieve an approximate layer thickness of 25mm, although this could nc be accurately measured. A roughened metal mesh was attatched to the slope of the impermeable plywood core section, to improve the keying of the filter layer to the smooth core section. Layer thickness of the armour layers will be considered in Section 5.4.1.

5.2 Shape of subsamples

5.2.1 Sampling

The material preparation (section 5.1) resulted in five batches each containing about 1000 blocks of model armourstone, a sufficient number to build the test sections for the flume tests. Each batch was designed to exhibit different combinations of gross and fine shape characteristics and the subsamples chosen for shape quantification should accurately reproduce these.

The weight of each particle in a batch test had already been logged on a microcomputer during the process of sizing the batches. Thus with a little extra computation, the blocks were ranked by weight and the exact floor locations of the blocks comprising each subsample were determined such that the 48 block subsample gave the same weight distribution as that of the whole batch. This systematic approach to selecting subsamples ensuring an even weight distribution was thought preferable to a random approach because of the possible correlation between size and shape sometimes noted within the products of commercial rock crushers (eg. see Thompson & Shuttler, Table 18, 1975).

Sample numbers in sedimentological studies of beach pebbles were discussed by Orford (1975). He noted that samples containing from 25 to 300 pebbles had been used but found a 30 pebble sample sufficient for his study. During the analysis of the shape descriptor results of this study, it was noted that when more than 40 blocks were included in the subsample, the average value of the significant descriptors became reasonably stable for the 'random' as well as the 'maximum' projections, suggesting that about 48 blocks was a sufficient subsample. However, differences between successive 'random' projections of the same 48 blocks were noted in Section 5.2.3, indicating perhaps that the sample number of 48 was not the only reason for a relatively poor sampling repeatability.

5.2.2 Gross shape and size from XYZ axial dimensions

The X,Y and Z dimensions of the enclosing cuboid of all 48 pieces in each subsample were measured to the nearest 0.1mm using vernier calipers. Results are summarized in Table 5.3. The average nominal cuboid diameter d_{xyz} from the five shape classes was 61.0mm. The values for the most irregular shape classes were larger by about 2mm and the more spherical shape classes were smaller by about 2mm. This is to be expected for subsamples designed to have essentially the same average weight, as reflected by the narrow range of D_{n50} of 49.1 ± 0.3mm (see Table 5.1), but which have different gross shapes.

For a comparison with other laboratory studies, the X/Z ratio data are presented in Table 5.2 and Figure 5.3. From the X/Z ratio exceedance curves it is immediately apparent that TABULAR is very different to all other classes. It was noted that an oblate/prolate index analysis of this shape class indicated equal proportions of extremely flat and extremely long pieces as intended by the selection procedure (Section 5.1), so that TABULAR is a misnomer in the strict sense. Remarkably, the grading curves for FRESH and SEMI ROUND are so similar that they reproduce the same kinks. This must be taken as evidence of their common parent material and the negligible effect on gross shape of the 5 to 10% weight losses during abrasion.

The vigorous action inside the cement mixer appears to have resulted in some fracture breakage of the most irregular blocks after the long period of tumbling during the preparation of the VERY ROUND material. The gross shape of the VERY ROUND is approaching that of the EQUANT.

It should be noted that the EQUANT, for which $(X/Z)_{50}$ =1.79 rather than the FRESH shape class is more comparable with that used in the model armourstone studies of Van der Meer and Thompson & Shuttler. Also, note that just over 30% of

EQUANT pieces have an X/Z ratio greater than the value 2.0 often quoted in specifications.

5.2.3 Image Analysis Results

The methods outlined in Sections 2.3 and 2.4 were used to obtain values of shape descriptors from each subsample block. One 'maximum' and two 'random' projections were analysed to check repeatability. This gave three sets of results for each of the five subsamples containing 48 blocks.

A complete record of the results is given in Appendix 1 so that it may be used future research as a data base for aspects of shape analysis. In this appendix, the digitized outline coordinates for all the projections analysed have been plotted to allow direct correlation of individual outlines with their descriptor results. For further visual comparison, photographs showing 'maximum' projections of each shape class, as analysed, are included. Average values for all the most pertinent descriptors of gross shape, roughness and size have been tabulated for each projection of each subsample.

The 'maximum' projection results are largely of academic interest since most practical applications of the Fourier and Fractal shape analysis methods will involve random projection field data. The main objective of the image analysis was to reduce the results of the two 'random' projection analyses of 48 blocks and thereby, to obtain one descriptor value summarizing the gross shape and one summarizing the roughness or surface texture of that subsample, together with an idea of the dispersion or variability of these descriptors throughout the subsample.

Percentage exceedance curves for P_C are shown in Fig.5.4. Both random projection sets of each shape class are presented. EQUANT, VERY ROUND and TABULAR provided very similar (i.e. repeatable) curves for each projection set whereas FRESH and SEMI ROUND resulted in diverging curves in the region of the 30% highest P_C values. The symmetric S-shaped exceedance curves indicate that the distribution of P_C values is approximately normal for each shape class. The mean value of P_C is therefore a good statistic to use for each subsample. A comparison of Fig.5.4 with Fig.5.3 reveals that the gross shape descriptor P_C carries essentially the same information as the X/Z ratio.

Percentage exceedance curves for P_R are shown in Fig.5.5. Again, there is a divergence between the two random sets for both FRESH and SEMI ROUND. This indicates that the procedure for setting up random projections, even using a 48 block subsample, can introduce quite considerable variability into any average statistic used to quantify shape characteristics of that subsample. The more asymmetric S-shaped curves of Fig.5.5 compared to Fig.5.4 indicate that the P_R values are skewed towards

their lower end and that the practise recommended in previous work, of using the logarithmic average to represent an average statistic of the subsample, is justified.

Table 5.3 is a summary from Appendix A. The results from the two sets of random projections have been combined and the 15 , 50 and 85% exceedance values of P_C and P_R are given. The mean Fractal coefficients F and F_{40} (corrected to an image size of $S_i = 40$) and the size parameters S_i and D_i are included. Note that the roughness measured by F_{40} is tuned to a scale of 1.7 to 6mm on the armourstone.

Recall that F_{40} and P_R are both designed to measure roughness of the block outline. It is therefore interesting to point out that the relative differences in F_{40} between the three unabraded shape classes are smaller than those given by P_R and that FRESH, EQUANT, TABULAR is the order of descending F_{40} values whereas TABULAR, FRESH, EQUANT is the order for P_R. This could be explained by a greater occurence of long and relatively straight sides in the TABULAR blocks which would tend to keep the F_{40} value lower than for the FRESH, whereas P_R is partially reflecting the effects of extreme difference in gross shape. The Fractal coefficient F_{40}, therefore appears from these results to be a more shape independant measure of surface texture than P_R for the unabraded blocks. Coincidentially, the asperity roughness P_R appears to be roughly proportional to the product of P_C and F_{40}.

The size parameter D_i from image analysis (see Section 2.3.5) is the diameter of the circle with area equal to the video image. The effective Fourier diameter of a block D_{ef} is therefore given by multiplying by the video image scale factor f, which was set at 0.58mm per pixel. The typical values obtained for D_{ef} were nearer 70mm than the 60mm expected. The increase is partly due to the distribution effect noted in Section 2.4.2 of assuming the correct f to be that given by the magnification at the light table surface and not where the projected outline is. This tendency to overestimate the size will be least apparent for the most equant blocks. Precise size measurement from image analysis cannot be recommended without further research to successfully remove scale distortions.

5.3 Layer thickness and fictitious porosity

5.3.1 Flume tests

Since Figure 3.25a for P = 0.1 in Van der Meer (1988) shows $t(armour) = 2D_{n50}$, the assumption was made that by placing the stones in a double layer, an armour thickness of $2D_{n50}$ would be achieved; that Van der Meer had used the same; and that actual construction methods used in the field would be simulated. A two layer placement technique as described in SR150 was therefore adopted without the

realisation that Van der Meer, as well as Thompson & Shuttler had used t(armour) of $2D_{50}$ (i.e. twice the median sieve diameter).

The layer thicknesses were calculated using a computer program to compare th difference in armour layer and filter profile heights. In fact, as shown in Table 4.1, the layer thickness achieved in the flume tests were about 77mm or $1.6D_{n50}$, i.e. about 20% lower than expected and 35% lower than Van der Meers' tests. However, Thomsen et al (1982) found no difference in laboratory performance for thicknesses of 1.4 to $2.9D_{50}$ although the minimum of $1.5D_{50}$ is often specified (Thompson & Shuttler 1975). Ahrens (1975) found little effect of layer thicknesses between 1.5 and $2.0D_{50}$ and therefore comparisons of the results in this report with those of Van der Meer may still be valid even though t(armour) $\approx 1.3D_{50}$ in this study.

The problem of achieving a specified layer thickness was also illustrated in the CIRIA study of a field site in the Wash by Young et al (1976, Table 7a,b,c,d). It demonstrates the potential for overestimating layer thickness. The target was $2.0D_{50}$ but they only achieved from 1.1 to $1.9D_{50}$ on their field test panels. Contractors are often required to provide a minimum thickness or 'payline' and they often use the laye coefficient k_Δ to estimate the thickness given by, say a two layer thick armour. Value of k_Δ are given in the Shore Protection Manual but there is evidence to suggest that these can often be inaccurate (see Latham et al, 1988).

The VERY ROUND and SEMIROUND stone as expected gave the thinnest layers with the EQUANT giving the largest two layer thickness. The total weight of stone placed on the test section was known for each shape. The cross section area of armour includes a 1.7m sloping section and a 0.2m horizontal toe section. The armou layer volume was calculated from the average armour thickness times the 1.9m slope length times the 1.2m flume width. The as laid bulk density ρ_b was therefore given b the weight of stone placed divided by the armour layer volume. The fictitious porosity P_f, which is the void space expressed as a percentage of the armour layer volume is then obtained from the as laid bulk factor (ρ_b/ρ_a) where ρ_a is the density of the rock armour. Note, the fictitious porosity is determined for a given layer thickness or number of layers and is the bulk porosity. These values are also shown in Table 4.1 and illustrate the effect of rock shape on the way that the armour layers pack. The very low porosity of the VERY ROUND rock, 28%, was due to its more rounded shape. Porosity for the other four shape classes was typically about 37%.

Placement throughout the tests was random and without preferred orientation. Differences in construction methods between the various studies, such as placement technique, are discussed in Section 7.1.4 and SR150.

5.3.2 Static model tests

To investigate layer thickness, packing density, block shape and topographic roughness a series of static models were built using 'fresh' and 'rounded' aggregate on a 1:2 slope (to simulate the flume tests) with a sublayer of D_{n50} = 10mm. For most models, the sublayer, first and second layer were surveyed using 5 profile lines separated by Δx = 30mm. Both tight and loose placement were used for the fresh and round stones, with nominal diameters of 21.5 and 22.2mm respectively. Thus the effect of placement on layer thickness and porosity could be investigated.

Layer thickness and porosity were measured in the laboratory using a 500mm long static model profiler. The profiler dropped 500 vertical pins of width w_p = 0.8mm and separation Δy = 1.0mm onto the models' surface and the image of the pin heights was recorded with a video image processing system.

Table 5.3.2 (from Latham et al, 1988, Table 6) shows the geometric parameters for the static models, including one and two layer thickness, porosity and layer coefficient k_Δ, for fresh and round stone, and also for spheres, cubes and dolosse (for a comparison). For round stone, the two layer thickness achieved varied from $1.7D_{n50}$ for a loose pack to $2.4D_{n50}$ for a tight pack. For fresh stone, the two layer thickness achieved varied from $1.6D_{n50}$ for a loose pack to $2.2D_{n50}$ for a tight pack. The gross shape and roughness of the fresh and round stone used in the static models was similar to those of the FRESH and VERY ROUND stone used in the flume tests - as described by the Fourier shape factor P_C and the Fourier asperity roughness P_R (c.f. Tables 5.2 and 5.4). In the flume tests, the thickness for FRESH was $1.6\ D_{n50}$ and for VERY ROUND was $1.5D_{n50}$, suggesting identical loose packing was achieved for the FRESH and fresh models given that their fictitious porosity values were P_f = 39 and P_f = 40 respectively.

Note, Table 5.4 also shows the two layer thicknesses of 3 artificial units - cubes, spheres and dolosse - which were 2.0, 2.0 and $1.4D_{n50}$ respectively, and the fictitious porosities, which were 37.7, 35.7 and 49.3 respectively. The high porosity of the dolosse agrees well with other studies such as Zwamborn (1980).

Perhaps surprisingly, the fictitious porosity values for loose and tight packing were very close, but again, as in the flume tests, the porosity of the round stone (34%) was less than that of the fresh stone (40%).

The layer coefficient k_Δ is often used in practice to estimate the layer thickness t that will be achieved for a given stone size. The standard layer thickness formula can be written in terms of nominal diameter D_{n50} as

$$t = n\ k_\Delta\ D_{n50}$$

where n is the number of armour layers. The Shore Protection Manual gives values of layer coefficient k_Δ. Compared with the static model test results in Table 5.4, for all shapes with loose packing, the SPM overestimates the values of k_Δ by about 10 to 20%. This would cause a breakwater designer/contractor to underestimate his layer thickness (given a certain stone size), and maybe cause unnecessary and inefficient topping up of the armour in order to meet the target thickness or 'payline' given in the specification. For the tightly packed stone, k_Δ was 10 to 20% higher, showing the variations that are possible due to placement technique, particularily if the test material is not very equant.

The values of layer coefficient k_Δ for the five shape classes used in the flume study were calculated and compared with the values given in the SPM (see Table 5.4). For TABULAR, EQUANT, SEMIROUND, VERY ROUND and FRESH, k_Δ was 0.76, 0.85, 0.73, 0.76 and 0.80 - in other words about 75% of the SPM values, showing the danger of underestimating layer thickness with the generally accepted values of the layer coefficient given in the SPM. (It should be pointed out that the experimental methods of Hudson upon which the values of k_Δ in the SPM are based, for example placement and survey method, are not generally considered). Further research is required to establish a standard set of values of layer coefficient for use by the breakwater designer/contractor.

5.4 Topographic roughness parameters from 'along slope' profiles on static model

For individual particle roughness, the Fourier asperity roughness P_R and the Fractal value F are the most significant shape parameters in this discussion. However, the topographic roughness of the entire 'macro-surface' gives a measure of the geometric character of the entire 'as-built' armour layer. Topographic 'along slope' profiles were taken on the static models as described in Section 5.3.2. These were high resolution profiles, surveyed using a probe width w_p of less than $0.1D_{n50}$ (compared a probe width of $0.5D_{n50}$ in the flume tests), and the sampling interval was also high resolution relative to the flume tests. Thus, accurate calculation of the topographic roughness parameters (corrected to be normal to the slope) was possible and was reported in Latham et al (1988).

The Fourier asperity roughness P_R was 0.0128 for fresh and 0.0039 for round. The value for round is very low and indicates the smooth nature of, what are basically beach pebbles, with minimal surface texture. (These figures do however relate to maximum projection image analysis and are slightly lower than for random projections).

The measure of topographic roughness σ in Table 5.4 shows that a loose pack tends to give lower roughness and that the fresh models topography is 10% rougher than the round. Another roughness parameter R_a, similar tc σ, is the centre-line-average roughness and can be used to compare the roughness of different rock slope surfaces and therefore their resistance to flow over the armour. This together with a measure of permeability within the structure could allow for a more accurate determination of wave energy and dissipation of wave energy generally. The permeability depends on the armour/filter/core configuration and the armour layer porosity, but there is no simple method available for estimating it apart from the figure (Fig.3.25) and the discussion given by Van der Meer in his thesis and 'engineering judgement'.

5.5 Downslope profiling in the flume tests

The test section was profiled before and after each test using a computer driven bed profiler developed at Hydraulics Research Ltd. specially for this flume study. Full details of the profiler operations are given in SR150. The profiler was mounted above the flume on a traversing beam which could be moved to relocateable positions across the width of the flume. The profiler probe had a touch sensitive switch fitted with a hemispherical foot of size 0.5 D_{n50} and was used to record levels along ten parallel survey lines, each 0.1m apart, down the slope of the test section. Each profile consisted of 67 points taken along the survey line at an interval of 0.03m. For a more detailed discussion of the importance of probe width, sampling interval and profiling techniques, see Latham et al (1988).

Downslope profiles of the armour layer were used to estimate layer thicknesses (see Section 5.4.1), erosion damage areas or volumes (see Section 6) and to examine a few low resolution topographic roughness descriptors.

Ten profiles from the flume tests were used to calculate the centre-line-average roughness R_a, for each shape (for one particular wave condition, H_s = 120mm, T_z = 1.4secs) at 0, 1000 and 3000 waves. Table 5.5 shows these values with the corresponding values of damage S for just these few tests. The trend was for roughness R_a to increase with damage S. This is to be expected since the definition of R_a has similarities with erosion area A_e when considering such low resolution profile data. It is interesting to note however, that for 0 waves, when the overall profile is expected to be straight, that VERY ROUND and TABULAR give lowest R_a values while tending to give very different damage values S. It is tempting to speculate that TABULAR may have a combination of higher stability but with higher runup also.

Note that the EQUANT topography is about 50% rougher than VERY ROUND. The effects of roughness on runup unfortunately could not be measured in these flume tests.

5.6 Shape of Van der Meer's test material

Four subsamples considered to be representative of the model materials which had been used in Van der Meer's (1988) experimental study of static stability were the subject of shape analysis using the imaging techniques already described in Section 2. Supplementary information given by Delft Hydraulics relating to each subsample was as follows :

DH1 - Broken brick, after 10 tests, not painted, Krumbein roundness = 0.43, $(X/Z)_{50}$ = 1.77, $(X/Z)_{15}$ = 1.46, $(X/Z)_{85}$ = 2.24

DH2 - Uniform stones, after 41 tests, not painted, Krumbein roundness = 0.52

DH3 - Uniform stones, after 106 tests, painted once, Krumbein roundess = 0.41, $(X/Z)_{50}$ = 1.76, $(X/Z)_{15}$ = 1.43, $(X/Z)_{85}$ = 2.00

DH4 - Riprap, after 134 tests, painted twice, Krumbein roundness = 0.50, $(X/Z)_{50}$ = 1.76, $(X/Z)_{15}$ = 1.39, $(X/Z)_{85}$ = 2.13

The uniform stones and riprap were called normal stone having a relative mass density Δ of 1.62, while for brick , Δ = 0.92. A subsample of crushed basalt was unavailable. An early observation upon seeing DH2 and DH3 was that perhaps as many as 50% of the normal stones appeared to have been prepared from the crushed products of quite smooth slightly larger boulders. At the start of the test programme, many pieces of model armour may have had smooth surfaces over up to half their surface areas. (This is the probable explanation for the different nominal diameter/sieve diameter ratios reported by Van der Meer (D_{n50}/D_{50} = 0.90) and that by Thompson & Shuttler (D_{n50}/D_{50} = 0.82)). It was therefore anticipated that roughness descriptors P_R and F would be lower for the Delft Hydraulics normal stones than in the samples tested at Hydraulics Research as reported by Thompson & Shuttler and the present study, reported in Section 5.3.3.

Each subsample consisted of 48 blocks and was subjected to only one random projection examination. As all subsamples were known to be relatively equant, further random projection analyses were considered unlikely to yield significantly different average descriptor values. Because of the wider grading in the riprap subsample, the

video camera magnification was set such that the smallest projected outlines still gave an image size of $S_i > 35$ pixels which is sufficient to ensure no size effects on the Fourier descriptors. For all subsamples, the same setting of f = 0.36 mm was used.

The digitized outlines and details of the average descriptor results of the shape analysis are given in Appendix B. The Delft Hydraulics subsample results have been presented in Table 5.6 in the same form as Table 5.1 for direct comparison. The P_C values confirm the X/Z supplementary details which indicate the equant character of all the Delft Hydraulics subsamples, and how remarkably similar they all are to EQUANT and to a lesser degree, to VERY ROUND, in terms of gross shape. The asperity roughness P_R shows a range of values from 0.0115 for DH1 to 0.0085 for DH4, representing a significant difference between broken brick and riprap. The uniform stones after 41 tests and after 106 tests show a decrease from $P_R = 0.0107$ to 0.0093 as might be expected if abrasive wear is occuring during testing and handling of the stones. The differences in F_{40} values for brick (DH1), and normal stones after 41 tests (DH2), also suggest that differences in roughness or surface texture are present (at the scale of 1 to 3.5mm, to which the Fractal parameter is tuned - see Section 2.2.3)

The results taken as a whole indicate that only the brick (DH1) closely resembles the gross shape, roughness and surface texture of the EQUANT material. Although the SEMIROUND material is not as equant as the DH2, DH3, and DH4 material, it seems reasonable to generalize and suggest that the normal stone throughout the Delft Hydraulics test programme would have exhibited about the same degree of roughness (expressed by P_R) as the SEMIROUND material. Notice that the Krumbein roundness values give no meaningful relationship or trend and may be ignored.

5.7 Summary

The preparation of the five shape classes was successful in the light of the wide range of gross shape and surface texture parameters that were associated with them. The image analysis techniques were applied very effectively to the armourstone used in this flume study and also to that used by Van der Meer. Although the Fourier shape contribution factor P_C values were similar to direct axial X/Z ratios from hand measurements, the important textural differences between the shape classes could only be measured objectively using the new imaging techniques. Krumbein roundness is not a satisfactory measure of texture or roughness for this study.

The Fourier asperity roughness P_R for the five shape classes are given in Table 5.3. The VERY ROUND has the lowest value (0.0046) having lost nearly all of its surface texture during the mechanical rounding process, and the SEMIROUND also has a lower than average value (0.0097). The low value of EQUANT compared to

FRESH (0.0138) or TABULAR (0.0165) is due to its compact shape. Clearly, P_R does not reflect surface texture alone and it will increase if the gross shape is increased. In contrast, the Fractal coefficient F_{40} is a more shape independant measure of surfac texture than P_R.

The material used by Van der Meer in his model tests was generally more equant (lower X/Z) than all shape classes tested in this study except EQUANT itself. This broken brick armour material strongly resembled the shape and texture of the EQUANT stones according to the image analysis descriptors P_C, P_R, and F. His tes material used most often to develop the design formulae probably had values of P_R more closely approximated by the SEMIROUND stones, because they were generally quite a bit more rounded than typical angular equant stones.

For each shape class, the thickness of the double layer was considerably less than twice the sieve diameter (as used in Van der Meer's study) and typically 20% lower than expected if a layer coefficient of $k_\Delta = 1.0$ is assumed. Using the same placement guidelines for each shape class, the layer thicknesses were slightly differen for each shape class, the most extreme being $t(EQUANT) = 1.7D_{n50}$ and $t(SEMIROUND) = 1.45D_{n50}$.

The effects of different packing/placement methods were examined in a series of separate static bench-top tests and it was noted that fictitious porosity P_f did not chang significantly when a tight pack was compared with a loose pack for both a very round batch and an angular/fresh batch of stones. For EQUANT material with parallel faces it is perhaps more likely that P_f could be reduced using careful tight packing but this would require further investigation. The layer thicknesses and thus armour placed pe unit area of slope varied greatly for the loose and tight packing. Layer thickness and therefore k_Δ depends mainly on gross shape and placement technique. Fictitious porosity P_f, however, may depend not so much on placement technique but on gross shape and surface texture and appears to show a correlation with the asperity roughness P_R in the flume and static models. The much lower P_f for the VERY ROUND (28%) compared with FRESH (39%) is a significant reduction in void space available for wave energy dissipation.

Although further research on the relationships between shape, layer thicknesses, fictitious porosity and placement methods is required before new recommendations can be given to the engineer, there is a pattern emerging with the new shape descriptors (see Table 5.7).

It is unfortunate that high resolution topographic profile data could not be measured for the flume models and that runup results were not available. The topographic roughness from the static models suggests that the profile roughness R_a

would be about 10% rougher for FRESH than for VERY ROUND even though their stone sizes are the same.

6. TEST RESULTS

6.1 Qualitative description of armour behaviour

Many obsevations relating to armourstone movements during testing were discussed in SR150. In order to create an eroded area A_e on the 1:2 slope, all shape choices indicated that armour is first dislodged or rocked during wave impact or upsurging and is then removed entirely from its previous position by rolling up or down over its lower neighbour during downrush. The rolling seems to be easiest for the very rounded and more equant stones and once they start rolling, they appear to roll further down the slope before coming to rest. It is probably unwise to make further generalisations unless they can be verified on video film. Future studies could benefit from video filming taken specifically to examine mechanisms of plucking out, rolling and mass movement of armour since block shape appears to play a role which is at present difficult to describe. It is tempting to suggest that the TABULAR material owes its greater stability noted in these tests to its resistance to rolling.

6.2 Calculation of damage

To calculate the damage caused to the test section by a given wave condition, profiles were taken. The mean slope profiles before and after wave action were differenced and the eroded area A_e used to calculate the dimensionless damage as follows

$$S = A_e/D_{n50}^2$$

This dimensionless damage number relates damage to the equivalent number of square sided stones of nominal diameter D_{n50} fitting into the eroded area. Broderick (1984) was the first to define the damage parameter S and it was used by Van der Meer to describe damage in his experimental programme. It is a simple and effective measure of damage and Table 6.1 presents the damage S after 1000 and 3000 waves for all tests.

An alternative damage parameter N_Δ was defined by Thomson & Shuttler (1975) as "the number of D_{50} sized spherical stones eroded from a 9 D_{50} width of slope which was obtained by dividing the product of the bulk density ρ_b, and the

eroded volume by the size of a spherical stone". This damage parameter estimates the actual number of displaced stones and is given by

$$N_\Delta = A_e \ \rho_b \ 9D_{50}/(\rho_a \ D_{n50}^3 \ \pi/6)$$

where

N_Δ = damage parameter

A_e = erosion area in a cross-section

ρ_b = bulk density of material as laid on the slope

D_{50} = diameter of stone which exceeds the 50% value of the sieve curve

ρ_a = mass density of the armour

The fictitious porosity $P_f = 100(1-\rho_b/\rho_a)$ varies for each shape class and is significantly lower for the VERY ROUND stone (see Table 4.1). Therefore, N_Δ would give a much higher relative damage than S for this shape class than for the others. The fact that the sieve diameters may also differ for each shape class would tend to further increase N_Δ for the more rounded and equant shape classes.

In contrast, the bulk density or fictitious porosity can be difficult to measure in the prototype and the nominal diameter is more convenient than the sieve diameter, particularily in an investigation of shape effects where it is important to separate size from shape. Therefore, all damage calculations were presented in terms of S, or else the dimensionless damage $S/\sqrt{N}$ where N is the number of waves.

Van der Meer (personal communication) also pointed out that a measure of damage should ideally reflect the forces resisting block removal. Since it is easier to remove an area A_e containing light rather than dense rocks, a damage parameter equal to $A_e/(\Delta D_{n50})^2$ might be better for future studies.

In the flume tests, the mass density and the sieve diameter are approximately constant and the bulk density depends on the porosity. Thus N_Δ is a function of the damage area and the porosity of the armour layer. The fictitious porosity $P_f = 100(1-(\rho_b/\rho_a))$ varies for each shape class, and is significantly lower for the VERY ROUND stone (see Table 4.1). The eroded area A_e and thus the damage S may be the same but N_Δ will be higher for the VERY ROUND stone. The damage N_Δ reflects the actual number of stones moved rather than the number of cubes that could occupy the eroded area.

In the report SR150, it was noted that the erosion area A_e could be calculated from the 10 downslope profile lines in two ways leading to two different results. The area A_e can be calculated independantly for each profile and then all 10 values are averaged to give one value of damage S_{md} for the whole test section. Alternatively, the area A_e and S, as used in this report and by Van der Meer, is based on the mean profile calculated by taking the mean height at each chainage point from a datum using a number of profiles. In SR150, the damage S_{md} appeared to give generally higher values than S.

Table 6.1 gives all the damage values S at 1000 and 3000 waves for each wave condition and shape class tested. In column 1 of Table 6.1, the first letter indicates the shape class, the second letter the wave condition, the third is for repeat tests. Plots of $S/\sqrt{N}$ against $H_s/\Delta D_{n50}$ are presented in SR150. In this report, the results have been presented (Section 7) in the form that most clearly shows their relationship to Van der Meer's equations.

7. ANALYSIS OF TEST RESULTS

7.1 Comparison of flume results with Van der Meer's stability equations

7.1.1 Choice of stability equation - discussion

Five different wave conditions were used in the flume. Generalizing for random waves, the surf similarity parameter ξ_m describes whether and how the waves will break. Below a critical value, plunging waves of high wave steepness break on the structure. Above this critical value, surging waves of low wave steepness surge up and down the slope of the structure. The transition, which is usually the most dangerous condition for stability is associated with collapsing waves and typically lies between $\xi_m = 2.5$ and 4.0. Because stability behaviour is quite different for surging and plunging waves, Van der Meer derived one equation for each wave condition. The equations intersect at a certain value of ξ_m given by:

$$\xi_m = (6.2\ P^{0.31}\ \sqrt{\tan\alpha})^{1/(P+0.5)}$$

The intersection point value of ξ_m depends on the permeability coefficient and the slope, and indicates the most dangerous conditions for stability. The above empirical equation was not discussed by Van der Meer. It does however strongly suggests that the permeability of the core will have an important effect on the phenomenon described as resonance by Bruun & Gunbak (1978). It is outside the scope of this report to consider mechanisms causing instability but it seems reasonable to speculate that the role of the constant with value 6.2 in the above expression should be one that is able to reflect the resistance to runup and rundown caused by the topographic roughness of the armour profile. This topographic roughness would have been relatively constant in Van der Meer's tests but was found to vary for the rounded and fresh block shapes measured on static models (see Section 5.4) and is likely, together with permeability and slope, to have some influence on the value of ξ_m for which resonance occurs. It should be noted that the value 6.2 in the above expression is derived by dividing the plunging equation constant 6.2 by the surging wave constant which was 1.0. Should these constants be found to be shape dependant variables, then so too is the intersection point value of ξ_m.

To find which equations to use, the available guidelines in Van der Meer (1988) implied that P = 0.1 was the lowest possible and therefore the best estimate. Substituting P = 0.1, tan α = 0.5 in the above equation gives ξ_m = 3.57. The wave conditions for each test were taken to be:

Test type	H_s	T_m	ξ_m	Av. wave condition	Steepness s_m
A	50	1.4	3.91	Surging	0.016
B	90	1.4	2.92	Plunging	0.029
C	120	1.4	2.53	Plunging	0.039
D	160	1.4	2.19	Plunging	0.052
E	90	2.0	4.17	Surging	0.014

Note that the test programme only considered a narrow range of ξ_m around the critical value but did have a good range of wave steepness. Therefore, results do cover the intended range of applicability of Van der Meer's two equations, although limited to five test types.

7.1.2 Plunging wave condition

Van der Meer's plunging wave equation was written as :

$$H_s/\Delta D_{n50} * \sqrt{\xi_m} = 6.2\ P^{0.18}\ (S/\sqrt{N})^{0.2}$$

It was confirmed in SR150 that the term $S/\sqrt{N}$ described accurately the increasing damage with number of waves for all the shapes tested. The exponents 0.2 and 0.18 were well established in Van der Meer's original programme of tests. To compare the damage results of Table 6.1 with predictions based on Van der Meer's plunging equation, the decision was taken to use linear regression and so to plot $(S/\sqrt{N})^{0.2}$ as the dependant variable against $H_s/\Delta D_{n50} * P^{-0.18} * \sqrt{\xi_m}$ (given the symbols S* and H* in Figs. 7.1 to 7.7). This is similar to Van der Meer's Fig. 3.27 except he has plotted $S/\sqrt{N}$ instead of $(S/\sqrt{N})^{0.2}$.

This approach, assumes the nonlinear form of Van der Meer's equation to be the best model for describing the new results. It is the simplest way of analysing the influence of armourstone shape and of comparing results with those of Van der Meer but the assumptions of this approach, discussed later, should not be overlooked. For convenience, the constant which had a value 6.2 will be given the symbol C_{pl} as for this study it will become the parameter describing the shape effect for plunging waves.

A linear least squares regression analysis was performed. Care was taken to ensure that each test contributed evenly weighted data so that if both 1000 and 3000 wave damage levels were to be included, sometimes an estimate of S was used if failure with filter exposure had occurred early. The slope of the regression line gives $1/C_{pl}$ which for Van der Meer's test results (approx. 600 points) would, it can be assumed, have given 1/6.2. The curve fitting model requires that the regression line should cut the origin and therefore the correlation coefficients for regression seem unusually high and the standard errors surprisingly low because of the narrow range of H* values. Treating C_{pl} as a stochastic variable, assuming a normal distribution, with a standard deviation given by the standard error, the 90% confidence levels for the expected value of the slope may be plotted in the same manner used in Van der Meer's thesis but here they are diverging straight lines rather than diverging curves. (Note that with such few data a t-distribution should have been used. This would have given slightly more widely diverging 90% confidence limits. Also, that the 90% confidence intervals for a prediction of each point (a reflection of scatter) would be wider apart and roughly parallel to the regression line). The plunging wave results are presented in this form in Figs.7.1 to 7.6 and the coefficients from regression ranging from 5.93 to 5.31 are as given below :

Plunging wave formula, assuming permeability coeff. P = 0.1

Shape	Coeff. C_{pl}	Standard error
Tabular	5.93	0.09
Equant	5.64	0.25
Fresh	5.39	0.24
Semiround	5.39	0.14
Very round	5.31	0.14
All	5.46	0.10
(Van der Meer	6.20	0.40)

These differences in C_{pl} are shown in Fig.7.7, for comparison with Van der Meer's value of 6.20. The TABULAR and VERY ROUND showed greatest and least stability. Comparing EQUANT and VERY ROUND rock shows the damage S to be $(5.64/5.31)^5 = 1.35$ times greater for VERY ROUND. The damage is 1.75 times greater for VERY ROUND than for TABULAR.

The scatter of the damage results for each shape class can be a consequence of (a) differences arising from the random behaviour of the rock slopes' geometric characteristics, (b) accuracy of measuring damage, (c) curve fitting to the Van der Meer model, (d) differences in test facilities (slope 1:52, etc.). Note that because of the thinner armour layer than in Van der Meer's tests, the filter layer became visible at lower values of S and therefore damage measurement was reliable over a relatively smaller range of S values. Van der Meer's statistic for the standard deviation value of 0.4 for the C_{pl} constant 6.2 is apparently the same as the standard error statistics given above. Since these errors are not greater than those for the other two studies, the results for C_{pl} invite a comparison with the value 6.2 for Van der Meer and Thompson & Shuttler's combined data, which probably owes its larger error to their much wider range of test conditions (eg. $\tan\alpha$, H_s, T_m, P).

Overall, the results shown here clearly indicate more damage than predicted by Van der Meer's equation, assuming that P = 0.1 correctly represents the permeability in the tests. There is a shape effect on stability, but it is not as significant as the results suggest for the surging wave condition - dealt with next.

7.1.3 Surging wave condition

Van der Meer's surging wave equation is as follows :

$$H_s/\Delta D_{n50} = 1.0\ P^{-0.13}\ (S/\sqrt{N})^{0.2} * \sqrt{\cot \alpha} * \xi_m{}^P$$

Following the same approach used in the previous section, the dependant variable $(S/\sqrt{N})^{0.2}$ was plotted against $H_s/\Delta D_{n50} * \xi_m{}^{-P} * P^{0.13} * \sqrt{\tan \alpha}$ (given the symbols S* and H** in the Figures). For surging conditions, the coefficient was given the symbol C_{su}. The regression line slope ($= 1/C_{su}$) for all the shape classes except FRESH (not enough data) are shown in Figs 7.8 to 7.11 and the values of C_{su} are as given below :

Surging wave formula, assuming permeability coeff. P = 0.1

Shape	Coeff. C_{su}	Standard error
Tabular	1.32	0.21
Equant	1.19	0.15
Semiround	1.10	0.07
Very round	0.95	0.06
All (incl. fresh)	1.10	0.06
(Van der Meer	1.00	0.08)

Although the data for this type of analysis are far from satisfactory (even fewer data than for plunging), the shape effect suggested by the regression analysis is clearly more significant than for plunging waves. For example, the relative stability comparing EQUANT and VERY ROUND shows the damage S to be $(1.19/0.95)^5 = 3.1$ times greater for

VERY ROUND. Compared with TABULAR, the VERY ROUND damage is 5.3 times greater.

The differences in values of C_{su} are compared in Fig.7.13 with the value of 1.0. They indicate that all classes except VERY ROUND show greater stability than Van der Meer's equation predicts.

7.1.4 Validity of a comparison with Van der Meer's equations

There were a number of differences between the Van der Meer and Thomson & Shuttler test conditions and those in this study. They stem from the fact that it is inappropriate to work with sieve sizes (particularily for making dimensionless parameters) when it is a shape effect that is under investigation. The important differences were

(i) Armour thickness : The armour in this study was laid as a double layer giving t(armour) ≈ $1.3D_{50}$. Probably three layers would have been required to produce t(armour) = $2D_{50}$ as used in the other studies. Note that because D_{50} varies considerably for each of the five shape classes, the armour layers would have required different thicknesses to achieve the specified t(armour) = $2D_{50}$ for each shape class. Alternatively, the average D_{50} given by EQUANT stone could have been used to set the armour thicknesses (see also Section 5.3.1).

(ii) Filter size and thickness : The filter thickness t(filter) ≈ $0.43D_{50}$ instead of $0.5D_{50}$ and filter size ratio D_{50}(armour)/D_{50}(filter) for EQUANT was about 5.4 instead of 4.5 (see section 5.1.4).

(iii) Placement technique : The blocks were placed individually by hand without preferred orientation in a manner intended to simulate prototype construction of a double layer from a grab. The construction method was discussed at length in SR150 where it was recognized that both shape and placement technique were likely to influence interlock. The 'tipping' placement technique used in other studies is more relevant to riprap construction. In retrospect, it may have been preferable to have adopted the same tipping technique as the effect of different construction techniques between studies is very difficult to evaluate. One way might have

been to compare the bulk factor (ρ_b/ρ_a) of the shape class of this study that most closely resembles Van der Meer's tests (EQUANT or SEMIROUND), with that for his uniform stones, but the data was not available and the bulk factor does not account for all the differences in placement method (see Section 5.3.2).

Other slight differences were in the profiling definition and its relation to damage definition. This was determined in SR150 and was considered not very significant. Also, Thompson & Shuttler's 'bedding in' of 1000 waves was apparently taken by Van der Meer to be insignificant.

The main problem raised by (i) and (ii) above is the uncertainty that it places on the validity of the P = 0.1 assumption for this study. Both (i) and (ii) would indicate a lower value of P is appropriate. Van der Meer (personal communication) suggested a value of 0.07 to 0.05, but this is only an estimate.

One consequence of changing the value of P is that this changes the value of ξ_m for which the plunging and surging equations intersect. Near the intersection value of ξ_m, the two equations give very close values of $H_s/\Delta D_{n50}$ for the same damage level. However, it is possible that data from say test type B could shift into the surging regime as the intersection value of ξ_m drops from 3.73 to below 2.92 (see Section 7.1.1) and the data regression analysis results might then be different. Substituting a value of P = 0.05, the regression analysis results for C_{pl} would tend to increase by a factor of about $(0.1/0.05)^{0.18} = 1.13$ which would bring an average value of 5.5 up to 6.2, as predicted by Van der Meer. For C_{su}, such an adjustment is more complex. A complete analysis with P = 0.05 was therefore repeated for both wave conditions.

Substituting P = 0.05 into the equation given in Section 7.1.1 gives the intersection value $\xi_m = 2.71$ so that test type B results should be included with the surging wave data and not with the plunging wave data.

The regression analysis results were as follows :

Plunging wave formula assuming permeability coeff. P = 0.05

Shape	Coeff. C_{pl}	Standard error
Tabular	6.76	0.12

Fresh	6.68	0.23
Equant	6.59	0.35
Semiround	6.14	0.20
Very round	6.03	0.11
All	6.39	0.10
(Van der Meer	6.20	0.40)

Surging wave formula assuming permeability coeff. P = 0.05

Shape	Coeff. C_{su}	Standard error
Tabular	1.00	0.09
Fresh	0.84	0.05
Equant	0.88	0.07
Semiround	0.86	0.04
Very round	0.81	0.05
All	0.93	0.03
(Van der Meer	1.00	0.08)

The relative effects are essentially the same as found for P = 0.1. However, assuming permeability conditions in the tests were best described by P = 0.05, then for the plunging condition, results generally show slightly greater stability than for Van der Meers equation while for the surging condition, results show much lower stability than predicted by his equation.

7.2 Synthesis of Van der Meer's shape data with the flume test results

Throughout Section 7.1, the approach followed has been based on the assumption that shape and texture of the armourstone is independant of all the variables appearing in Van der Meer's design formulae. Unfortunately the permeability may depend to some extent on shape of the armourstone, particularily

since the fictitious porosity was noticeably lower for VERY ROUND rock. Expressed in terms of P, which reflects the whole core/filter/armour configuration, the differences in permeability due to armour shape could be quite insignificant for most structures except perhaps for those with an impermeable core.

Supposing that shape of armour does not affect the permeability coefficient P, it is still possible that a pronounced shape effect on stability could occur at low permeabilities of around P = 0.1 but which may not be significant or could have a different trend altogether (in terms of C_{pl} and C_{su}) for structures with a permeable core and a P value of about 0.5. In this case C_{pl} and C_{su} would not be ideal parameters to quantify the armour shape effect on stability because they would not be independant of P. Further tests could investigate the shape effects at higher core permeabilities, but until further results are available, the tentative conclusions accounting for shape effects in Van der Meer's equations will only apply to so called impermeable structures ($P \approx 0.1$).

It might be suggested that to keep the design formulae as simple as possible, the coefficient P could be redefined to accomodate the shape effect on permeablity and that the constant values 6.2 and 1.0 in the formulae would continue to give sufficient accuracy. The argument against this suggestion is that the engineer will have more difficulty and uncertainty in selecting the appropriate P value for the structure. More fundamentally, the effect of armourstone shape on stability is a combination of its effect on interlock and resistance to rolling with its effect on the void ratio, so that P alone cannot do the job of describing the armour shape effect.

One further possibility worth investigating is to introduce a shape effect correction to the slope of the structures since a reduction in surface texture appears to have the same effect as increasing the slope.

The asperity roughness P_R was chosen as the shape parameter most likely to correlate with the different coefficients derived from the regression analysis of Section 7.1.2 and 7.1.3. In Fig.7.14, the coefficients C_{pl} and C_{su} calculated assuming P = 0.1 have been plotted against P_R , together with the shape analysis results DH1, DH2, DH3 and DH4 for the Van der Meer material. The plot was interpreted as follows :

(i) With the exception of the FRESH rock, as P_R increases, the coefficients C_{pl} and C_{su} also increase.

(ii) For surging wave conditions, the relationship is approximately linear ($C_{su}/P_R \approx 30$ by eye).

(iii) For plunging wave conditions, the relationship is less certain and may not be as linear. ($C_{pl}/P_R \approx 50$ by eye).

(iv) Taking SEMIROUND as the shape class most similar to DH2, DH3 and DH4 (for which the values $C_{su} = 1.0$ and $C_{pl} = 6.2$ were obtained), C_{su} is 1.1 times higher in this study than predicted and C_{pl} is lower than predicted by a factor of 0.9. If $P = 0.1$ was correct for conditions in these tests, then the damage S was 60% greater and 60% less than that predicted by the plunging and the surging equations.

(v) Comparing DH4(riprap) with DH2(normal stones after 41 tests) assuming (ii) and (iii) above gives a 30% lower damage for DH2 than DH4 under surging waves and a 9% lower damage under plunging waves. This fits in well with the damage differences observed by Van der Meer which he considered might be due to rounding effects (see Section 3).

(vi) Comparing DH1(brick) with DH2, a small difference in roughness as given by P_R, assuming (ii) above, gives a 12% lower damage for brick under surging waves. Compared with DH3, there is a 30% lower damage for brick. This helps to explain Van der Meers observations giving greater stability for brick than normal stones (see Section 3).

(vii) The intersection point value of ξ_m between the plunging and surging equations is also a function of C_{pl}/C_{su} which is different for different shapes : TABULAR ≈ 4.5 , EQUANT ≈ 4.9 , VERY ROUND ≈ 5.6 (for $P = 0.1$).

(viii) Some of the variability in Van der Meers damage data will be due to combining results from Thompson & Shuttler, which most likely used material with P_R values similar to EQUANT (i.e., 0.0115), with his own results which includes P_R ranging from 0.0085 to 0.0115. Note that in Van der Meer's Figure 3.28

(1988) for surging waves, Thompson & Shuttlers damage results generally fall below his own test results.

(ix) If damage were to have been measured using N_Δ rather than S, because N_Δ gives a measure of the actual number of stones displaced, the much lower fictitious porosity for VERY ROUND compared with the other shape classes is also important. It would imply an even greater removal of mass from the slope for VERY ROUND than is implied by comparing S values for the different shapes.

Fig.7.15 is an alternative plot to Fig.7.14 where the coefficients C_{pl} and C_{su} were recalculated assuming P = 0.05 (tabulated in Section 7.1.4), the equivalent interpretations to those given above in (ii), (iii), (iv) and (vii) are that $C_{su}/P_R \approx 10$, $C_{pl}/P_R \approx 60$ and that C_{su} is lower (i.e lower stability) by a factor 0.85 and C_{pl} is about the same or just higher than the values predicted by Van der Meer and that C_{pl}/C_{su} for TABULAR ≈ 6.8 and for VERY ROUND ≈ 7.4.

Clearly, it would be possible to 'fine tune' the value of P to give the best correspondence between the model test results and Van der Meer's equations. Such a P value surely lies between 0.1 and 0.05. There will always be some doubt about the value of P in models and full scale structures. However, it is reasonable to suppose that engineers, given appropriate guidelines (see Van der Meer's discussion, Section 3.5.3, 1988), could estimate P quite precisely, just as in these model tests, an initial estimate of P = 0.07 could have been made upon examining the test section conditions and comparing them with those of Van der Meer's tests.

Given an accurate estimate of P and knowing the shape characteristics of Van der Meer's test material, it is reassuring to find such a high degree of compatibility with his predictions. That the asperity roughness P_R can apparently be used to compute an estimate of the effect of armourstone shape on stability may prove extremely useful. For example, assuming that Van der Meer's formulae are based on model material with average P_R values of 0.010, the shape effects observed in this study (see Figs. 7.14 & 7.15) for an impermeable core structure can be summarized as :

$C_{su} = 0.8+20P_R$ for the surging condition

$C_{pl} = 5.6+60P_R$ for the plunging condition

It can be argued that until the shape effects suggested in this discussion are substantiated with further test results, that (i) the scanty and scattered data do not warrant such detailed analysis as presented in this report and that (ii) the armour shape effect on stability suggested by the above relations is insignificant compared with the other variables and the uncertainty in predicting H_s for a given site.

Nonetheless, the above relations, perhaps with minor modifications in future, do appear to account for the complex effect of block shape in a surprisingly simple systematic manner (with the possible exception of the FRESH rock). The effect is most pronounced for the surging condition which suggests a 55% greater damage for EQUANT than for TABULAR material and a 100% greater damage for VERY ROUND than for EQUANT.

8. MEASUREMENTS OF PROTOTYPE ROUNDING AND WEIGHT LOSS

8.1 Large scale testing and field observations of 'New Bern' limestone from North Carolina, (Allison & Savage, 1976)

Allison & Savage (1976) tested a breakwater section armoured with 100 to 200kg 'New Bern' limestone from North Carolina. After 14 tests with an average of about 750 waves each inflicting about 5 to 10% 'erosion damage', weight losses just above and below the still water level were 10.4 and 7.9% with an average for all armourstones of 5.5%. Typically for this shelly limestone, the wet specific gravity was 2.0g/cm^3 and water absorption after 24 hours between 2 and 6%, which gives an indication of its poor durability.

Armourstone of the same 100 to 200kg size range of 'New Bern' limestone were, in the same study, the subject of a field investigation in which 13 blocks were placed among larger armourstones on a jetty in Fort Macon, North Carolina. The stones were periodically removed, weighed and replaced for about 18 months. They concluded that abrasion and to a lesser extent solution of solids contributed significantly to the loss of weight in these rocks. The weight loss within 0.5 years was on average about 18% for blocks of about 150kg (D_{n50} = 0.42m). On the basis of the volume to surface area relationship (see section 8.2), the same 18% weight loss for a block weighing 8 tonnes would take just under 2 years!

8.1 Theoretical considerations using field observations of Portland Limestone from West Bay, Dorset (Clark, 1988)

Clark (1988) described an experiment, set up in 1983, to monitor the loss of material from 4 blocks of Portlandstone armour each one weighing about 10 to 15 tonnes. The 4 blocks were selected to represent different lithology and working environment. Material losses were measured by profiling the rock surface between two permanent phospho-

bronze reference pins at two-monthly intervals from February 1983 to March 1984.

Block A, from the area suffering the most severe wave attack and attrition from shingle was subject to considerable but not untypical storm wave conditions during the winter of 1984. Blocks B and C were less exposed than Block A. Block D consisted of slightly more durable lithology but was exposed to severe conditions, comparable perhaps to those of Block A.

From the profiles presented in the reference, the material losses normal to the surface over a 1.25 metre length, for the 13 month period, were calculated to be A : 25mm, B : 6mm, C : 1-2mm, D : 5mm.

To illuminate these observations by converting to fractional weight loss estimates, it is necessary to make several assumptions. Assume first that block A is a 15 tonne cube of specific gravity 2.5 tonnes/m^3. Assume now that (a) one face (b) two faces (c) six faces are attacked at 25mm per year. After one year the block which was originally of D_{n50} = 1.82m loses (a) 0.207 tonnes, $W/W_0 = 0.986$ (b) 0.413 tonnes, $W/W_0 = 0.972$ (c) 1.205 tonnes, $W/W_0 = 0.9197$. If the block were a sphere weighing 15 tonnes and therefore of diameter 2.25m and it lost an outer shell of thickness 0.25mm in one year, then another weight loss estimate (d) gives $W/W_0 = 0.935$. A value between condition (a) and (b) giving $W/W_0 = 0.98$ (i.e. total losses equal to 1.5 times the losses from the most exposed face) seems a reasonable guess for block A which at 15 tonnes is unlikely to lose weight from rocking or any other mechanisms apart from attrition. (Apparently, block A toppled over in 1985). These theoretical abrasion conditions are plotted in Fig.8.1.

It should be noted that if the rate of removal of material is essentially governed by the surface area of the block, then for two blocks of equal shape but different size (equivalent diameter), the two values of W/W_0 are in inverse proportion with their initial sizes. For example, if the cubic block was 2.5 tonnes (D_{n50} = 1.0m) for condition (a) after one year it loses 0.062 tonnes and $W/W_0 = 0.975$. For (b) $W/W_0 = 0.950$. It is well known that for surface degradation, smaller bocks of the same shape lose weight faster, relative to their initial weights, than larger blocks

precisely because of the surface area to volume relationship which is simple to calculate (see Fig.8.1)

The more complex relationships between shape change together with size reduction and weight fraction were considered at length in Latham & Poole (1988). Because corners and asperities present on new blocks are more easily removed, W/W_0 falls more rapidly at first. It is therefore interesting to consider these relationships since available laboratory data on the abrasion resistance of Portlandstone can be used to put some limit on the calibration factors needed to correlate laboratory abrasion rates with prototype rates. Also it is possible to compute rates of rounding given laboratory data on weight loss.

In Fig.8.1 and Table 8.1, the data for the laboratory mill abrasion of Portlandstone with dry density of 2.50 tonnes/m^3 is given with time expressed in units of 1000 revolution in the mill. Considering blocks of 15 tonnes, the equivalent wear factor x that specifies the number of years exposure to the environment (in this example, those conditions suffered by block A) that is equivalent in terms of fractional weight loss and shape change to 1000 revolutions in the abrasion mill test, appears to be about 1.0. However, if the armourstone weight was lower, for the same environmental conditions of extremely high shingle attack, for 8, 2.5 and 1.0 tonne blocks, the equivalent wear factors would be 0.81, 0.55 and 0.41 respectively. Note that in Latham & Poole (1988), the authors failed to point out that the suggested equivalent wear factors were based on observations of rounding of prototype blocks weighing nominally 8 tonnes. In that paper, the suggestion that for a highly aggressive environment the value of $x = 0.5$ compares well with the value of about 0.8 obtained for conditions of wear on block A, assuming that it had weighed about 8 tonnes.

Considering blocks B, C and D which were from a 10 tonnes designated area, block D was almost certainly of more durable rock than that tested in the mill. Block B performance after one year suggests an equivalent wear factor for 10 tonne blocks at this particular more sheltered site of about 3.0.

All these estimates of x would be too high if the rock type used in the mill is more durable than that at the site and if the abrasion losses occur

on the site such that volume losses on the whole block exceed the volume losses from the most exposed face by more than the assumed amount of 1.5 times. The comparison is not valid if the initial shape of the blocks used in the mill is significantly different from those in the prototype. Also, whereas abrasion takes place evenly throughout the rock surface during rolling in the mill, abrasion will be concentrated more on certain sides of prototype blocks while other sides may receive protection from neighbouring blocks. Therefore to some extent the way shape is modified in the mill may be different to that for statically stable breakwater armour. For armourstone which is expected to move by rocking or rolling under severe wave attack such as in some berm breakwaters and other dynamically stable designs, the comparison with mill abrasion may be more valid. Note in Fig.8.1 how much faster the weight losses develop for material removed from all six sides of a cube (c) than from a sphere of the same volume (d), indicating one fundamental reason why weight losses are faster from angular irregular blocks compared with smooth spherical ones especially if subject to rolling.

Estimates of asperity roughness P_R based on the mill abrasion theory in Latham & Poole (1988), are given in Table 8.1. A recent visual comparison of the rounding of the most extremely abraded blocks from the region near block A at West Bay, five years after construction (see Fig.8.2), is quite compatible with a degree of rounding intermediate between the SEMIROUND (P_R = 0.0097) and the VERY ROUND (P_R = 0.0046) test material used in the flume tests, but this was not confirmed by image analysis of block outlines because they were too large and insufficient in number. In some instances, the shingle assisted abrasion has produced fluting features in these armourstones.

8.3 Rounding observations using image analysis of Whin Sill dolerite from Buckhaven, Scotland

This revetment structure, which is at Buckhaven in Scotland, was constructed in 1975 and was reported to have been designed at a 1 in 2 slope and built with 1 to 2 tonne armourstone quarried from the Whin Sill dolerite. It is underdesigned with storms frequently causing rocks to roll

down onto the foreshore. It is one of the only UK examples of a structure resembling a rock beach where block mobility and shingle attrition have combined to produce dramatic rates of wear against perhaps one of the most durable rock types in the UK. A typical angular block and a well rounded block are shown in Figs C.1 and C.2 and a general view is shown in Fig.8.3. Digitized outlines of 8 upper blocks and 8 lower blocks are shown in Figs C.3 and C.4.

Although these block outlines are not statistically representative samples, for illustration, the upper blocks values may be equated with the initial condition during construction and the lower block values with 12 years wear. The gross shape parameter P_C has hardly changed while the asperity roughness P_R has fallen from 0.0149 to 0.0062. Details of the shape analysis results are given in Table C.1 where the F_{40} values should be noted. Mill abrasion results were not available for this rock type but it is known to have a very high fracture toughness ($K_{1c} \approx 3MPa.m^{-0.5}$) and density ($\approx 3.0$ tonnes/m^3).

On this basis and comparing with test results for the toughest granites, a conservative estimate of the abrasion resistance index and other mill abrasion constants can be calculated. Applying the theory outlined in Latham & Poole (1988) with the available measured and estimated data suggest that 50,000 revolutions in the mill would give the observed P_R value of 0.0062 and at a weight loss of 9%. The equivalent wear factor x for these semi-mobile blocks of about one tonne is therefore 12/50 = 0.25. However, for 8 tonne blocks, the value would be 0.5.

It might be expected that equivalent wear factors on dynamic structures would be lower (i.e. faster wear) than for statically stable structures. It is possible that the value of 0.5 for 8 tonne blocks which, was suggested in Latham & Poole (1988) for extremely aggressive environments on statically stable structures is slightly too low and is more representative of a structure which has greater mobility in the design (eg. $H_s/\Delta D_{n50} \approx 6$).

8.4 Rounding observations using image analysis of Scandinavian granite at Herne Bay, Kent

Blocks from the top (T) and from the base (S) of the Herne Bay coastal protection structure were photographed for the first preliminary trials of prototype image analysis only one winter season after project completion. The evidence of shingle attrition on the lower blocks was easily visible to the eye even for this abrasion resistant rock. Results of the Fourier and Fractal analysis based on a total of 32 block outlines are given in Table C.1. (The individual results were given in full in Latham, 1987).

The Fractal coefficient is tuned to the fine scale roughness at lengths on the prototype of 15 to 50mm (f = 5mm). The difference between the means of F is statistically significant at a confidence level of about 98% using the Student's T-distribution, indicating that the S blocks are significantly smoother than the T blocks. However, comparing P_C values indicates that the gross shapes are different and that the S blocks are probably the less equant. As P_R to some extent reflects gross shape as well as the finer irregularities, and tends to have a high variability about its mean for irregular blocks, the higher value of P_R for the S blocks is not surprising since the rounding action of the shingle is in fact very insignificant.

This example illustrates that in many cases of relatively minor abrasion, P_R may not detect differences in surface roughness that could perhaps be detected by the Fractal coefficient.

8.5 Summary

To relate wear on a prototype structure with wear inside an abrasion mill, the concept of the equivalent wear factor x was introduced in Latham & Poole (1988). This extremely simplified approach to estimating rates of wear (rounding and weight loss) considers the problems in terms of three factors : the material properties of the rock as indicated by abrasion resistance indices from a laboratory mill test, all the environmental conditions at the site of the blocks under consideration

grouped together (eg. climate, wave energy, attrition agents, block mobility) and the approximate initial sizes of the armourstone blocks.

A first revision of the range of suggested x values from Latham & Poole (1988) is given in Table 8.2. The choice of x most appropriate to the environmental site specific conditions still leaves a large degree of uncertainty. However, the methodology offers some guidance for predicting wear rates.

Using this approach coupled with results from the hydraulic analysis of Section 7, it will be possible to deduce loss of stability due to rounding in service and due to weight loss. For example, the extreme differences in block shape measured at Buckhaven would result in 2.4 times more damage for surging wave conditions, for the rounded (lower) stones than if the more irregular fresh (upper) stones were placed throughout the structure (assuming an impermeable core) The weight loss of 9% would be responsible for a further 20% more damage.

9. CONCLUSIONS AND RECOMMENDATIONS

9.1 Image analysis of armourstone shape

For the model studies in the flume, the parameters P_C, P_R and F_{40} obtained from image analysis were able to quantify the shape characteristics of the five batches of armourstone extremely effectively.

The Fourier asperity roughness factor P_R, obtained by summing the 11th to 20th harmonic amplitudes, is the most revealing parameter because of its apparently simple correlation with hydraulic stability for impermeable structures (see Section 7.2) and because it describes almost completely the contribution that shape makes to the rate of weight loss during abrasion (see Latham & Poole, 1988). Although it is predominantly a measure of texture, it is partly dependant on gross shape and this is why, in terms of physical processes, it is such a meaningful measure of roughness.

The Fourier shape contribution factor P_C, which sums the first 30 harmonic amplitudes, gives very useful gross shape information similar to the directly measured axial ratio X/Z. For greater compatibility with P_R, future studies could use the practically identical Fourier shape factor P_S obtained by summing the 1st to 10th harmonic amplitudes instead of P_C. (The difference between $P_C/10$ and P_S is at most 3%).

The Fractal coefficient F_{40} as defined in this study (i.e. a specific range of step lengths and image size correction is required), is very sensitive to fine scale roughness and is less sensitive to gross shape than P_R. An image size correction has been worked out and the length range on the object to which the roughness refers should always be quoted with the F_{40} value. There may be problems of interpretation when comparing samples of different size rocks (eg. 0.5 and 15 tonnes) or ones containing a wide grading of sizes.

This type of image analysis is not difficult to implement and the results can clearly be rewarding. Several sedimentology laboratories already have similar software and imaging systems and hydraulic laboratories are encouraged to set up such facilities. The essential parameters P_R and P_S are relatively simple to obtain from outline coordinates. Other features covered in this report including outline reconstructions, Fractal coefficients, additional Fourier and outline size parameters

may be unnecessary for coastal engineers but have a place in research and development of new analytic tools. The transfer of model test material (or carefully taken silhouette photographs) to Queen Mary College for shape analysis is an alternative which was carried out successfully with Van der Meer's test material from Delft Hydraulics.

For prototype blocks in the quarry or on a structure, the image analysis techniques can be applied using photographs (see Section 2.3.1 for guidelines). Many block outlines (at least 30) are required to sample block shape at one location on a structure and above 10 to 15 tonne blocks, the photography may be impractical or considered dangerous. If results from the prototype shape analysis are to be used together with predictive models for hydraulic stability and amounts of wear, then the implicit assumption that the prototype photographs represent random projections will require careful consideration.

One warning concerning the use of P_R is that for random projections, the repeatability of a determination of the average P_R may not be as good as some other site or model parameters. A difference of 0.001 between two successive determinations may be typical of most samples of block shapes but rather high for equant blocks. Further investigation of the parameter P_R would allow an estimate of the error associated with the P_R value determined for a sample of random projections of different armour block shapes.

9.2 Hydraulic stability

The results of this limited series of flume tests are probably not sufficient on their own to modify design practise. The results have been analysed so that provisional conclusions can be presented for the design of impermeable core structures with different shaped rock armouring within the framework of Van der Meer's design equations. The conclusions are tentative until confirmed by further information.

Armour consisting of a mixture of extremely tabular and elongate blocks (the TABULAR rock of this study) is significantly more stable than relatively equant blocks when they are placed randomly in a double layer. In future, this hydraulic advantage should be evaluated and compared with the handling and structural disadvantages that these weaker shapes would impose.

As rock becomes more rounded it also becomes more unstable. Stability under surging waves is more sensitive to armour shape than under plunging waves.

Further guidance is required for the accurate determination of the permeability coefficient P. It was reasonable to assume that P was between 0.1 and 0.05 in the flume tests, in which case Van der Meer's predictions, taking into account the shape effects on stability, were confirmed.

Van der Meer's equations may be written with an additional coefficient to include the armour shape effect. For an impermeable core structure they are :

Plunging waves :

$$H_s/\Delta D_{n50} * \sqrt{\xi_m} = C_{pl} * P^{0.18} * (S/\sqrt{N})^{0.2}$$

Surging waves

$$H_s/\Delta D_{n50} = C_{su} * P^{-0.13} * (S/\sqrt{N})^{0.2} * \sqrt{\cot \alpha} * \xi_m P$$

where

$$C_{pl} = 5.6 + 60\ P_R$$

$$C_{su} = 0.8 + 20\ P_R$$

The values of P_R can be determined directly from image analysis or estimated using the data in Appendices A and C which contain outlines and photographs for visual comparison. Most of Van der Meer's test material had a P_R value of 0.0010 and was typical of slightly rounded equant stones (see Tables A3,A.4 and B.1). In this study, the PR values were : TABULAR 0.0165, FRESH 0.0138, EQUANT 0.0117, SEMIROUND 0.0087, VERY ROUND 0.0046.

9.3 Rates of Armourstone wear

An approach for predicting the rates of armourstone wear by rounding and weight loss was presented in Latham & Poole (1988). Using the results of a laboratory abrasion mill test to obtain the most appropriate material properties of a rock type, it was proposed that time on the breakwater built with the same rock could be directly related to revolutions in the mill test. The outstanding problem was to relate the site specific wear conditions to the equivalent wear factor x that relates prototype time to mill abrasion time.

Evidence in Section 8 from prototype structures has allowed some modifications to be made to the originally proposed values of x and the importance of the initial block size on x has been included assuming the surface area to volume

relationship. The new x values imply a slightly slower rate of wear on prototype structures generally.

The possibility exists that the influence of wear on stability could be estimated using a systematic approach. In practice, many more observations and refinements will be required to give confidence to these methods of estimating stability losses through wear with time.

10. REFERENCES

Ahrens, J.P. (1975) 'Large wave tank tests of riprap stability' U.S. Army Corps of Engineers, Coastal Engineering Reseach Centre, Tech. Memo 51

Allison, D.M.& Savage, R.P. (1976) 'Tests of low-density marine limestone for use in breakwaters' U.S. Army Corps of Engineers, Coastal Engineering Research Centre, Tech. Paper No. 76-4

Allsop, N.W.H. , Bradbury, A.P. , Poole, A.B. , Dibb, T.E. & Hughes, D.W. (1985) 'Rock durability in the marine environment ' Hydraulic Research Ltd., Report No. SR11

Allsop, N.W.H. & Latham, J-P. (1987) 'Rock armouring to unconventional breakwaters : the design implications for rock durability' Seminar on Unconventional Rubble-Mound Breakwaters, NRC, Ottawa, Canada, Paper No. 2

Barrett, P.J. (1980) 'The slope of rock particles, a critical review' *Sedimentology*, Vol. **27**, p.291-303

Bergh, H. (1984) 'Riprap protection of a road embankment exposed to waves' Hydraulic Laboratory, Royal Institute of Technology, Stockholm, Sweden. Bulletin No. TRIA-VBI-123

Bradbury, A.P., Allsop, N.W.H., Latham, J-P., Mannion, M.B. & Poole, A.B. (1988) 'Rock armour for rubble mound breakwaters, sea walls and revetments : recent progress' Report no. SR150, Hydraulics Research

Broderick, L.L. (1984) 'Riprap stability versus monochromatic and irregular waves' M.thesis, George Washington University, USA

Bruun, P. & Gumbak, A.R. (1978) 'Stability of sloping structure in relation to $\xi = \tan\alpha/\sqrt{H/L_0}$' *Coastal Engineering*, Vol. **1**, p.287-322

Clark, M.W. (1981) 'Quantitative shape analysis, a review'
Mathematical Geology, Vol. **13**, p.303-320

Clark, A.R. (1988) 'The use of Portland Stone rock armour in coastal protection and sea defense works' *Q.J eng Geol.*, London, Vol.**21**, p.113-136

Czernecka, E. & Gillott, J.E. (1977) 'A modified Fourier method of shape and surface texture analysis of planar sections of particles' *'Journal of testing and evaluation'* ASTM. Vol. **5**: p.292-298

Dibb, T.E., Hughes, D.W. & Poole, A.B. (1983) 'Controls of size and shape of natural armourstone' *Q.J eng Geol.*, London, Vol. **16**, p.31-42

Ehrlich, R., Brown, P.J. , Yarus, J.M. & Przygocki, R.S. (1980) 'The origin of shape frequency distributions and the relationship between size and shape'
Journal of Sedimentary Petrology, Vol. **50**, No. 2, p.475-484

Ehrlich, R. & Weinberg, B. (1970) 'An exact method for characterizing grain shape'
Journal of Sedimentary Petrology, Vol. **40**, p.205-212

Fookes, P.G. & Poole, A.B. (1981) 'Some preliminary considerations on the selection and durability of rock and concrete materials for breakwaters and coastal protection works' *Q.J.Eng Geol* , Vol. **14**, p.97-128

Fookes, P.G. & Thomas, R.S. (1986) 'Rapid site appraisal of potential breakwater rock at Qeshm, Iran' *Proc I.C.E.* Part 1, I.C.E., London

Hudson, R.Y. (1959) 'Laboratory investigation of rubble-mound breakwaters'
Journal of the Waterways and Harbors Division, Proc. of the American Society of Civil Engineers, WW3,p.95-119

Jensen, O.J. (1984) 'A monograph on rubble mound breakwaters'
Danish Hydraulic Institute, Denmark

Latham, J-P. (1987) 'Size and shape of prototype armourstone using image analysis'
Internal Report, Queen Mary College, London

Latham, J-P. & Poole, A.B. (1987a) 'The application of shape descriptor analysis to the study of aggregate wear' *Q.J eng Geol.*, Vol. **20**, p.297-310

Latham, J-P. & Poole, A.B. (1987b) 'Pilot study of an aggregate abrasion test for breakwater armourstone' *Q.J.eng Geol* , Vol. **2**, p.311-316

Latham, J-P. & Poole, A.B. (1988) 'Abrasion testing and armourstone degradation' *Coastal Engineering*, Vol. **12**, p.233-255

Latham, J-P. et al (1988) 'Developments in the analysis of armour layer profile data' *Proc. I.C.E. Breakwaters '88 Conference*

Mandelbrot, B.B. (1982) 'The Fractal geometry of Nature' W.H.Freeman, San Francisco, Calif., 460pp

Markle, D.D. & Davidson, G.G. (1979) 'Placed stone stability tests, Tillamook, Oregon' Tech. Report HL-79-16, U.S. Army Corps of Engineers, W.E.S., Missisipi

Orford, T.E. (1975) 'Discrimination of particle zonation on a pebble beach' *Sedimentology*, Vol. **22**, p.441-463

Orford, T.E. & Whalley, W.B. (1983) 'The use of the fractal dimension to quantify the morphology of irregular-shaped particles' *Sedimentology*, Vol. **30**, p.655-68

Poole, A.B., Fookes, P.G., Dibb, T.E. & Hughes, D.W (1984) 'Durability of rock in breakwaters' Breakwaters - design and construction, p.31-43, Thomas Telford Ltd., London

Schwarcz, H.P. & Shane, K.C. (1969) 'Measurement of particle shape by Fourier analysis' *Sedimentology*, Vol. **13**, p.213-31

Schwarz, H. & Exner, H.E. (1980) 'The impementation of the concept of fractal dimension on a semi-automatic image analyser' *Powder technology*, Vol. **27**, p.207-13

Shore Protection Manual (1984) Volume II, US Army Corps of Engineers, Coastal Engineering Research Centre

Thomsen, A.L., Wohlt, P.E. & Harrison, A.S. (1972) 'Riprap stability on earth embankments tested in large and small scale wave tanks' U.S. Army Corps of Engineers, Coastal Engineering Research Centre, Tech. Memo 37

Thomson, D.T. & Shuttler, R.M. (1975) 'Riprap design for wind wave attack. A laboratory study in random waves' CIRIA Report No.61, Hydraulics Research Ltd., Wallingford

Van der Meer, J.W. (1988) 'Rock slopes and gravel beaches under wave attack' Thesis, Delft Hydraulics Communication No. 396

Van der Meer, J.W. & Pilarczyk, K.W. (1984) 'Stability of rubble mound slopes under random wave attack' *Proc. 19th ICCE*, Houston, USA, Chapter 176

Young, R.M., Pitt, J.D., Ackers, P. & Thompson, D.M. (1976) 'Riprap design for wind wave attack : longterm observations on the Offshore bank in the Wash' CIRIA Tech. Note 101

Zwamborn, J.A. (1986) 'The quantification of breakwater armour profiles for design purposes' *Coastal Engineering*, Vol. **10**, p.253-273

11. ACKNOWLEDGEMENTS

This report describes work funded by the Science and Engineering Research Council under Grants GR/D/00832 and GR/D/66921. The major part of the work for the project, 'Armour durability and breakwater performance' (Phases 1 and 2), was carried out at Queen Mary College. The flume tests were performed at Hydraulics Research, Wallingford, who funded two thirds of the cost of the test programme. Ir. J.W. Van der Meer of Delft Hydraulics supplied samples of test material for shape analysis.

12. APPENDICES

Appendix A - Details of projected block outlines and shape analysis results of the five subsamples used in the flume tests

Appendix B - Details of projected block outlines and shape analysis results from four batches of armour tested at Delft Hydraulics Laboratories

Appendix C - Details of projected block outlines and shape analysis results from photographs of prototype armourstones at Buckhaven, Scotland and Herne Bay

TABLES

A.1 TABULAR rock shape descriptors
A.1 FRESH rock shape descriptors
A.1 EQUANT rock shape descriptors
A.1 SEMIROUND rock shape descriptors
A.1 VERY ROUND rock shape descriptors

B.1 Delft Hydraulics Laboratory samples DH1-DH4, shape analysis descriptors

C.1 Shape analysis of prototype armourstones from Buckhaven and Herne Bay
C.2 Individual block shape descriptors from Buckhaven

FIGURES

A.1 TABULAR block outlines as digitized (a) max projection (b) random projection 1 (c) random projection 2
A.2 FRESH block outlines as digitized (a) max projection (b) random projection 1 (c) random projection 2
A.3 EQUANT block outlines as digitized (a) max projection (b) random projection 1 (c) random projection 2
A.4 SEMIROUND block outlines as digitized (a) max projection (b) random projection 1 (c) random projection 2
A.5 VERY ROUND block outlines as digitized (a) max projection (b) random projection 1 (c) random projection 2
A.6 TABULAR blocks - photograph in maximum projection
A.7 FRESH blocks - photograph in maximum projection
A.8 EQUANT blocks - photograph in maximum projection
A.9 SEMIROUND blocks - photograph in maximum projection
A.10 VERY ROUND blocks - photograph in maximum projection

B.1 Delft Hydraulics laboratory sample (DH1) random projection
B.2 Delft Hydraulics laboratory sample (DH2) random projection
B.3 Delft Hydraulics laboratory sample (DH3) random projection
B.4 Delft Hydraulics laboratory sample (DH4) random projection

C.1 A typical angular block from Buckhaven upper photograph
C.2 A typical very round block from Buckhaven lower photograph
C.3 Digitized outlines of 8 upper blocks from Buckhaven
C.4 Digitized outlines of 8 lower blocks from Buckhaven

Table A.1 : TABULAR rock shape descriptors

Average value of descriptor	Maximum projection		Random projection (1)		Random projection (2)	
	Mean	Std.Dev.	Mean	Std.Dev.	Mean	Std.Dev.
SIZE :						
N'	453.5	47.4	410.8	58.6	405.3	67.6
S_i	2.19	6.55	54.63	9.16	53.99	9.96
D_i	136.40	14.10	122.86	19.72	121.49	21.46
GROSS SHAPE :						
P_C	2.206	0.910	2.706	1.271	2.645	1.152
Circ	0.864	0.057	0.836	0.084	0.839	0.080
R_d	0.778	0.268	0.917	0.402	0.903	0.376
ROUGHNESS :						
P_R (log mean*)	0.0150		0.0162		0.0169	
P_R (mean*)	0.0157	0.0049	0.0178	0.0091	0.0186	0.0096
F	0.0146	0.0024	0.0137	0.0020	0.0143	0.0025
T	4.602	0.614	4.665	0.732	4.604	0.682
T_C	2.396	0.948	1.959	1.056	1.958	0.864

Note 1 : mean* = arithmetic mean

Note 2 : log mean* = log average transform i.e. antilog (average of log P_R for each particle)

Table A.2 : FRESH rock shape descriptors

Average value of descriptor	Maximum projection		Random projection (1)		Random projection (2)	
	Mean	Std.Dev.	Mean	Std.Dev.	Mean	Std.Dev.
SIZE :						
N^I	391.0	53.6	378.3	54.0	364.5	49.1
S_i	55.50	7.89	53.67	8.05	51.39	7.09
D_i	123.68	17.23	118.57	17.82	114.76	16.31
GROSS SHAPE :						
P_C	1.753	0.683	1.825	0.643	1.934	0.882
Circ	0.892	0.045	0.891	0.042	0.888	0.057
R_d	0.657	0.225	0.674	0.223	0.686	0.283
ROUGHNESS :						
P_R (log mean*)	0.0136		0.0134		0.0142	
P_R (mean*)	0.0142	0.0045	0.0142	0.0045	0.0152	0.0063
F	.0145	0.0027	0.0156	0.0031	0.0156	0.0032
T	4.529	0.628	4.380	0.625	4.344	0.623
T_C	2.776	0.857	2.555	0.858	2.409	0.889

Note 1 : mean* = arithmetic mean

Note 2 : log mean* = log average transform i.e. antilog (average of log P_R for each particle)

Table A.3 : EQUANT rock shape descriptors

Average value of descriptor	Maximum projection		Random projection (1)		Random projection (2)	
	Mean	Std.Dev.	Mean	Std.Dev.	Mean	Std.Dev.
SIZE :						
N^i	378.4	37.9	352.9	45.8	366.0	43.2
S_i	54.75	5.03	51.73	6.95	53.29	6.23
D_i	119.36	9.99	114.47	14.31	117.09	12.96
GROSS SHAPE :						
P_C	1.442	0.443	1.418	0.510	1.438	0.545
Circ	0.910	0.027	0.921	0.030	0.916	0.032
R_d	0.543	0.135	0.523	0.170	0.530	0.177
ROUGHNESS :						
P_R (log mean*)	0.0121		0.0117		0.0117	
P_R (mean*)	0.0124	0.0033	0.0120	0.0029	0.0122	0.0041
F	0.0153	0.0023	0.0149	0.0025	0.0152	0.0023
T	4.612	0.529	4.163	0.474	4.300	0.548
T_C	3.170	0.840	2.745	0.736	2.863	0.848

Note 1 : mean* = arithmetic mean

Note 2 : log mean* = log average transform i.e. antilog (average of log P_R for each particle)

Table A.4 : SEMIROUND rock shape descriptors

Average value of dscriptor	Maximum projection		Random projection (1)		Random projection (2)	
	Mean	Std.Dev.	Mean	Std.Dev.	Mean	Std.Dev.
SIZE :						
N^I	385.2	49.3	361.0	50.2	361.1	45.8
S_i	55.70	6.76	51.28	6.64	51.56	7.15
D_i	122.54	14.28	113.86	15.16	115.51	14.74
GROSS SHAPE :						
P_C	1.667	0.752	1.891	0.902	1.878	0.965
Circ	0.911	0.048	0.896	0.059	0.898	0.062
R_d	0.604	0.241	0.674	0.289	0.664	0.298
ROUGHNESS :						
P_R (log mean*)	0.0089		0.0102		0.0093	
P_R (mean*)	0.0102	0.0056	0.0113	0.0052	0.0106	0.0057
F	0.0105	0.0019	0.0106	0.0020	0.0101	0.0016
T	4.061	0.702	4.197	0.591	4.149	0.669
T_C	2.394	0.935	2.306	0.833	2.271	0.935

Note 1 : mean* = arithmetic mean

Note 2 : log mean* = log average transform i.e. antilog (average of log P_R for each particle)

Table A.5 : VERY ROUND rock shape descriptors

Average value of descriptor	Maximum projection		Random projection (1)		Random projection (2)	
	Mean	Std.Dev.	Mean	Std.Dev.	Mean	Std.Dev.
SIZE :						
N'	347.9	42.3	334.1	41.8	338.8	41.3
S_I	51.77	5.69	49.16	5.83	50.25	5.73
D_I	115.30	11.13	109.67	13.23	111.78	13.03
GROSS SHAPE :						
P_C	1.444	0.558	1.605	0.743	1.496	0.615
Circ	0.937	0.033	0.926	0.044	0.933	0.035
R_d	0.502	0.183	0.564	0.239	0.521	0.192
ROUGHNESS :						
P_R (log mean*)	0.0042		0.0047		0.0044	
P_R (mean*)	0.0046	0.0022	0.0053	0.0026	0.0047	0.0019
F	0.0078	0.0009	0.0079	0.0012	0.0081	0.0009
T	3.401	0.605	3.528	0.657	3.433	0.672
T_C	1.957	0.600	1.923	0.640	1.937	0.574

Note 1 : mean* = arithmetic mean

Note 2 : log mean* = log average transform i.e. antilog (average of log P_R for each particle)

Table B.1 : DHL subsample shape analysis

Average value of descriptor	DH1 Brick after 10 tests		DH2 Uniform stone after 41 tests		DH3 Uniform stone after 106 tests		DH4 Riprap after 134 tests	
	Mean	Std. dev.	Mean	Std. dev.	Mean	Std. dev.	Mean	Std. dev.
SIZE								
N^i	424.0	57.9	453.1	45.9	451.5	50.2	362.1	92.1
S_i	61.60	8.91	66.34	7.59	66.40	7.71	53.13	13.37
D_i	134.42	19.18	145.82	16.77	145.63	16.33	115.93	28.73
GROSS SHAPE								
P_C	1.510	0.531	1.516	0.552	1.428	0.479	1.461	0.508
Circ	0.912	0.030	0.919	0.032	0.924	0.030	0.924	0.032
R_d	0.554	0.162	0.553	0.193	0.529	0.153	0.541	0.166
ROUGHNESS								
P_R (log mean*)	0.0118		0.0107		0.0093		0.0085	
P_R (mean*)	0.0121	0.0031	0.0112	0.0036	0.0098	0.0033	0.0089	0.0030
F	0.0138	0.0026	0.0115	0.0028	0.0104	0.0014	0.0119	0.0031
T	4.464	0.642	4.055	0.767	4.095	0.591	4.082	0.537
T_C	2.954	0.978	2.539	1.018	2.667	0.757	2.621	0.663

Table C.1 : Shape analysis of prototype armourstone

Average descriptor	Buckhaven		Herne Bay	
	Upper (U)	Lower (L)	Top (T)	Base (S)
SIZE				
N	391.6	352.0	525.1	536.1
S_i	56.6	52.1	74.4	77.0
D_i	122.5	113.1	164.2	167.9
GROSS SHAPE				
P_C	1.441	1.409	1.778	1.849
Circ	0.9072	0.9295	0.8913	0.8909
R_d	0.5559	0.5339	0.6502	0.6512
ROUGHNESS				
P_R (log mean)	0.0149	0.0062	0.0135	0.0144
P_R (mean)	0.0141	0.0064	0.0138	0.0151
F	0.0237	0.0104	0.0205	0.0166
F_{40}	0.0195	0.0093	0.0147	0.0118
T	4.684	4.062	4.485	4.435
T_C	3.243	2.653	2.708	2.586

Note : f = 5mm, F and F_{40} tuned to lengths of 15 to 50mm on prototype blocks

	N	T_c	P_c	P_R	F	
1	594	3.2538	1.4849	1.7689	.010111	.013644	
2	353	5.4222	4.6977	.7245	.014877	.023276	
3	445	5.5790	4.6588	.9203	.015434	.022730	
4	442	3.7904	1.8475	1.9429	.011580	.011290	UPPER
5	336	4.3634	2.3770	1.9865	.012575	.017481	
6	385	5.2421	3.8127	1.4294	.020821	.024671	
7	265	5.3850	4.3574	1.0276	.015105	.021298	
8	313	4.4350	2.7059	1.7292	.022373	.021645	
1	409	3.9273	2.8282	1.0991	.005269	.009050	
2	397	3.6316	2.5078	1.1237	.008320	.009175	
3	323	4.1975	3.2305	.9670	.003853	.009631	
4	382	3.9494	1.2359	2.7135	.006891	.009112	LOWER
5	328	4.8288	3.2083	1.6206	.007776	.008662	
6	304	4.1968	2.5584	1.6384	.007154	.009559	
7	379	4.3471	3.5653	.7818	.004875	.009507	
8	294	3.4198	2.0907	1.3292	.006964	.009699	

	N	L_{P3}	L_{P1}	S_i	D_i	L_n	Circ	R	R_d	
1	594	628.13	658.62	86.60	183.16	6.8587	.9161	1.2600	.5326	
2	353	387.98	410.58	52.88	116.23	6.6760	.9412	1.2006	.3265	
3	445	495.59	522.46	65.47	145.84	6.7966	.9245	1.2458	.4641	
4	442	479.50	502.48	62.97	136.62	7.0196	.8951	1.4712	.7325	UPPER
5	336	371.05	389.85	46.99	103.79	7.1500	.8788	1.4155	.7282	
6	385	408.47	428.49	54.75	116.17	7.0325	.8935	1.2196	.5486	
7	265	278.93	294.41	38.76	81.60	6.8365	.9191	1.3359	.4572	
8	313	341.44	364.78	44.40	96.86	7.0501	.8912	1.3957	.6577	
1	409	430.30	445.04	61.70	129.83	6.6285	.9479	1.2167	.4069	
2	397	426.44	447.12	60.06	129.04	6.6097	.9506	1.2484	.4522	
3	323	352.00	368.98	48.88	106.54	6.6079	.9509	1.1821	.4026	
4	382	416.08	435.02	51.94	113.14	7.3548	.8543	1.4862	.9013	LOWER
5	328	376.60	392.62	47.47	109.01	6.9092	.9094	1.3999	.6484	
6	304	338.98	355.36	44.49	99.22	6.8333	.9195	1.3993	.6812	
7	379	395.06	410.89	57.82	120.53	6.5551	.9585	1.2025	.3476	
8	294	332.62	349.50	44.23	100.08	6.6468	.9453	1.2040	.4312	

C.2 Individual block shape descriptors from Buckhaven

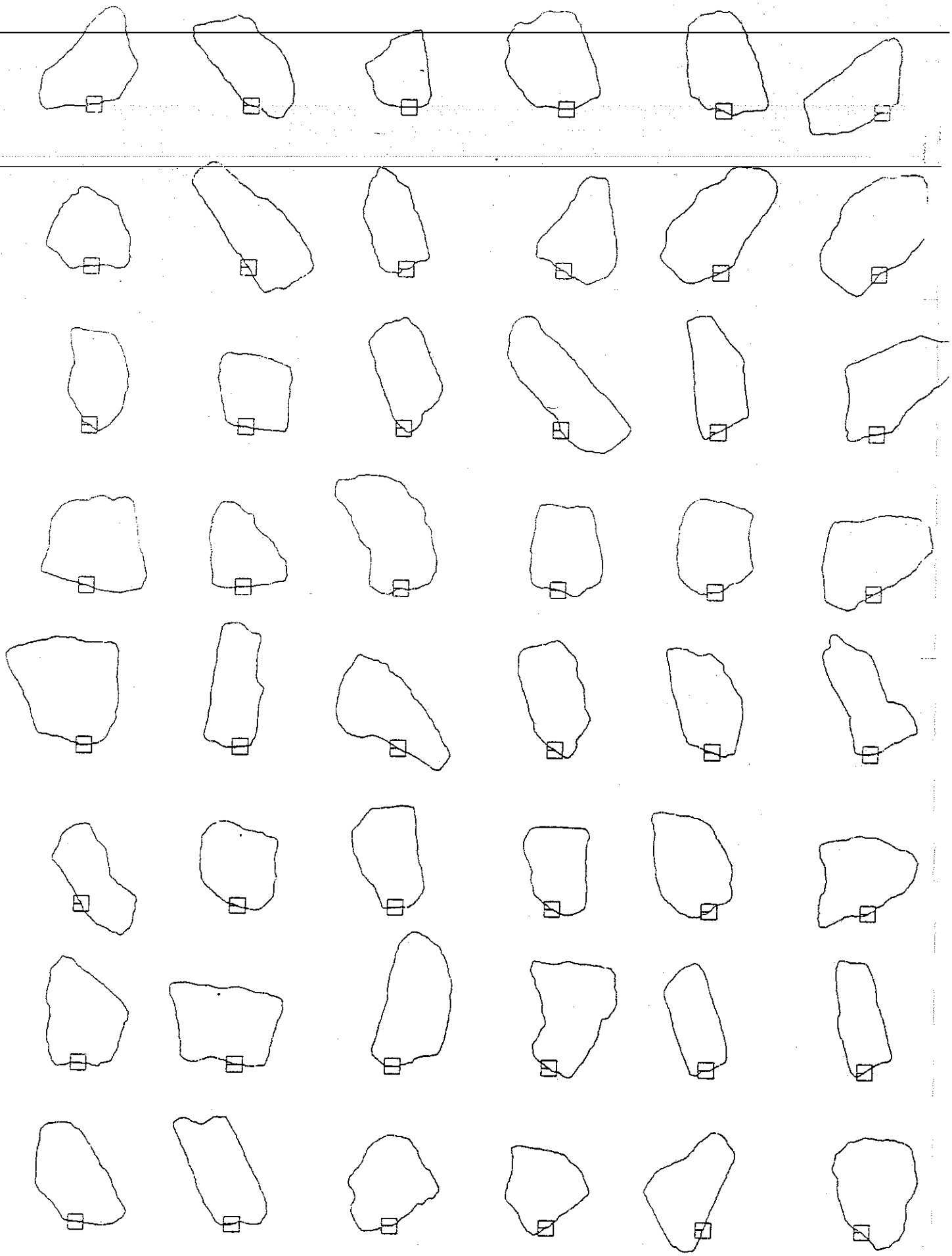

Figure A.1 TABULAR block outlines as digitized (a) max projection

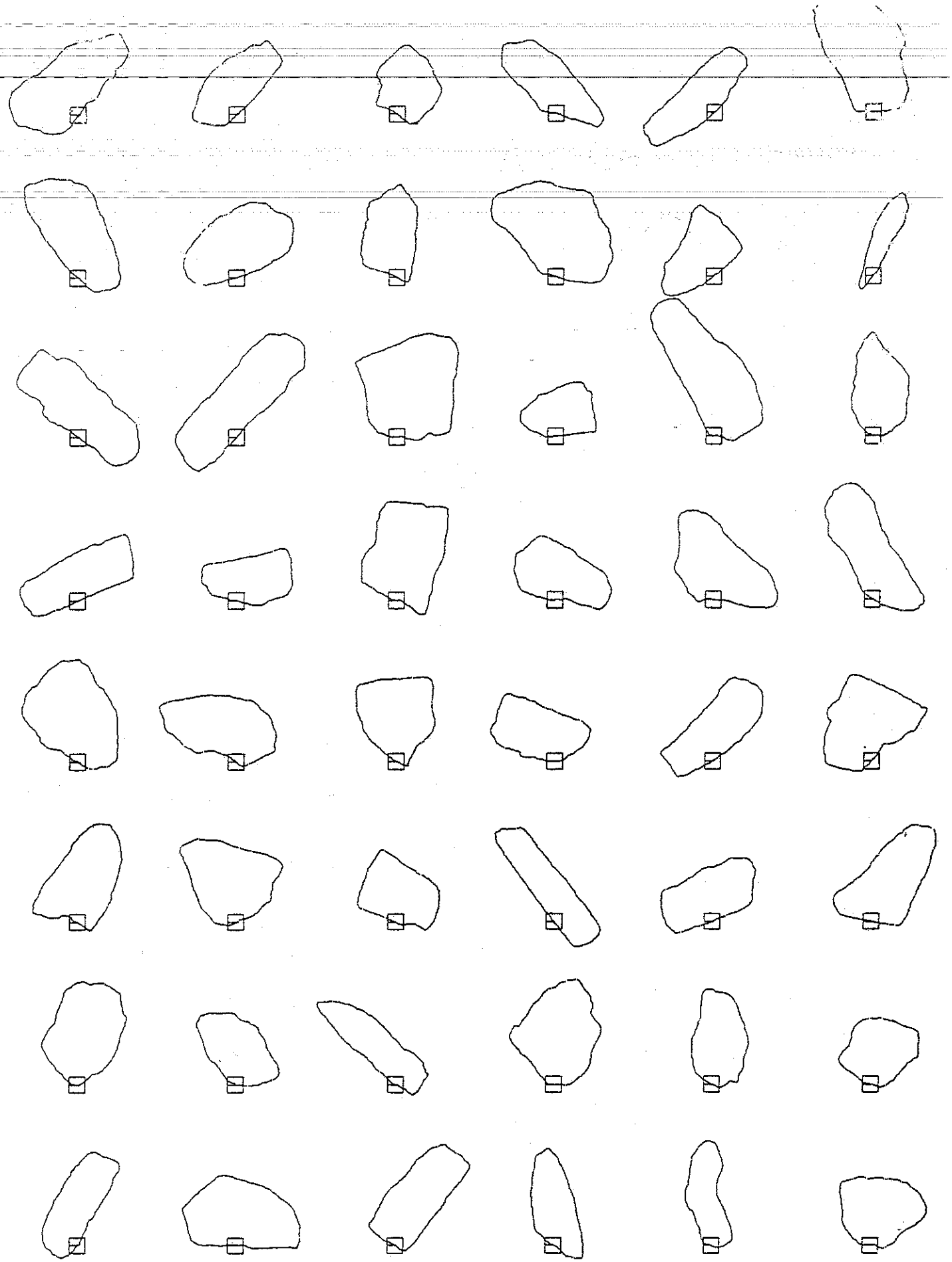

Figure A.1 TABULAR block outlines as digitized (b) random projection 1

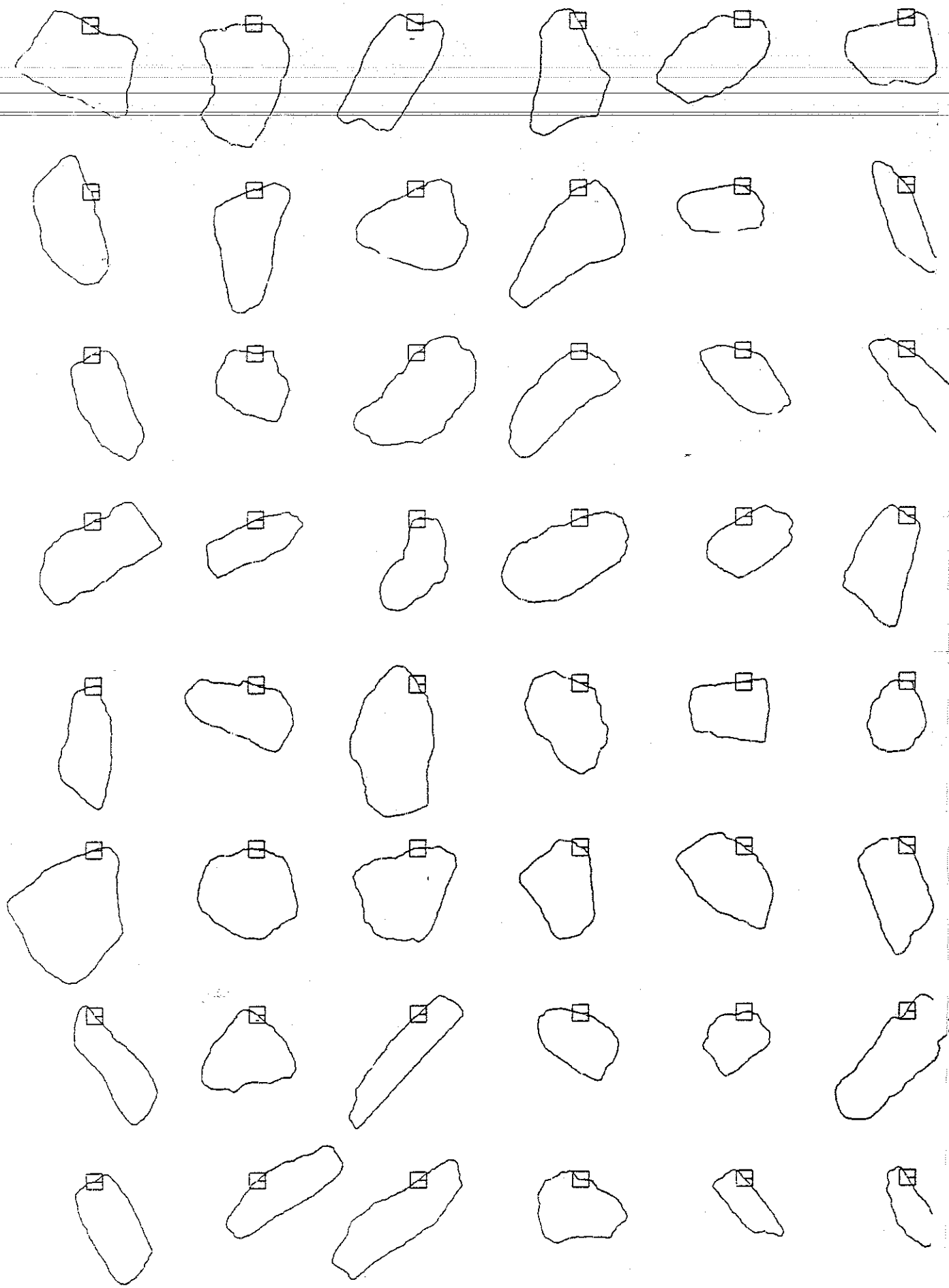

Figure A.1 TABULAR block outlines as digitized (c) random projection 2

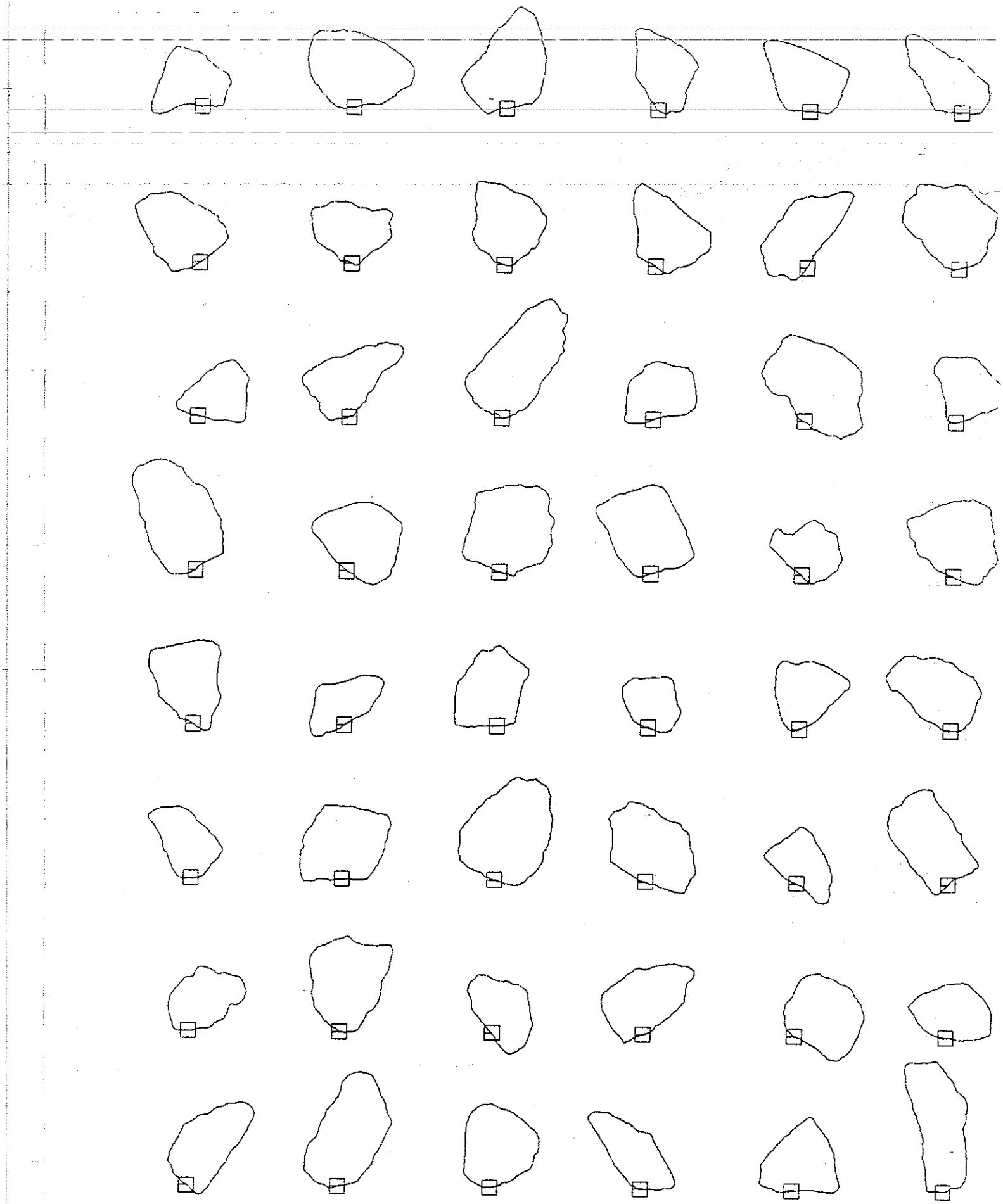

Figure A.2 FRESH block outlines as digitized (a) max projection

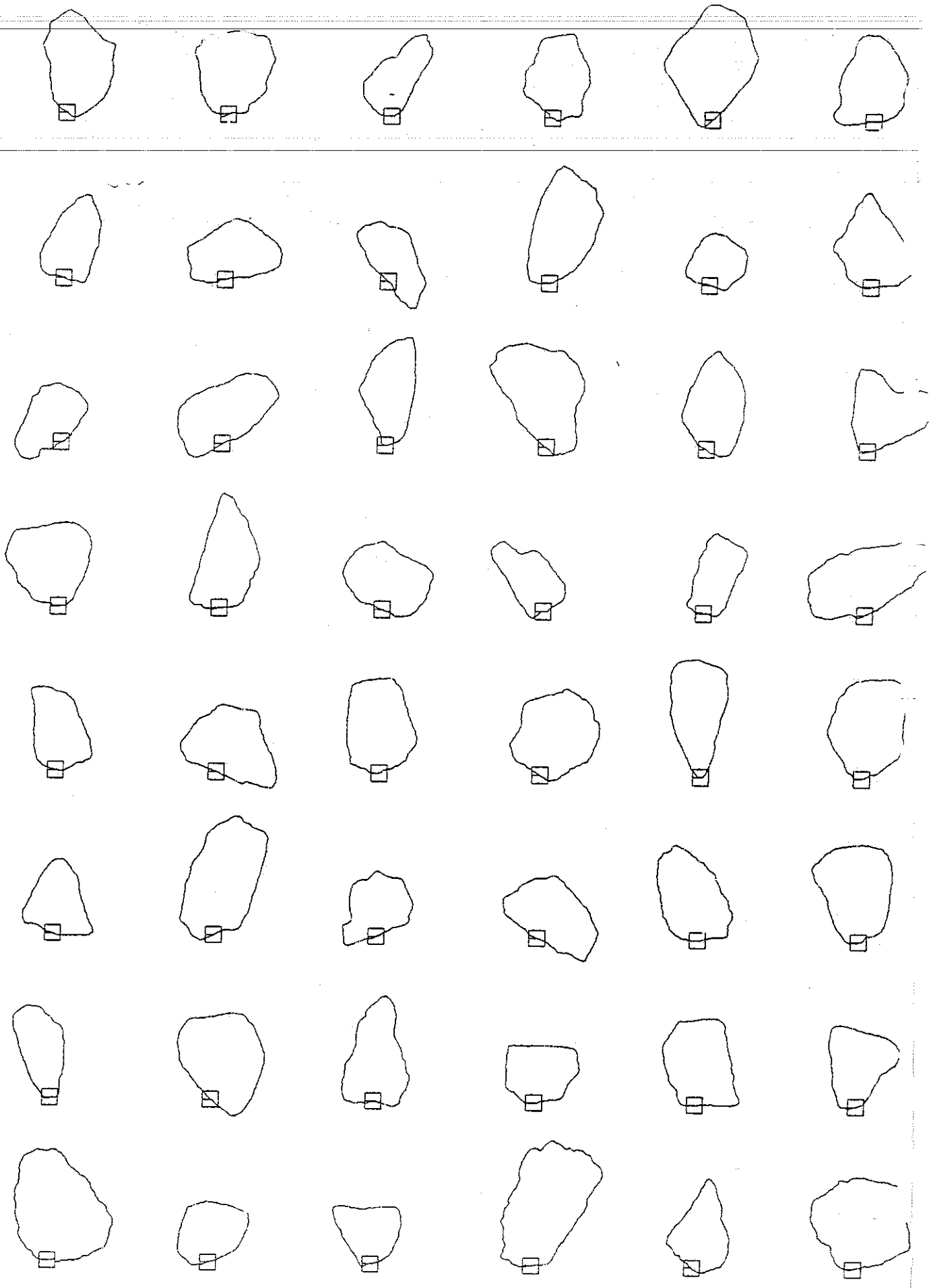

Figure A 2 FRESH block outlines as digitized (b) random projection 1

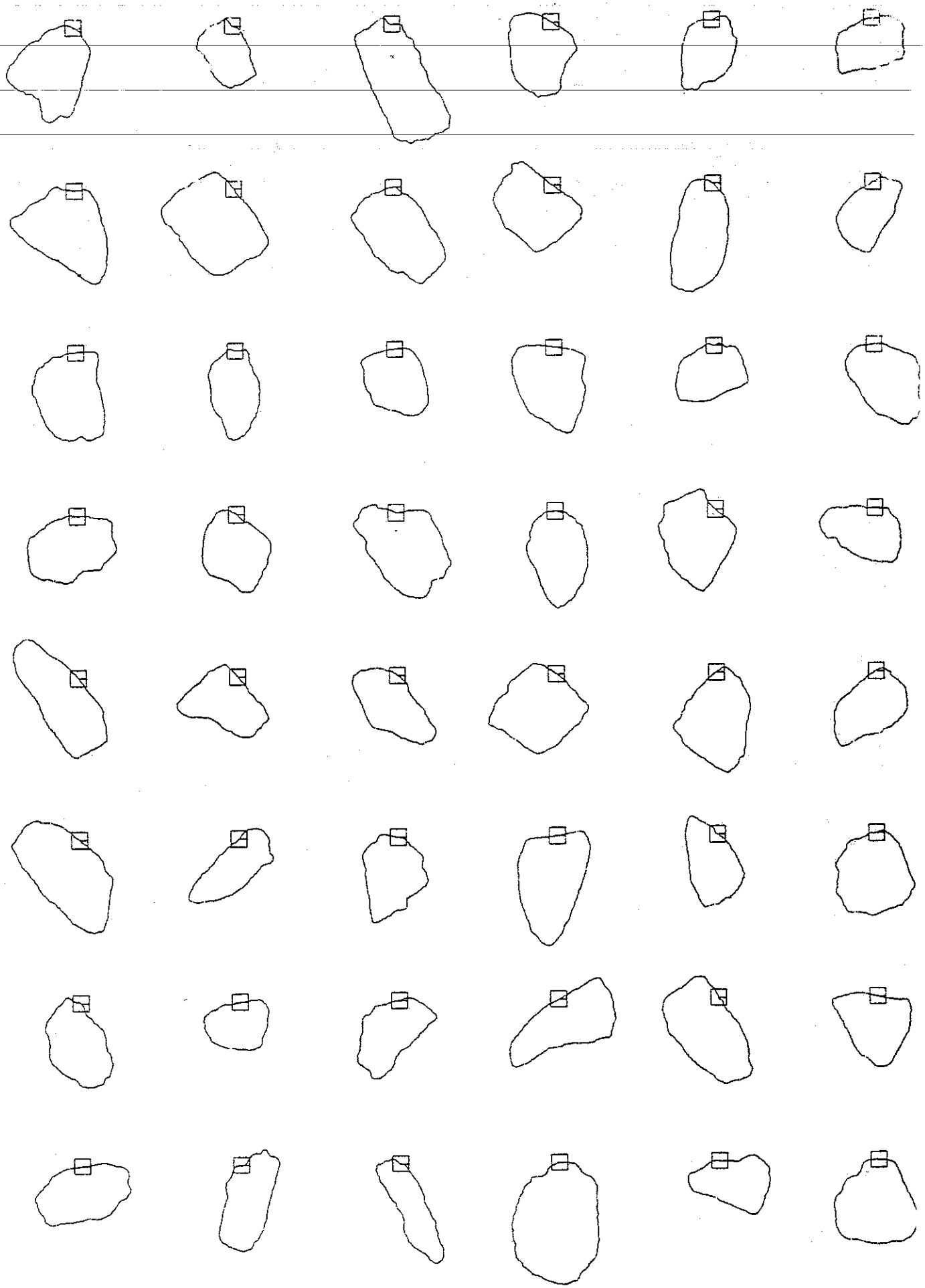

Figure A.2 FRESH block outlines as digitized (c) random projection 2

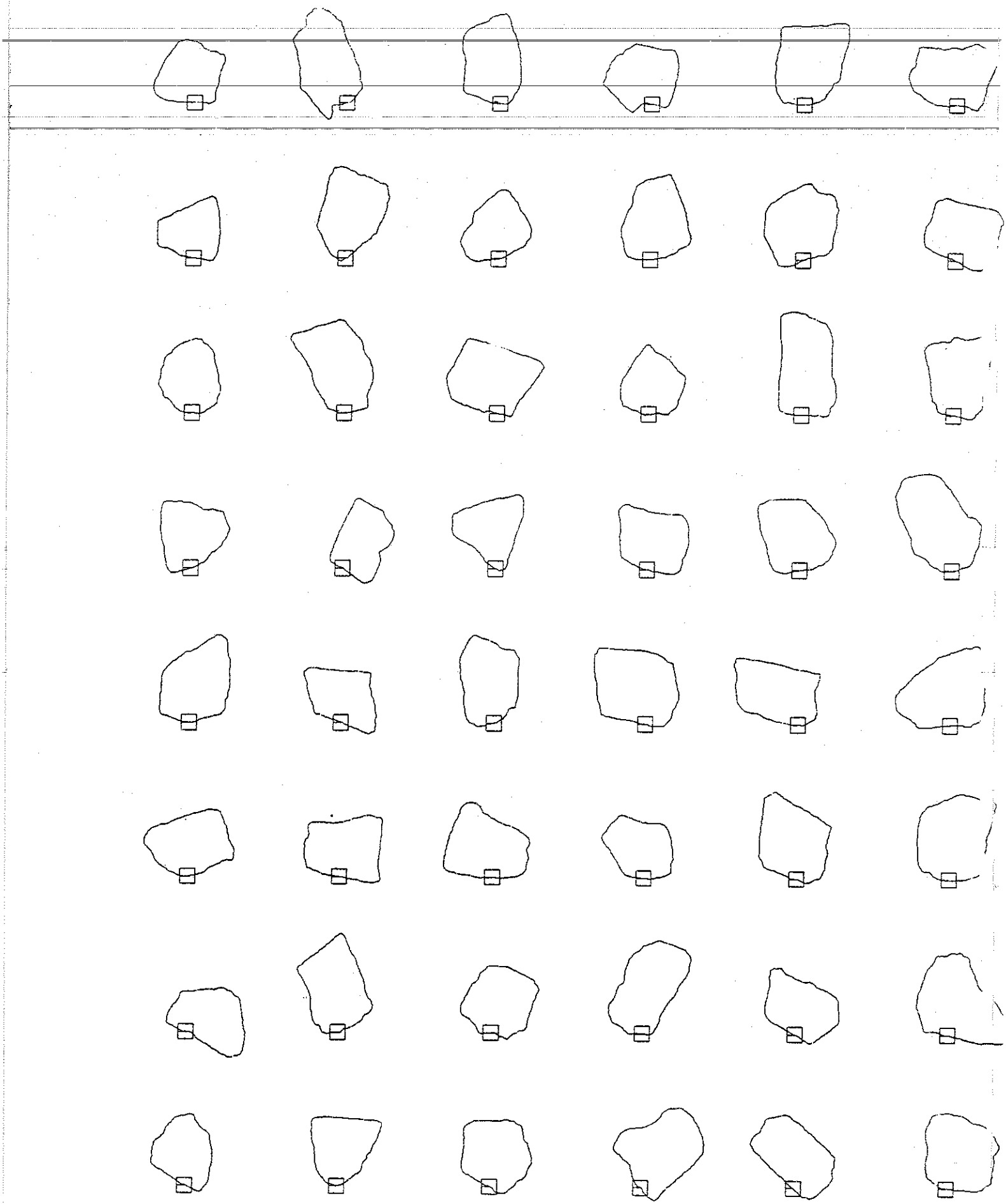

Figure A.3 EQUANT block outlines as digitized (a) max projection

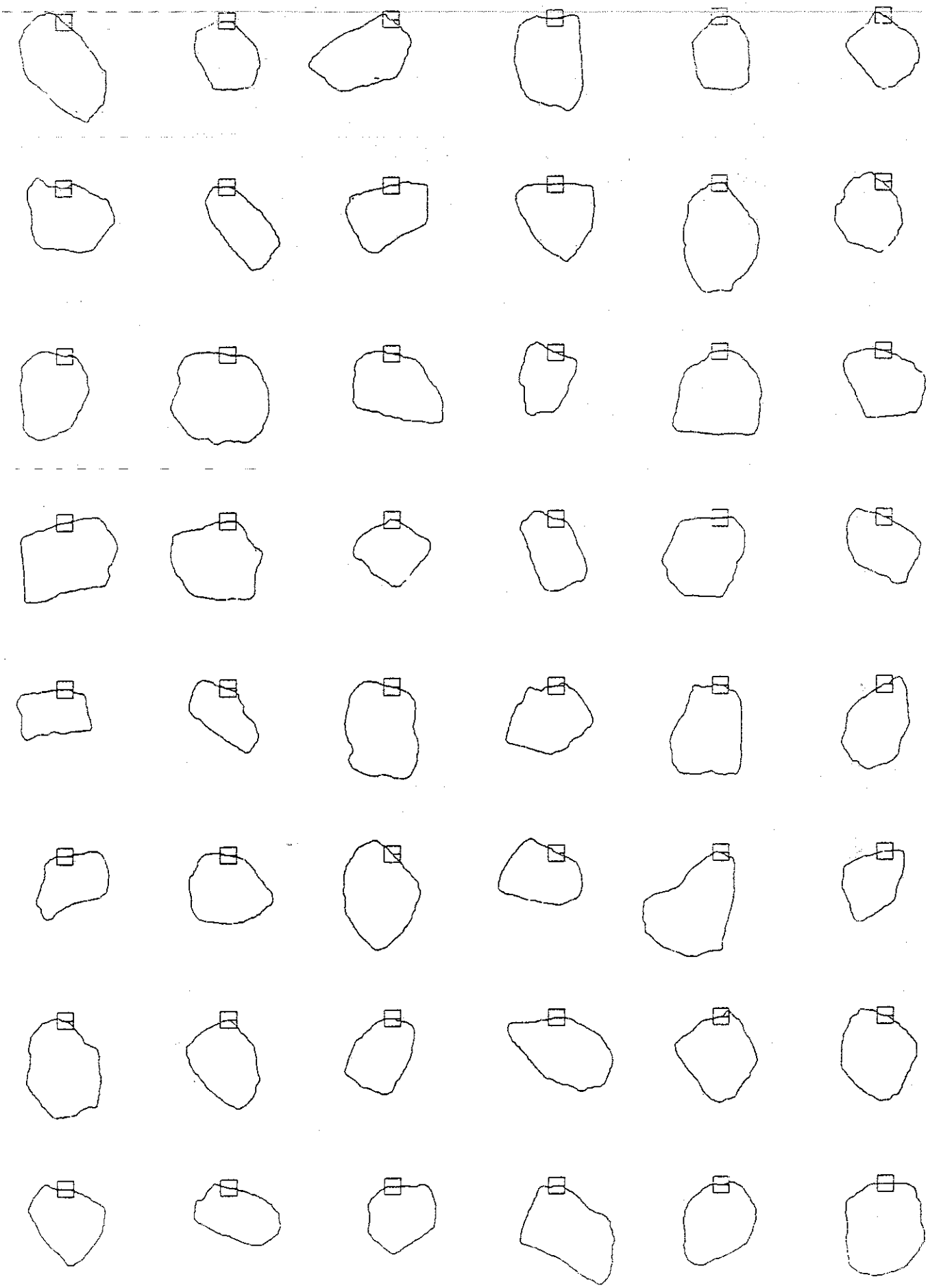

Figure A.3 EQUANT block outlines as digitized (b) random projection 1

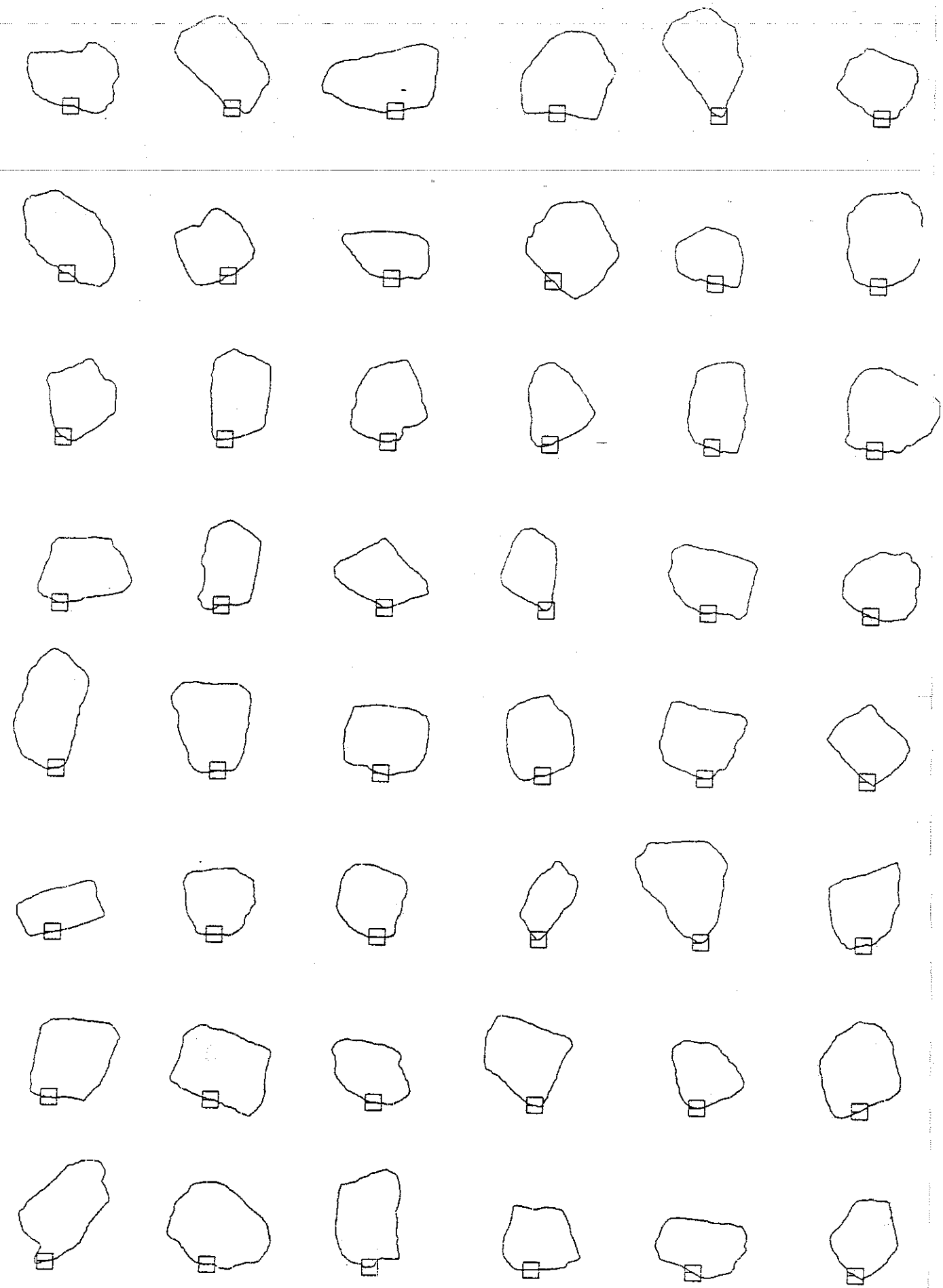

Figure A.3 EQUANT block outlines as digitized (c) random projection 2

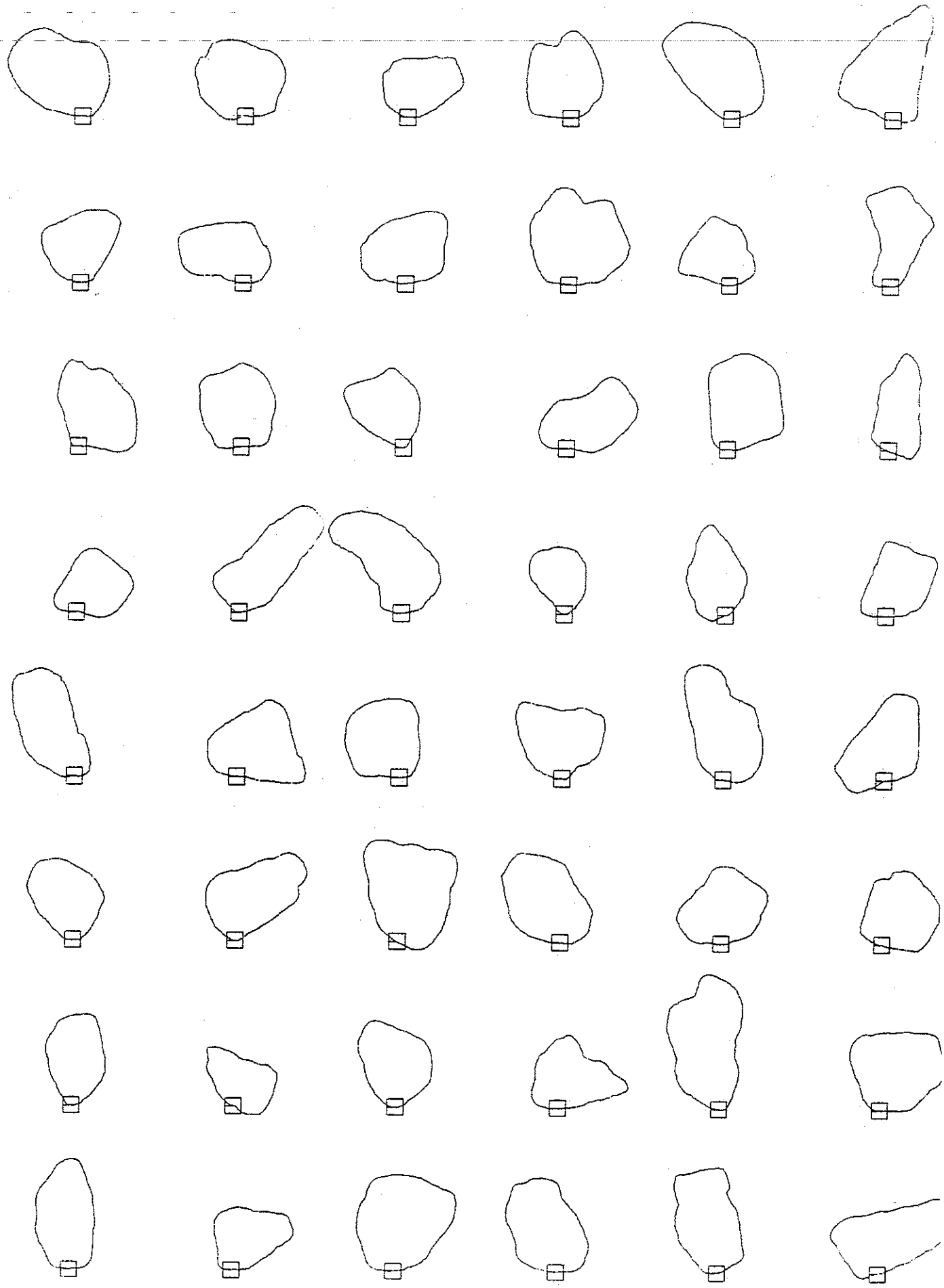

Figure A 4 SEMIROUND block outlines as digitized (a) max projection

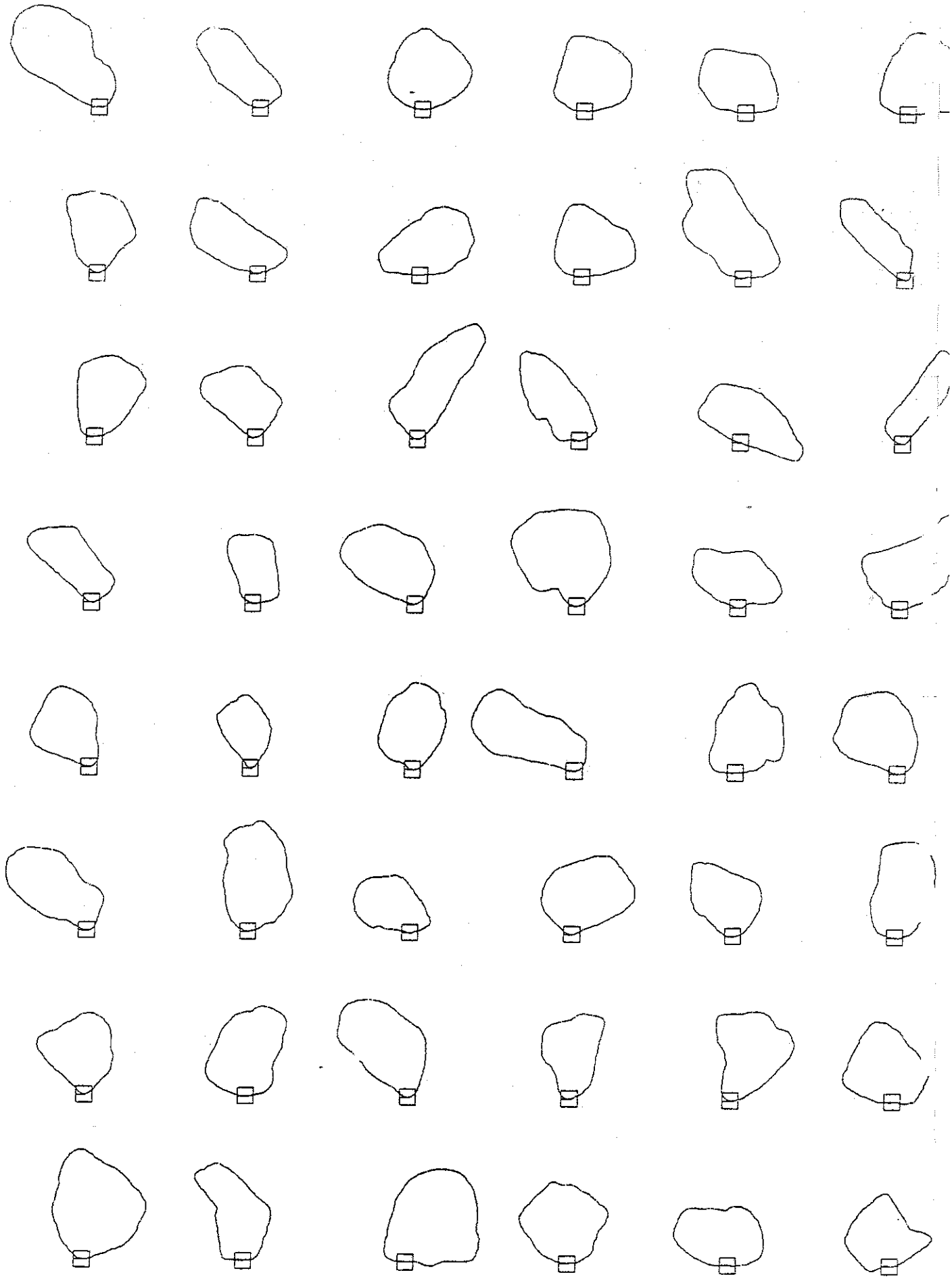

Figure A.4 SEMIROUND block outlines as digitized (b) random projection 1

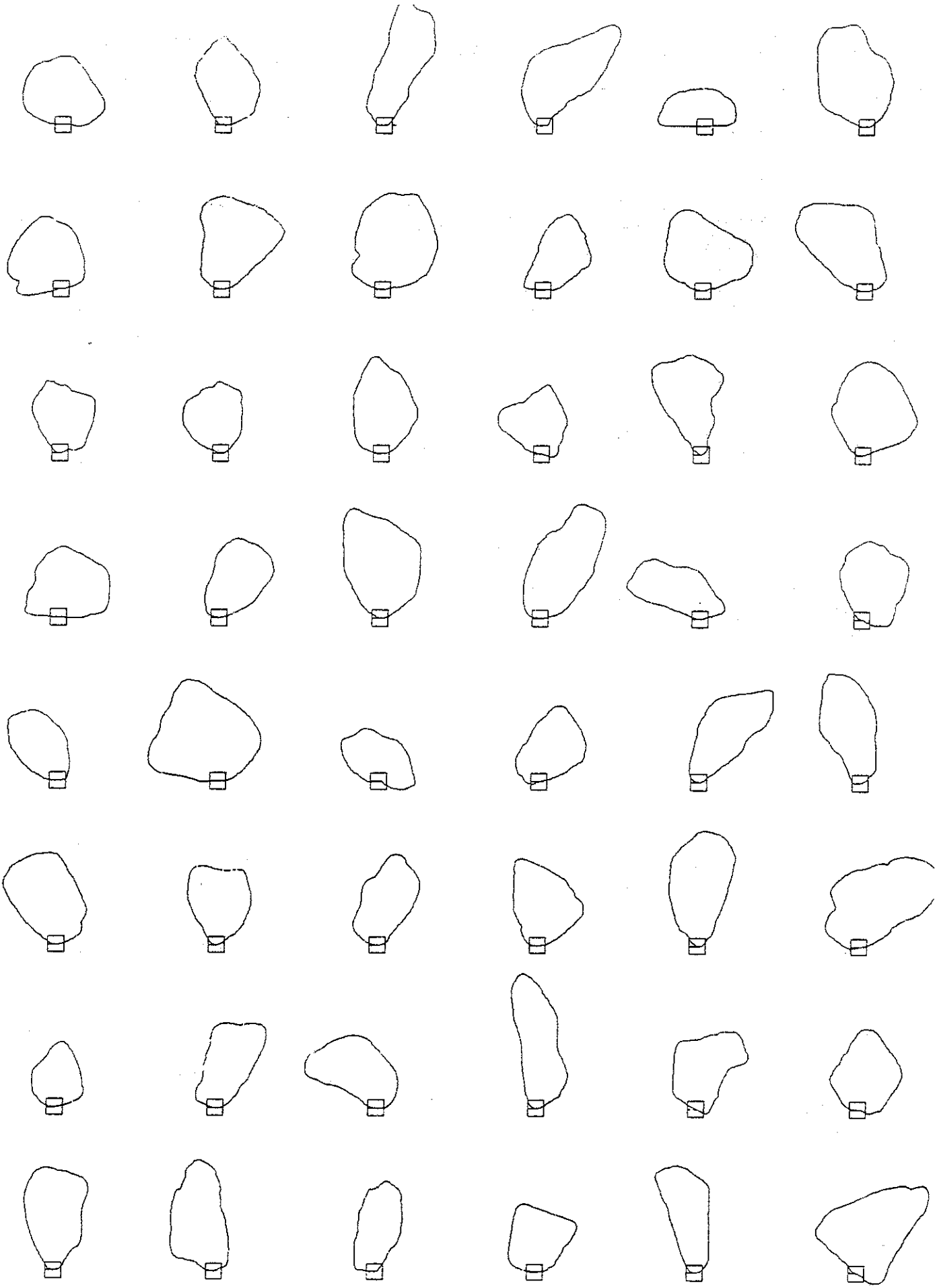

Figure A.4 SEMIROUND block outlines as digitized (c) random projection 2

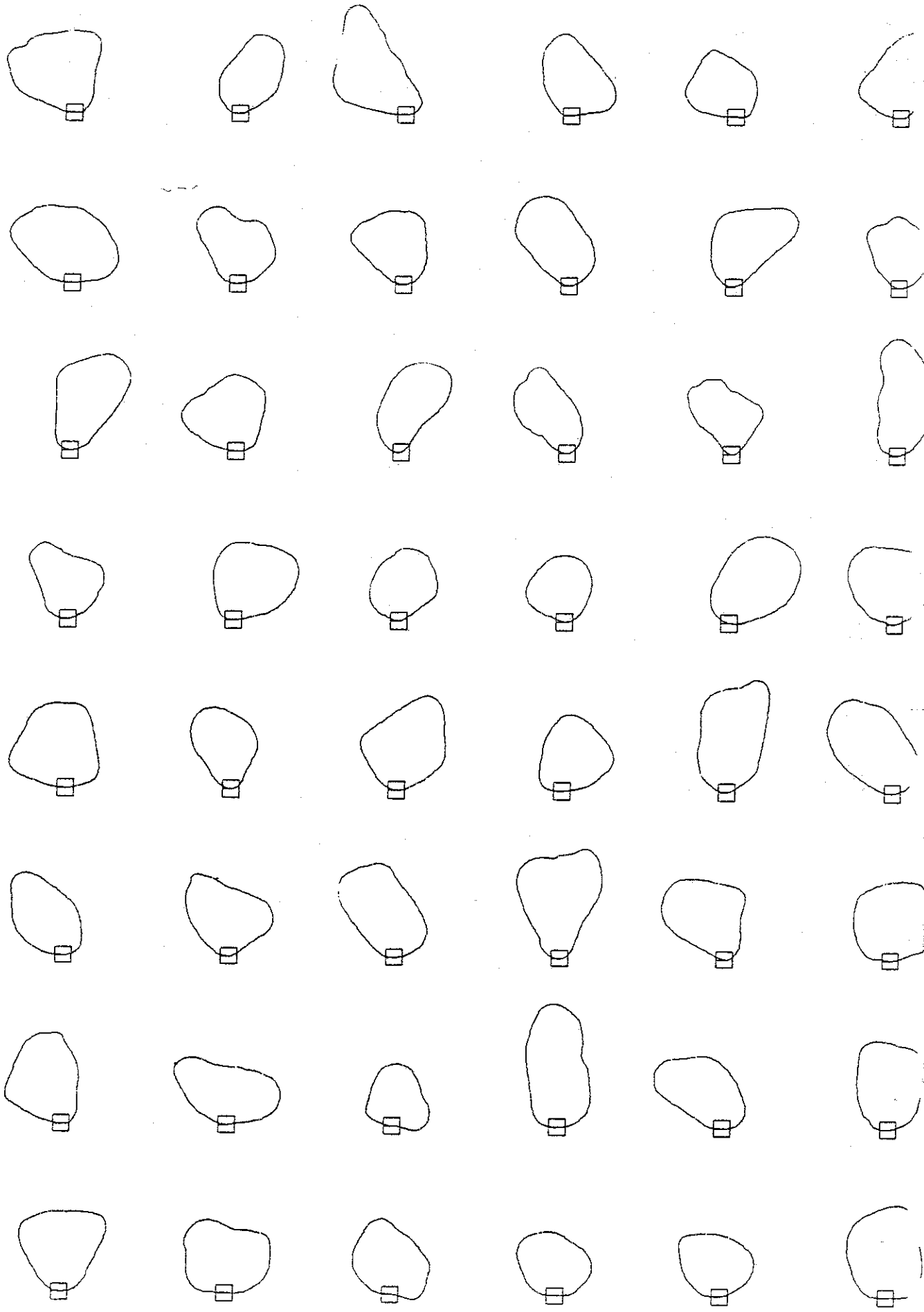

Figure A.5 VERY ROUND block outlines as digitized (a) max projection

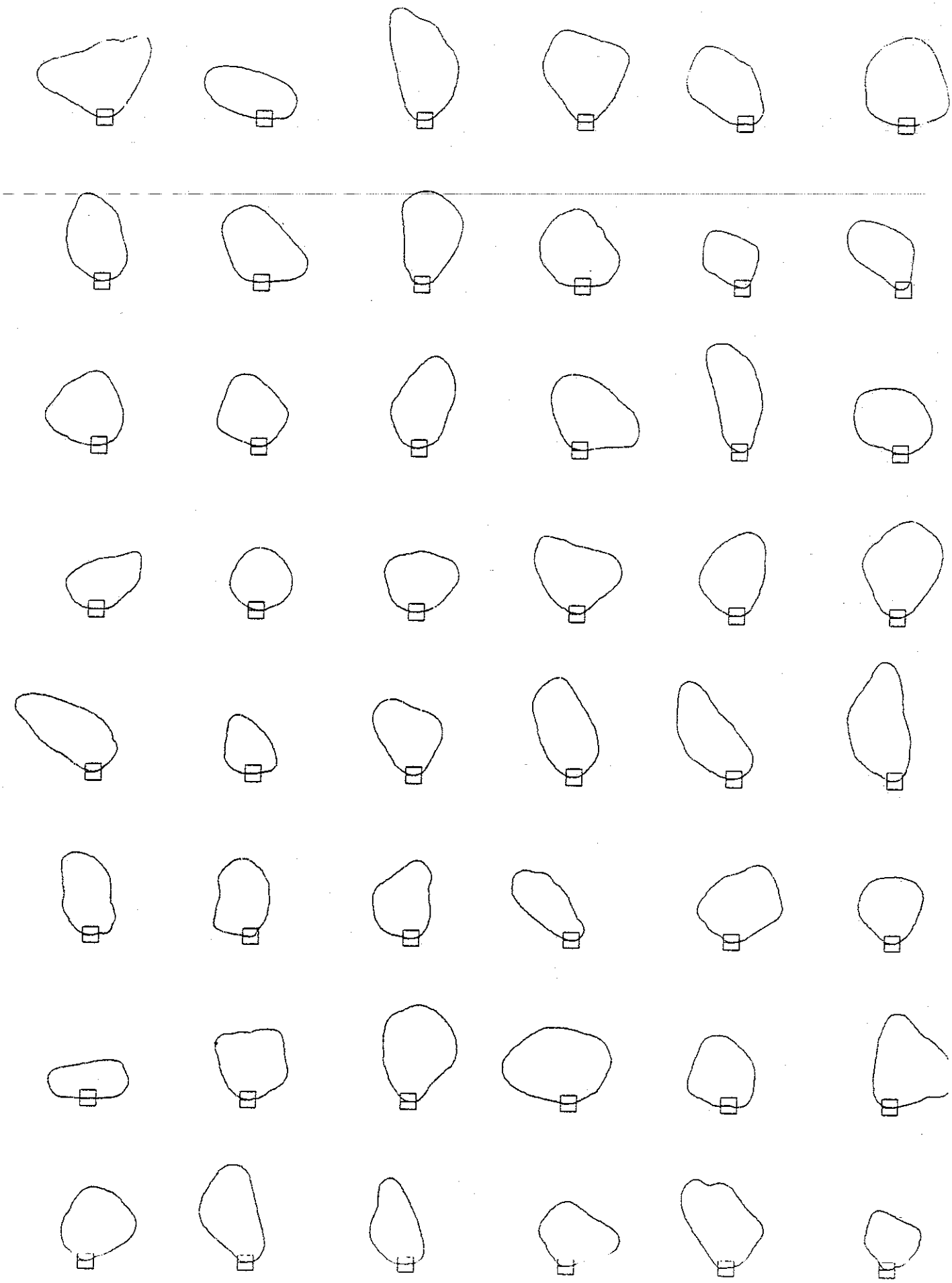

Figure A.5 VERY ROUND block outlines as digitized (b) random projection 1

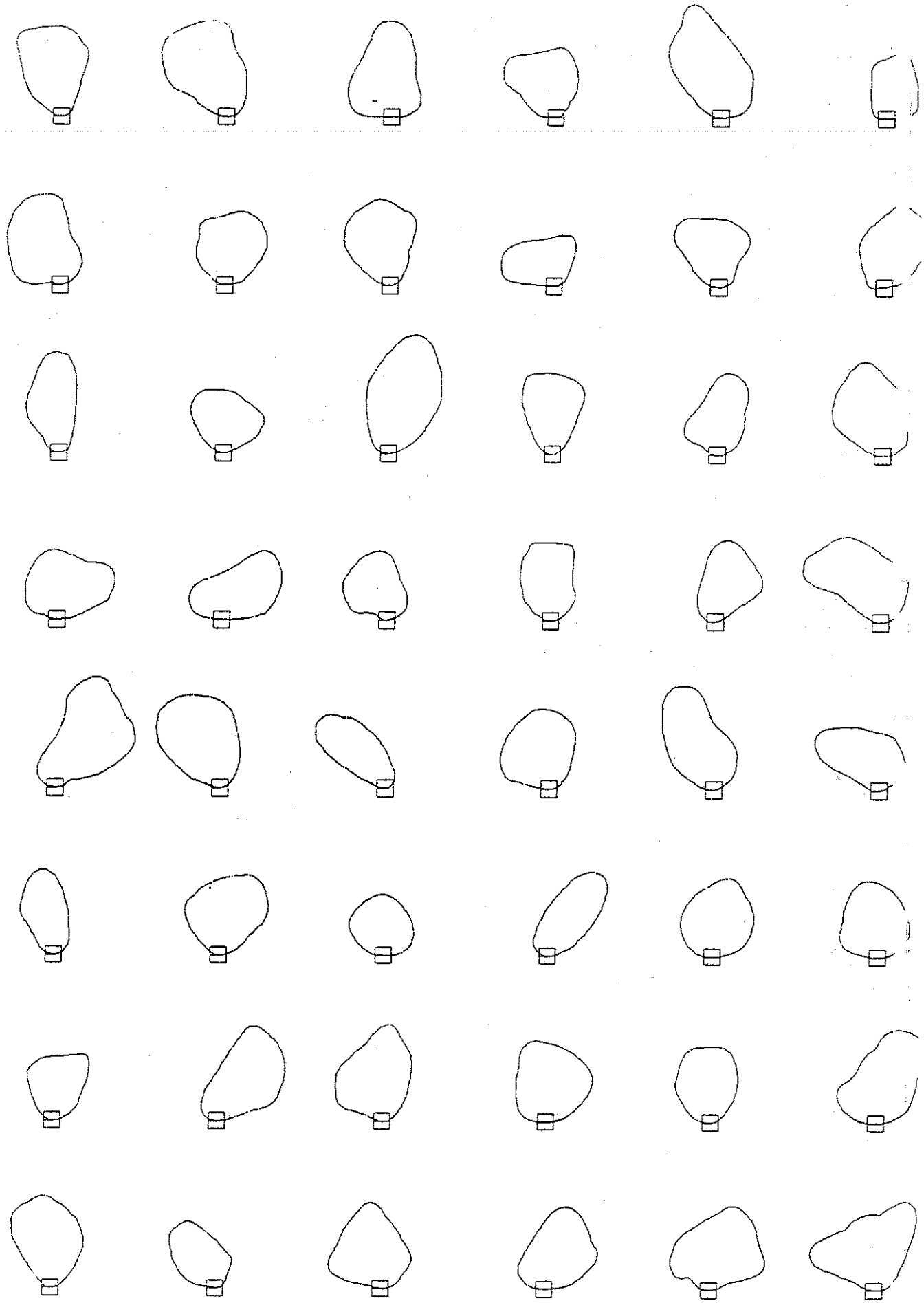

Figure A 5 VERY ROUND block outlines as digitized (c) random projection 2

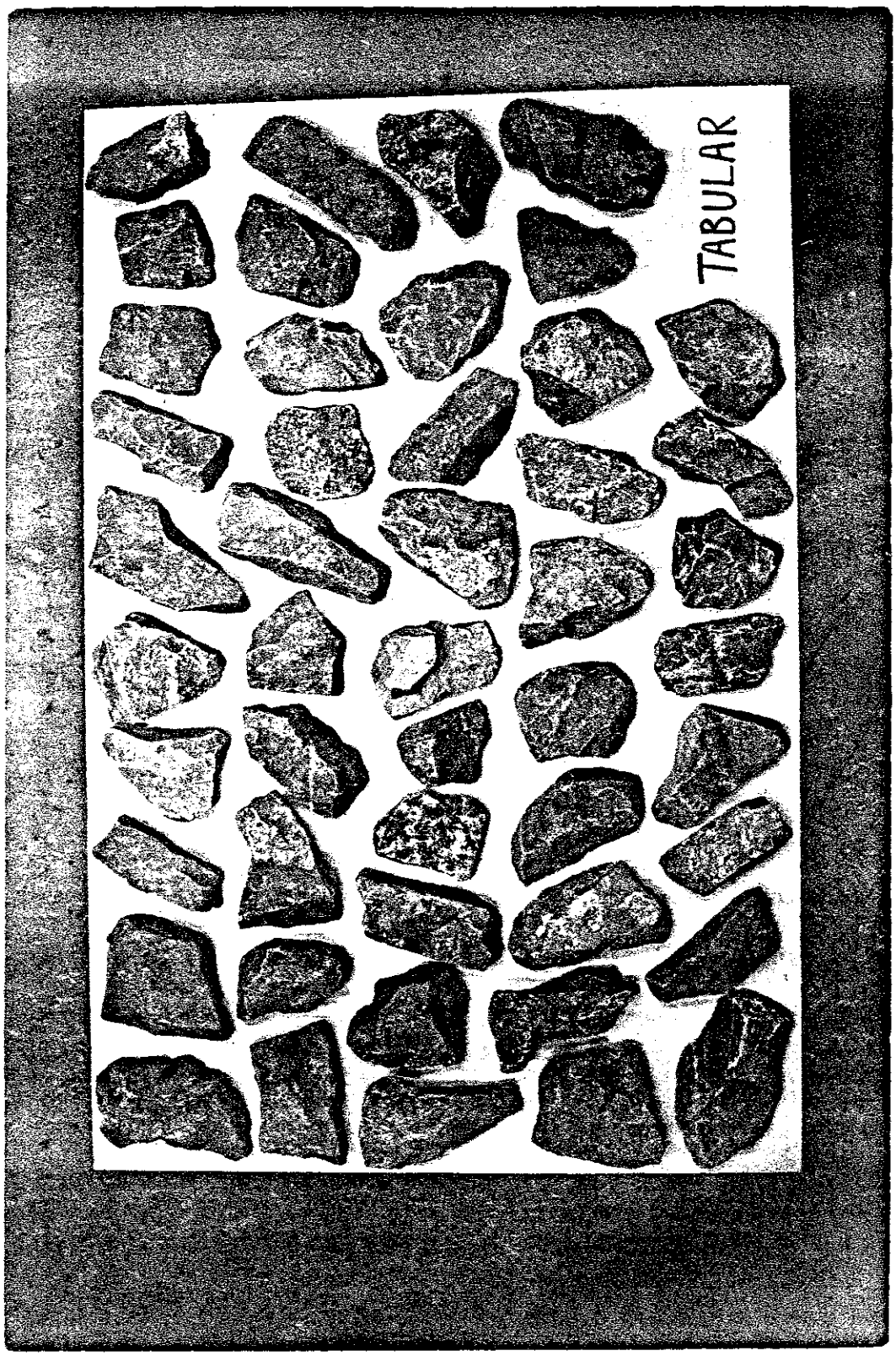

A.6 TABULAR blocks - photograph in maximum projection

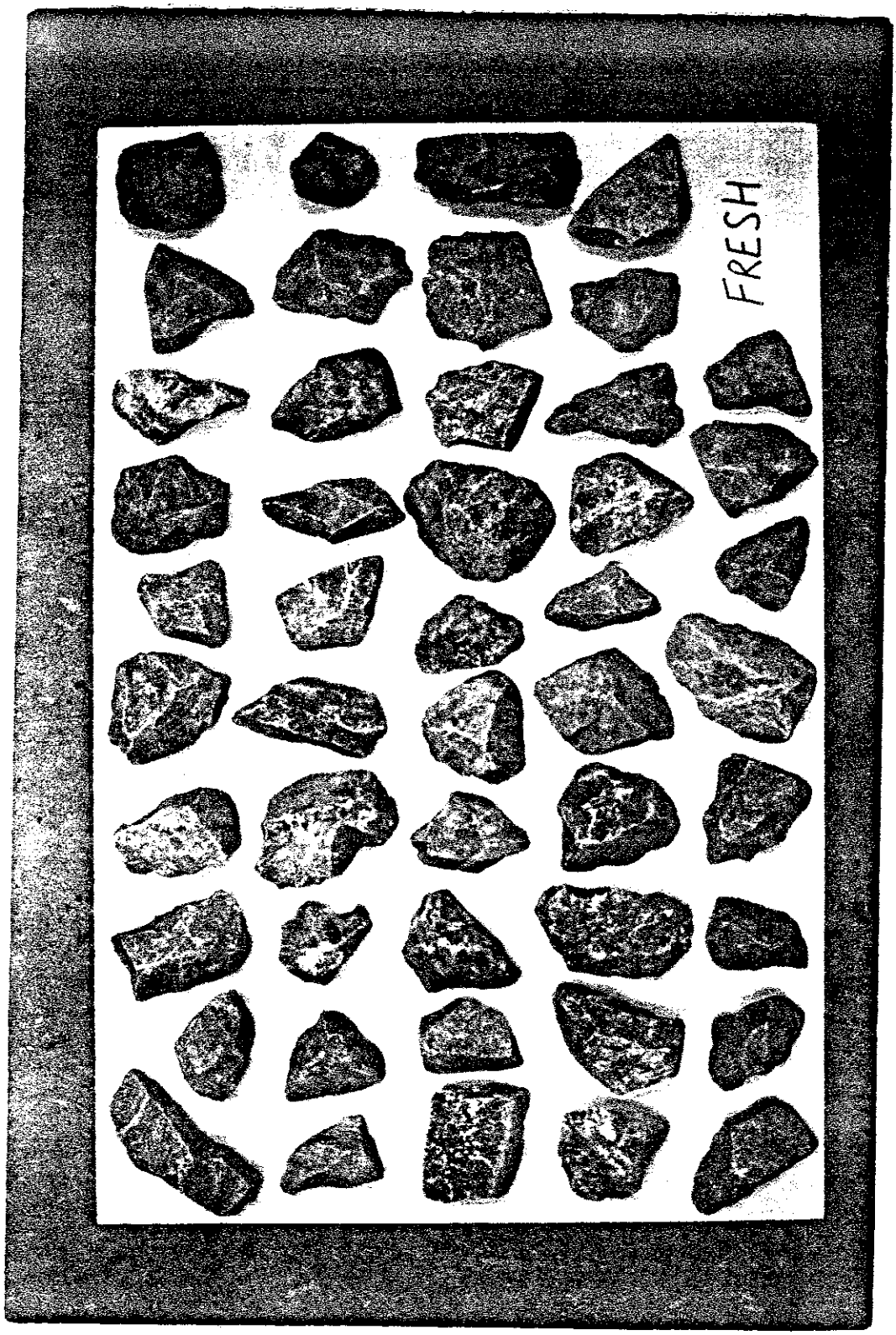

A.7 FRESH blocks - photograph in maximum projection

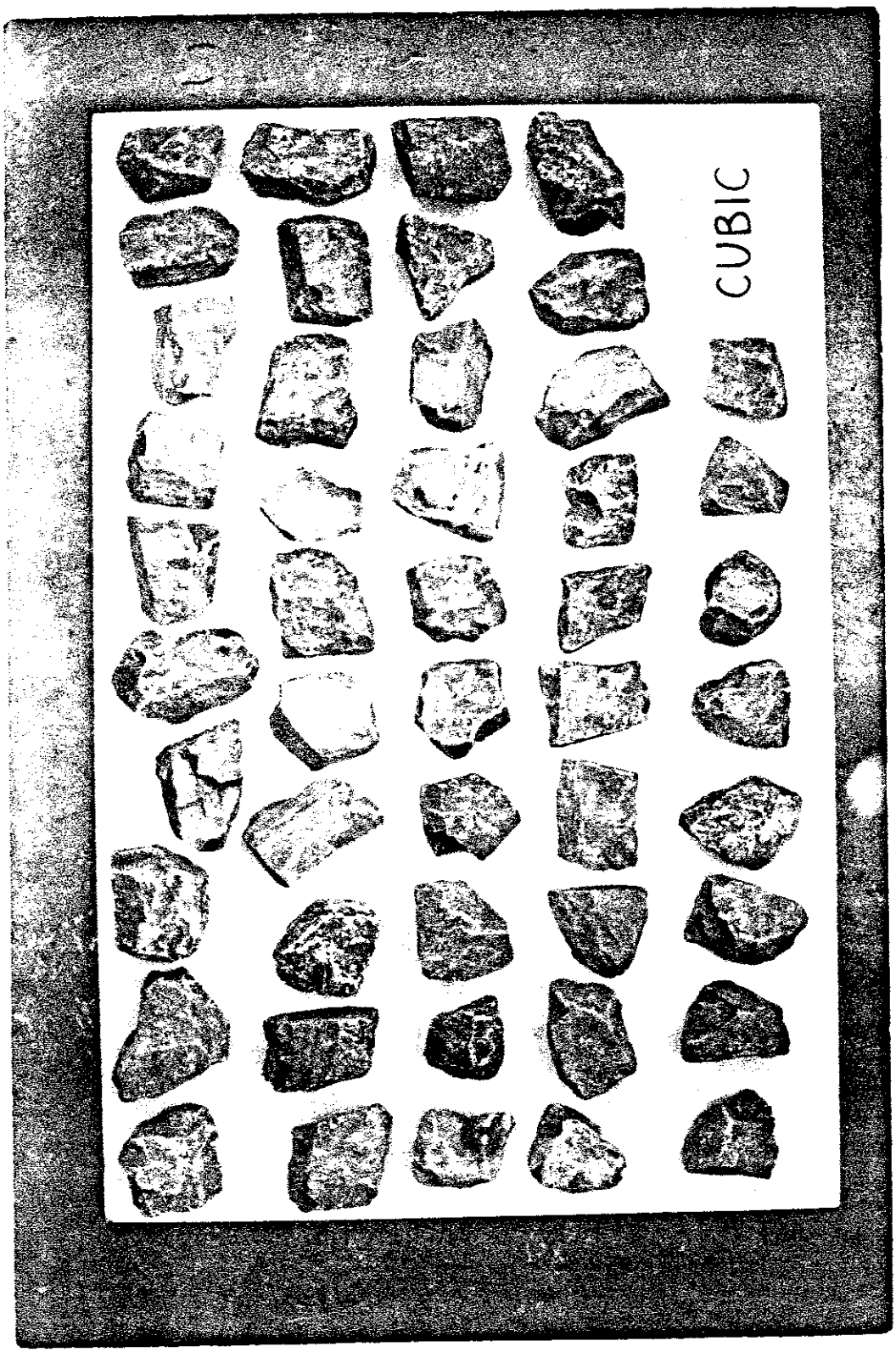

A.8 EQUANT blocks - photograph in maximum projection

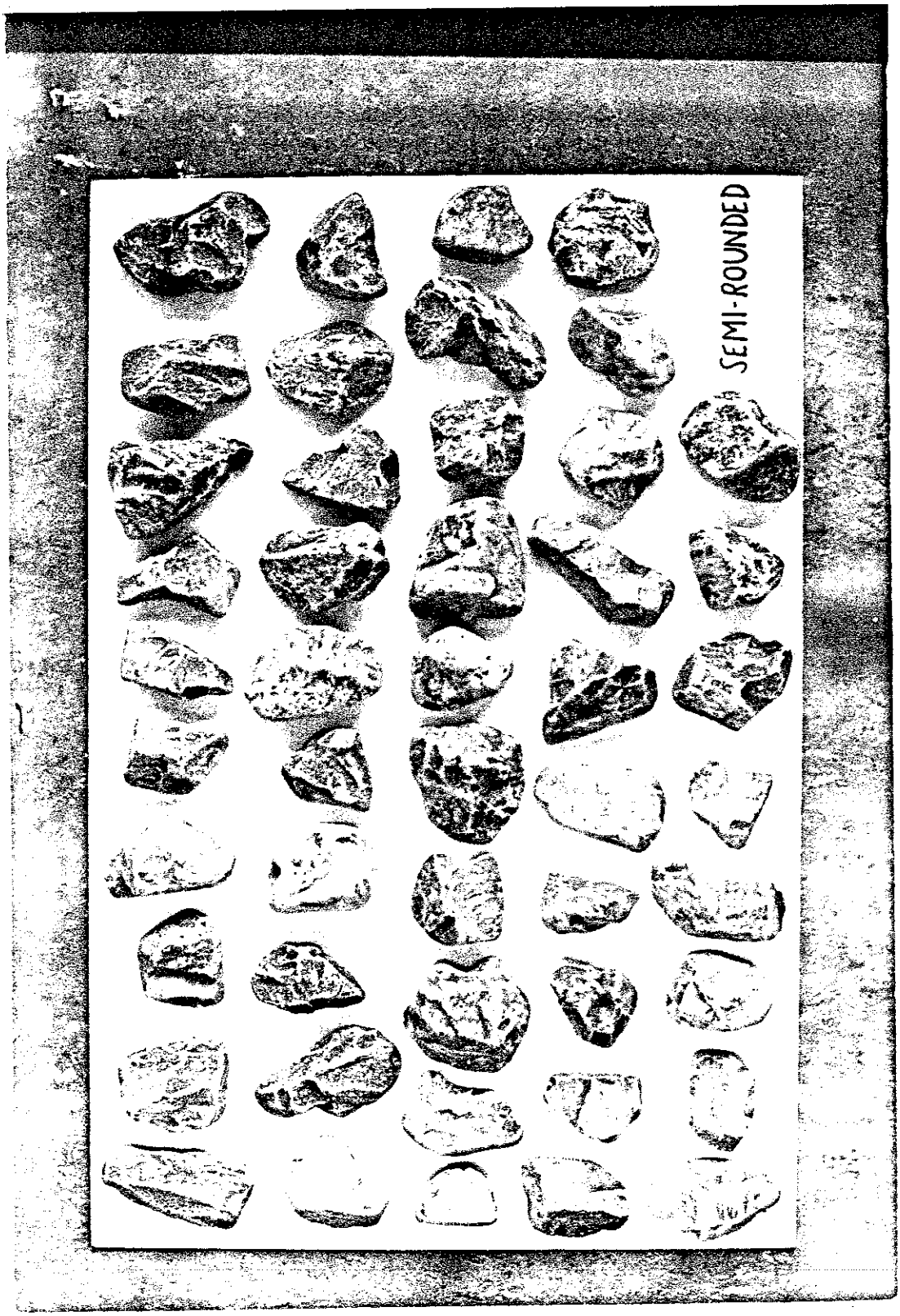

A.9 SEMIROUND blocks - photograph in maximum projection

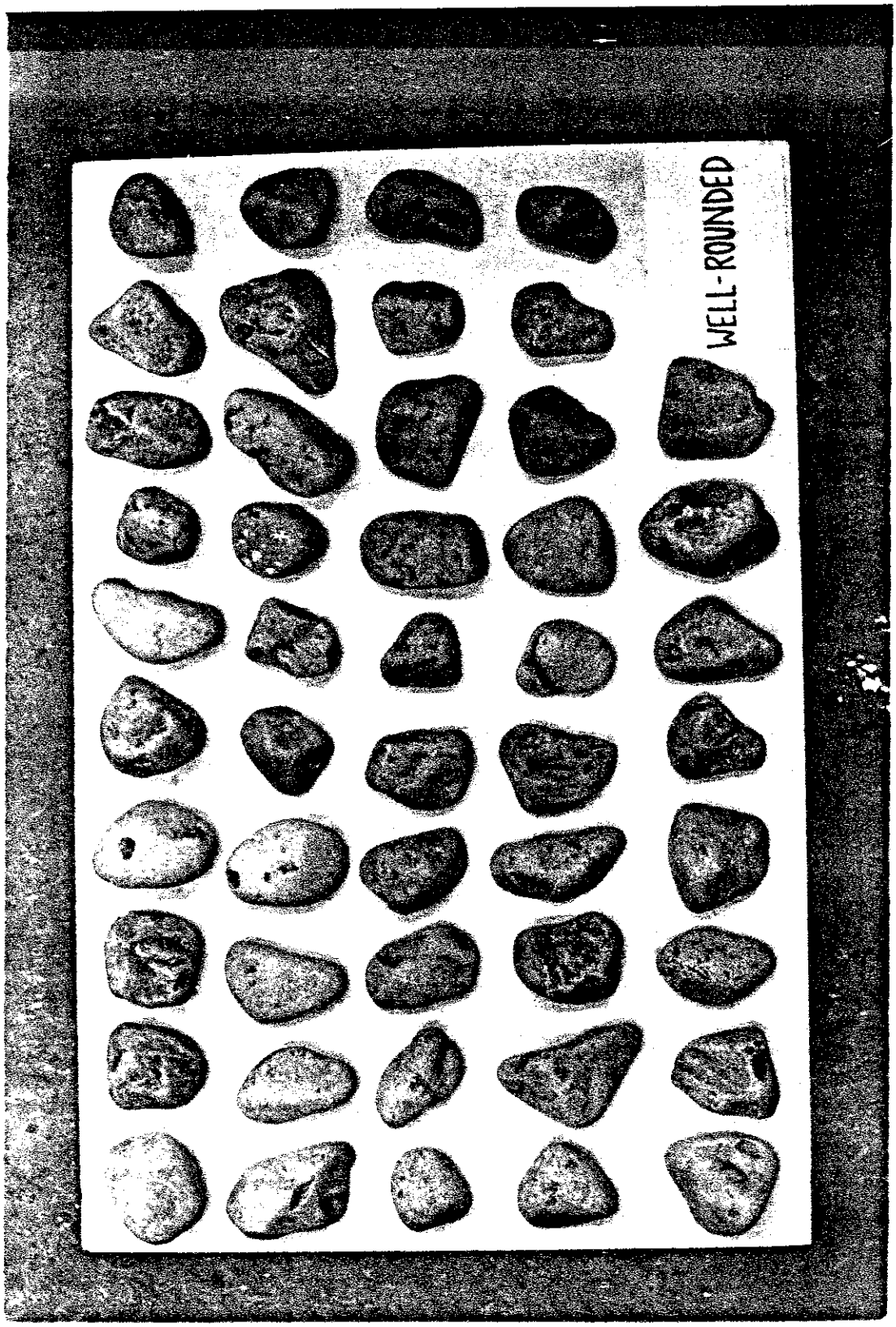

A 10 VERY ROUND blocks - photograph in maximum projection

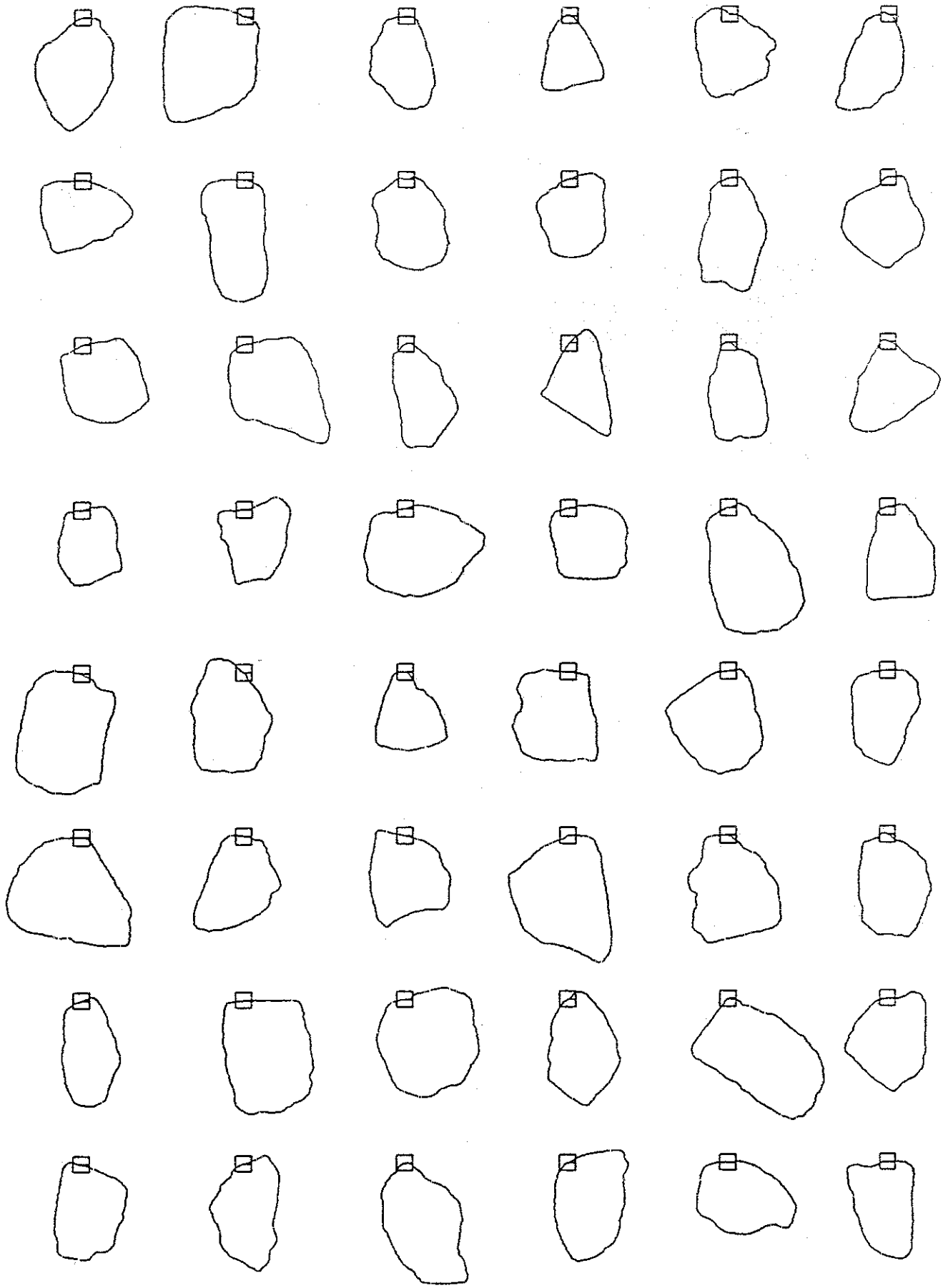

B.1 Delft Hydraulics laboratory sample (DH1) random projection

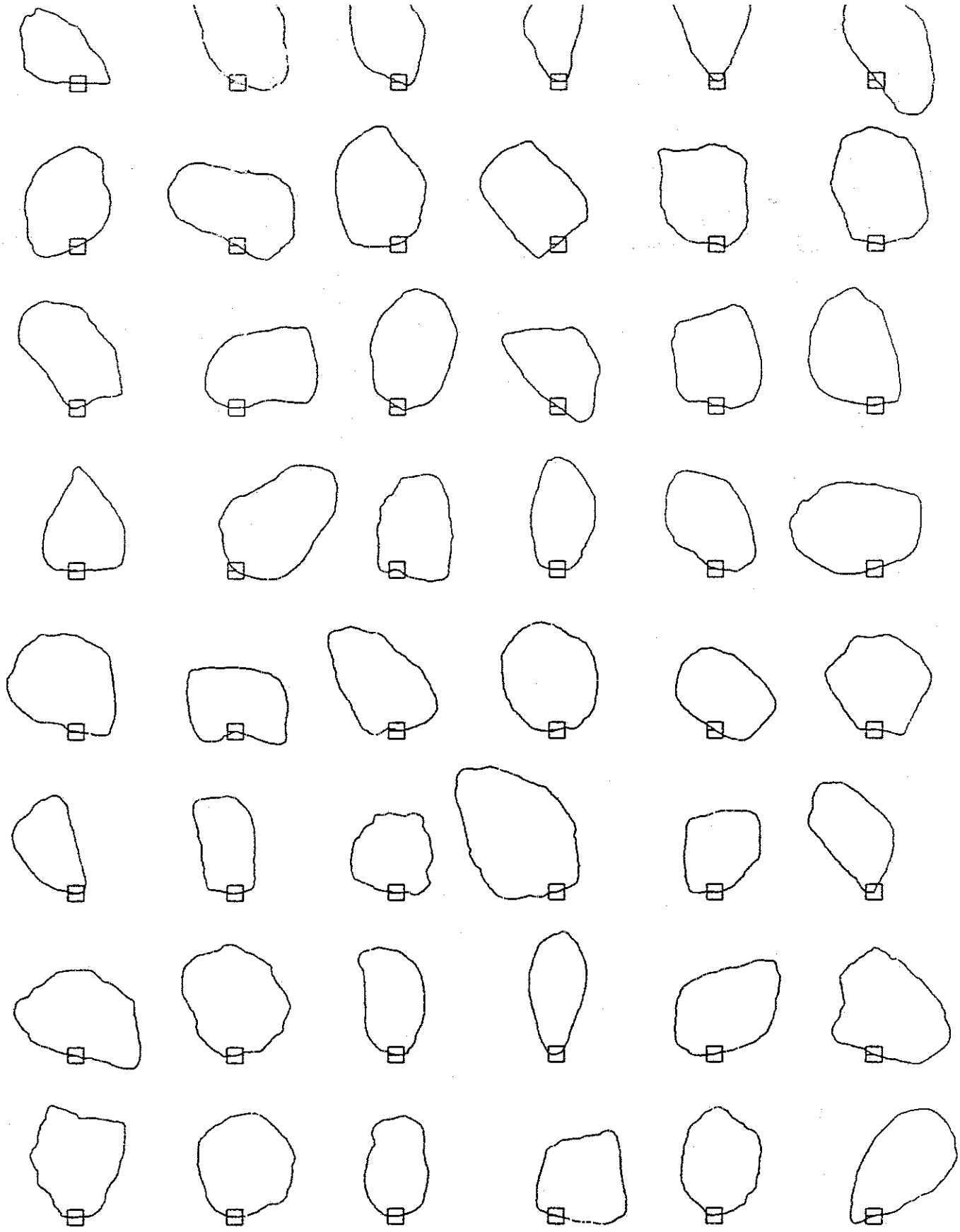

B.2 Delft Hydraulics laboratory sample (DH2) random projection

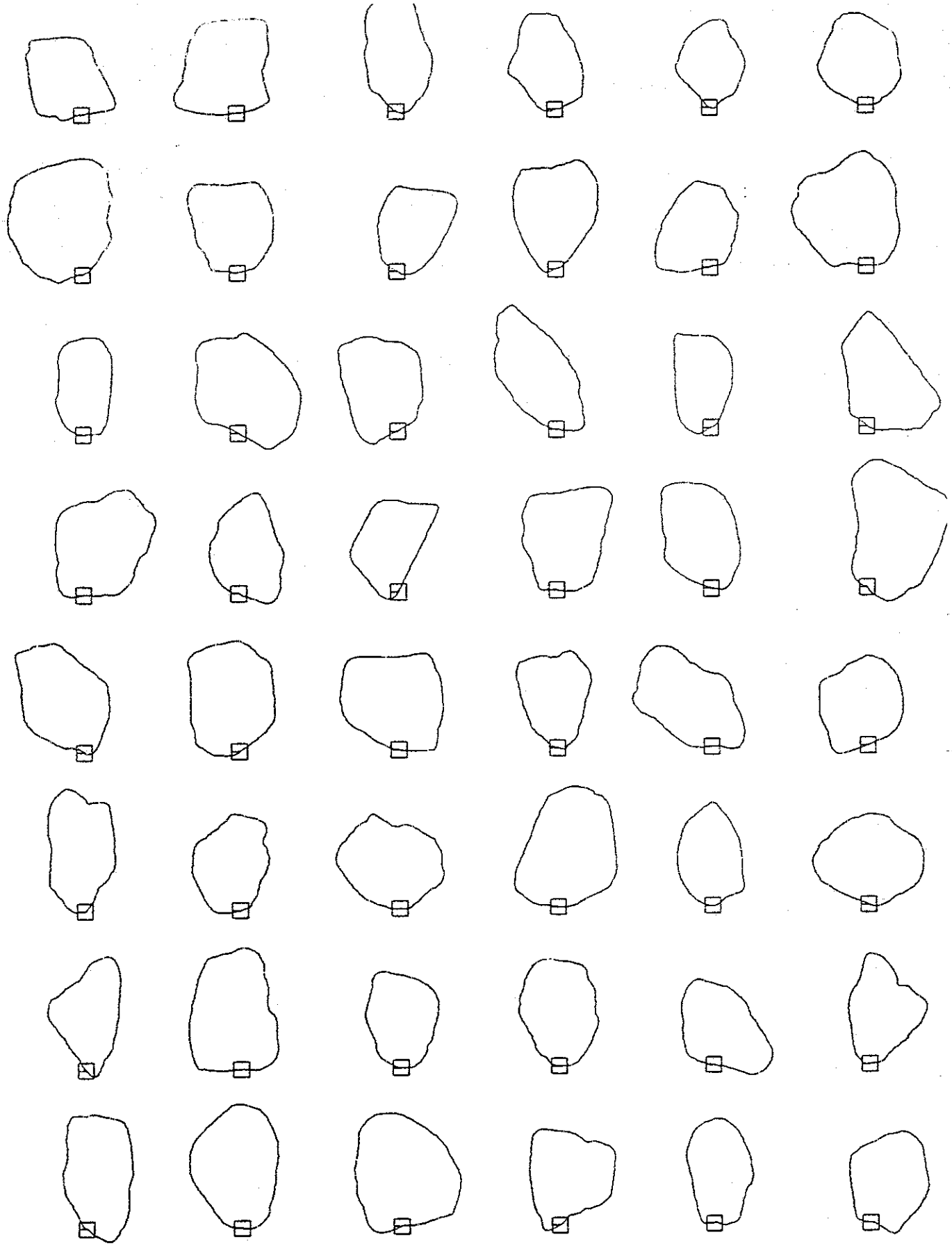

B.3 Delft Hydraulics laboratory sample (DH3) random projection

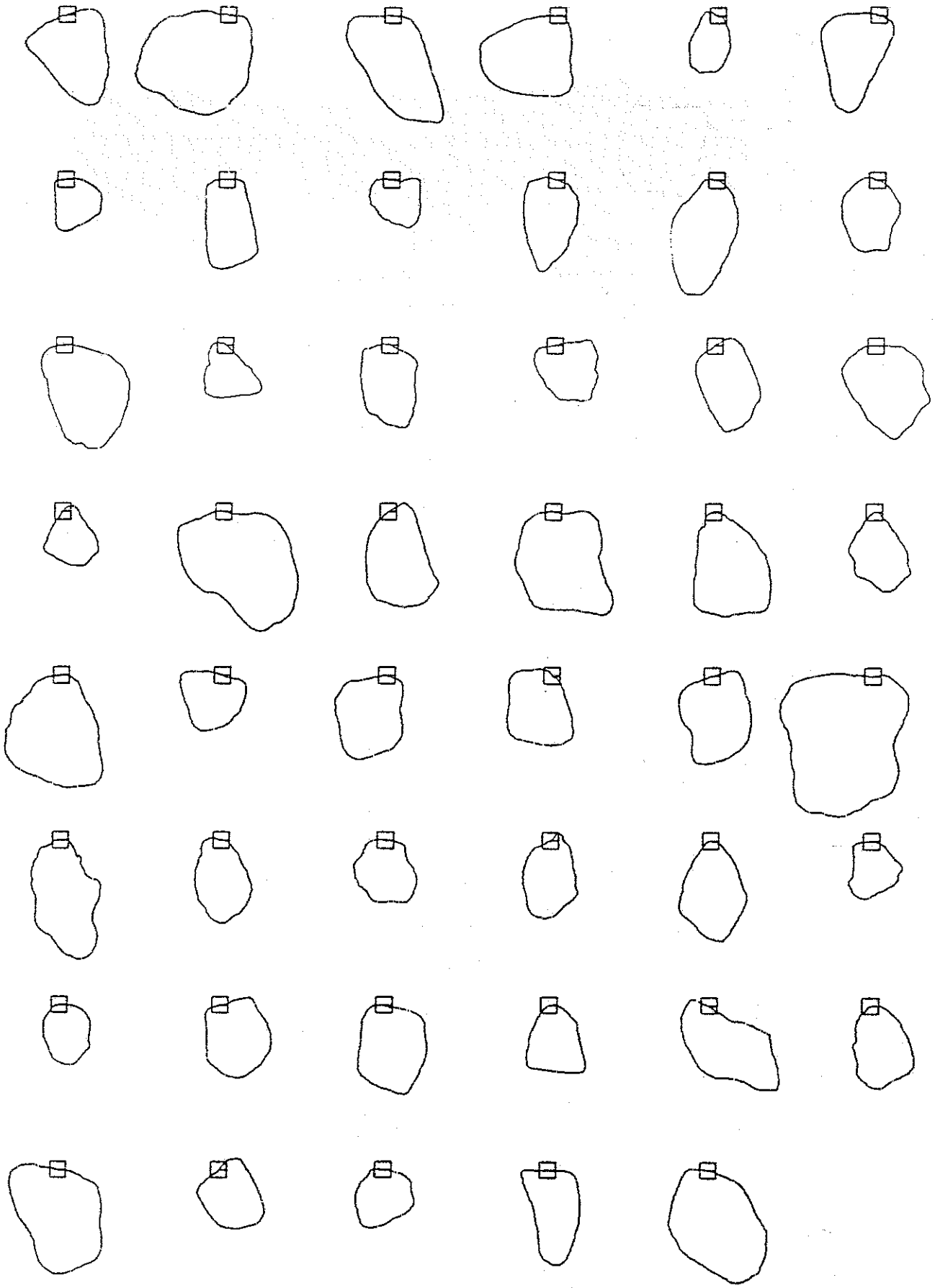

B.4 Delft Hydraulics laboratory sample (DH4) random projection

C.1 A typical angular block from Buckhaven upper photograph

C.2 A typical very round block from Buckhaven lower photograph

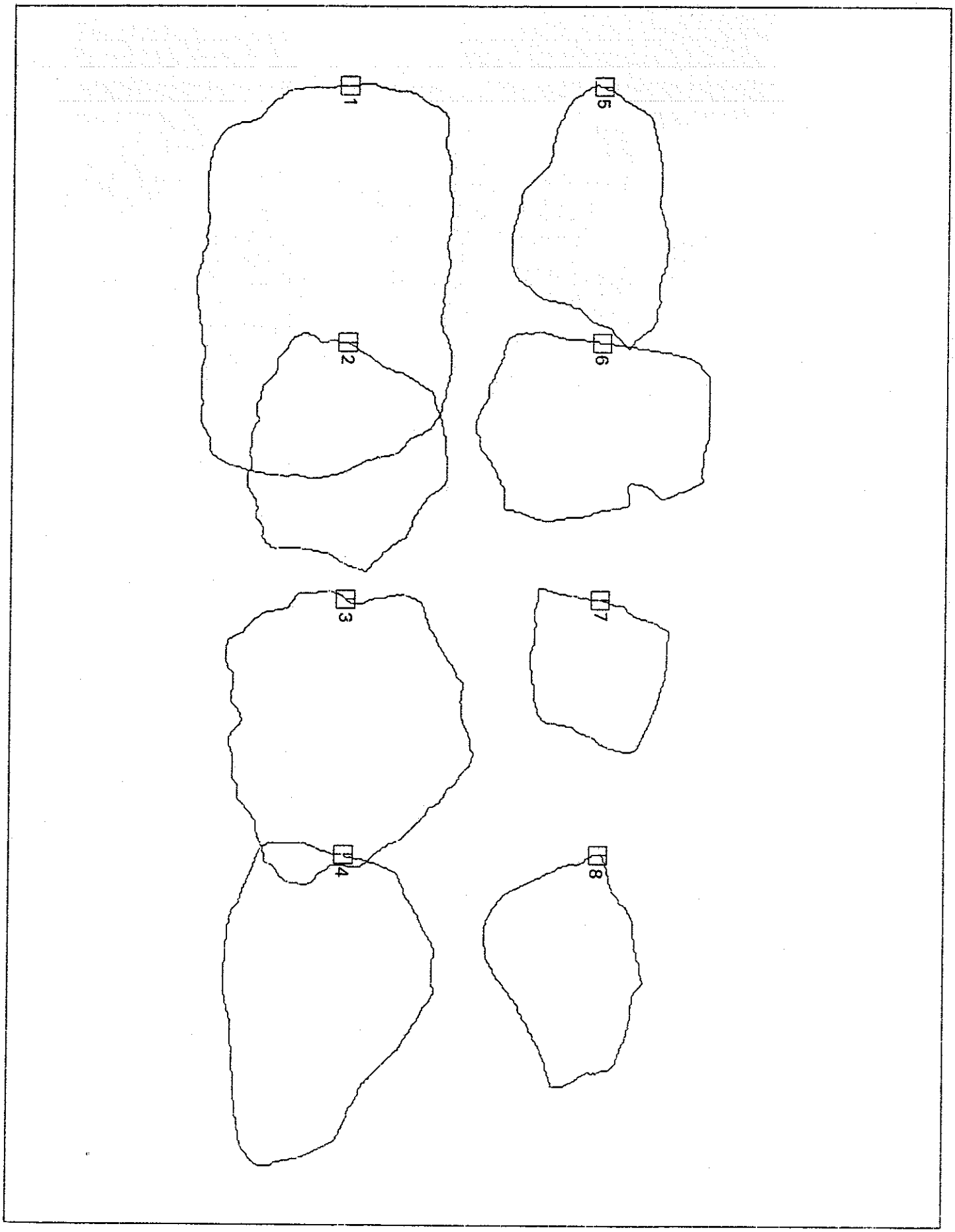

C.3 Digitized outlines of 8 upper blocks from Buckhaven

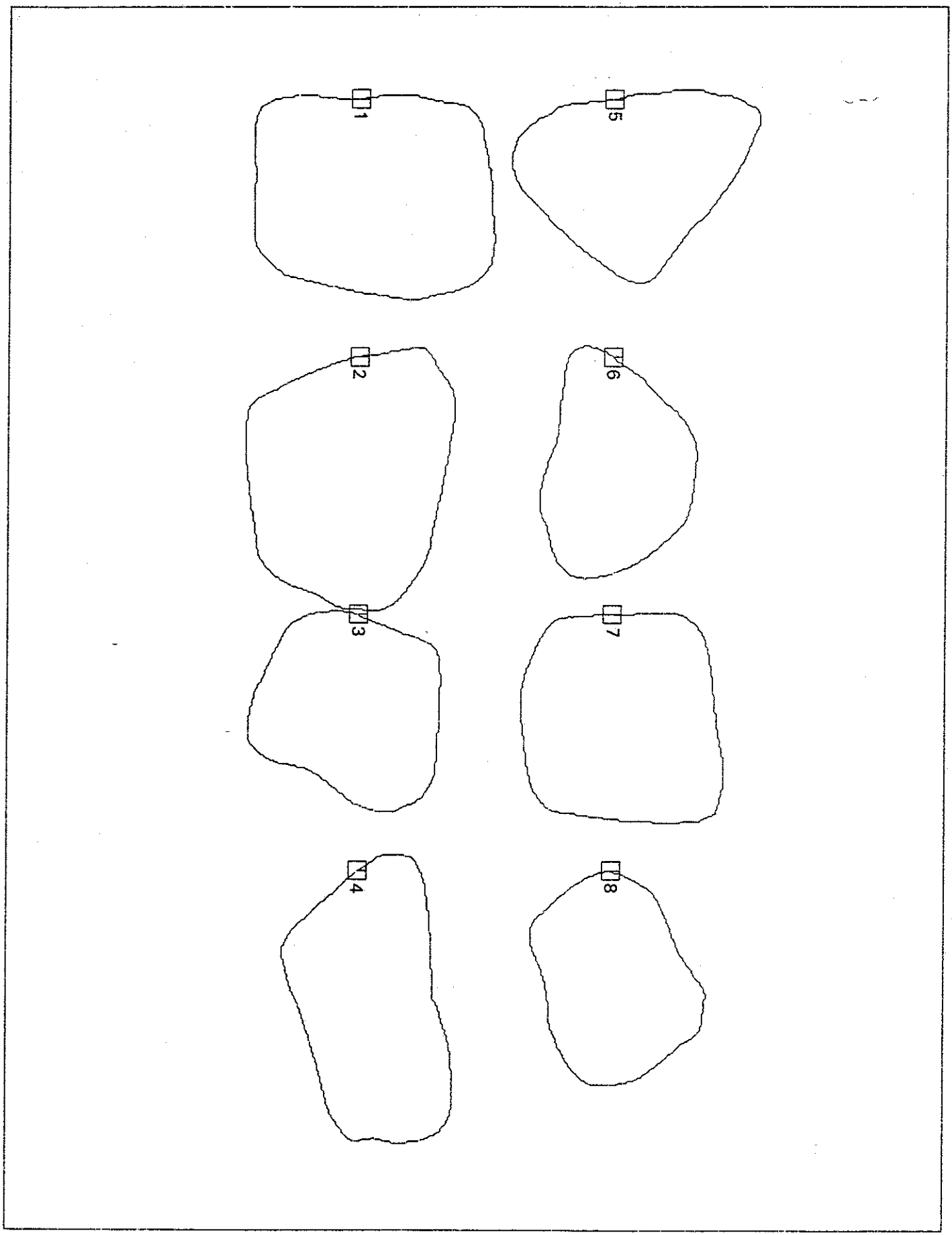

C.4 Digitized outlines of 8 lower blocks from Buckhaven

Table 4.1 : Test conditions

Test	Significant wave height H_s (mm)	Mean Period T_m (secs)	Cross section area A_e (m^2)	Standard deviation of profiles	Armour thickness t(armour) (m)	As laid bulk density (kg/m^3) ρ_b	As laid bulk factor ρ_b/ρ_a	Fictitious Porosity P_f (%)
FRESH :								
FA	50	1.4	0.152	0.006	0.080	1649	0.60	39.58
ZA	50	1.4	0.143	0.008	0.075	1753	0.64	35.78
FB	90	1.4	0.154	0.005	0.081	1628	0.60	40.37
FBR	90	1.4	0.151	0.008	0.079	1660	0.61	39.18
ZB	90	1.4	0.155	0.007	0.082	1618	0.59	40.75
ZBR	90	1.4	0.145	0.008	0.076	1729	0.63	36.66
ZC	120	1.4	0.147	0.009	0.077	1706	0.62	37.53
ZCR	120	1.4	0.149	0.008	0.078	1683	0.62	38.36
ZD	160	1.4	0.148	0.008	0.078	1694	0.62	37.95
FD	160	1.4	0.153	0.010	0.081	1639	0.60	37.98
FF	180	1.4	0.151	0.007	0.079	1660	0.61	39.18
FE	90	2.0	0.152	0.006	0.080	1649	0.60	39.58
FER	90	2.0	0.152	0.009	0.080	1649	0.60	39.58
					0.079	**1670**	**0.61**	**38.81**
EQUANT :								
CA	50	1.4	0.164	0.007	0.086	1661	0.61	39.16
CAR	50	1.4	0.160	0.005	0.084	1702	0.62	37.64
CB	90	1.4	0.150	0.004	0.079	1816	0.67	33.49
CBR	90	1.4	0.161	0.010	0.085	1692	0.62	38.03
CC	120	1.4	0.149	0.005	0.078	1828	0.67	33.04
CCR	120	1.4	0.161	0.006	0.085	1692	0.62	38.03
CD	160	1.4	0.147	0.005	0.077	1853	0.68	32.13
CDR	160	1.4	0.159	0.006	0.084	1713	0.63	37.25
CE	90	2.0	0.164	0.008	0.086	1661	0.61	39.16
CER	90	2.0	0.166	0.022	0.087	1641	0.60	39.90
					0.083	**1726**	**0.63**	**36.78**
SEMIROUND :								
SA	50	1.4	0.132	0.009	0.069	1800	0.66	34.07
SAR	50	1.4	0.136	0.110	0.072	1747	0.64	36.01
SB	90	1.4	0.136	0.010	0.072	1747	0.64	36.01
SBR	90	1.4	0.136	0.008	0.072	1747	0.64	36.01
SC	120	1.4	0.137	0.007	0.072	1734	0.64	36.47
SCR	120	1.4	0.134	0.008	0.071	1773	0.65	35.05
SD	160	1.4	0.136	0.009	0.072	1747	0.64	36.01
SDR	160	1.4	0.136	0.005	0.072	1747	0.64	36.01
SE	90	2.0	0.137	0.011	0.072	1734	0.64	36.47
SER	90	2.0	0.136	0.012	0.072	1747	0.64	36.01
					0.071	**1752**	**0.64**	**35.81**

Table 4.1 (continued) : Test conditions

VERY ROUND :

VA	50	1.4	0.147	0.006	0.077	1875	0.69	31.33
VAR	50	1.4	0.143	0.007	0.075	1927	0.71	29.41
VB	90	1.4	0.138	0.009	0.073	1997	0.73	26.85
VBR	90	1.4	0.138	0.008	0.073	1997	0.73	26.85
VC	120	1.4	0.146	0.008	0.077	1888	0.69	30.86
VCR	120	1.4	0.144	0.008	0.076	1914	0.70	29.90
VD	160	1.4	0.147	0.005	0.077	1875	0.69	31.33
VDR	160	1.4	0.136	0.011	0.072	2026	0.74	25.77
VE	90	2.0	0.140	0.007	0.074	1968	0.72	27.90
VER	90	2.0	0.136	0.025	0.072	2026	0.74	25.77
XB	90	1.4	0.136	0.007	0.072	2026	0.74	25.77
XC	120	1.4	0.138	0.007	0.073	1997	0.73	26.85
XCR	120	1.4	0.139	0.007	0.073	1983	0.73	27.38
XD	160	1.4	0.141	0.005	0.074	1954	0.72	28.41
					0.074	**1961**	**0.72**	**28.17**

TABULAR :

TA	50	1.4	0.146	0.010	0.077	1645	0.60	39.75
TAR	50	1.4	0.139	0.008	0.073	1728	0.63	36.71
TB	90	1.4	0.147	0.010	0.077	1634	0.60	40.16
TBR	90	1.4	0.144	0.007	0.076	1668	0.61	38.91
TC	120	1.4	0.144	0.010	0.076	1668	0.61	38.91
TCR	120	1.4	0.143	0.007	0.075	1679	0.62	38.48
TD	160	1.4	0.140	0.006	0.074	1715	0.63	37.17
TDR	160	1.4	0.146	0.010	0.077	1645	0.60	39.75
TE	90	2.0	0.147	0.008	0.077	1634	0.60	40.16
TER	90	2.0	0.136	0.007	0.072	1766	0.65	35.32
					0.075	**1678**	**0.61**	**38.53**

Table 5.1 : Weight characteristics of armourstone batches used in the tests

Shape	W_{50} (g)	Armour grading D_{85}/D_{15}	Number of stones	Total weight (kg)	Mean weight (g)	Nominal diameter D_{n50} (mm)
TABULAR	330.2	1.21	946	288.186	304.6	49.4
EQUANT	323.2	1.22	1084	326.848	301.5	49.1
FRESH	328.7	1.27	1031	300.863	291.8	49.3
SEMIROUND	318.3	1.27	1012	285.122	281.7	48.9
VERY ROUND	317	1.26	1142	330.698	289.6	48.8
Average	323.5	1.25	1043	306.343	293.6	49.1

Table 5.2 : Subsample gross shape characteristics based on XYZ axial dimensions

SHAPE	SIZE $\sqrt[3]{XYZ}$		FLATNESS[1] (X+Y)/2Z		SPHERICITY[2] $\sqrt[3]{Z/(XY)}$		$(X/Z)_{50}$	$(X/Z)_{85}$	$(X/Z)_{15}$	(X/Z)	
	Mean (mm)	Std. dev. (mm)	Mean	Std. dev.	Mean	Std. dev.				Mean	Std. dev.
TABULAR	62.16	6.24	2.64	0.54	0.549	0.082	3.25	2.81	4.09	3.23	0.67
EQUANT	59.66	5.30	1.64	0.32	0.739	0.089	1.79	1.49	2.26	1.82	0.40
FRESH	63.03	6.80	1.87	0.47	0.689	0.094	2.20	1.81	2.98	2.22	0.57
SEMI ROUND	61.27	7.07	1.88	0.46	0.686	0.106	2.16	1.73	3.07	2.19	0.59
VERY ROUND	59.02	6.13	1.67	0.35	0.734	0.096	2.02	1.47	2.64	1.92	0.48

Note 1 : Wentworth (1922)
Note 2 : The maximum projection or effective settling velocity sphericity, Sneed & Folk (1958)

Table 5.3 : Summary of Fourier and Fractal shape descriptors and size estimates from image analysis of the five shape classes

SHAPE	GROSS SHAPE				ROUGHNESS				SURFACE TEXTURE		SIZE	
	Fourier Shape Contribution Factor P_C				Fourier Asperity Roughness P_R				Fractal Coefficient F		S_i	D_i
	Mean	P_{C50}	P_{C85}	P_{C15}	P_R*	P_{R50}	P_{R85}	P_{R15}	Mean	F_{40}	Pixels	Pixels
TABULAR	2.67	3.03	1.82	4.65	.0165	.0180	.0125	.0325	.014	.017	54.3	122.1
EQUANT	1.43	1.52	1.00	2.21	.0117	.0124	.0095	.0166	.015	.018	52.5	115.8
FRESH	1.88	2.08	1.38	3.06	.0138	.0150	.0107	.0216	.016	.019	52.5	116.6
SEMIROUND	1.89	2.13	1.22	3.19	.0097	.0121	.0080	.0153	.010	.012	51.4	114.7
VERY ROUND	1.55	1.80	1.05	2.64	.0046	.0053	.0035	.0092	.008	.009	49.7	110.7

Note : * indicates log mean P_R

Table 5.4 : Summary of geometric characteristics of armour layers from static models

Name	Symbol	Unit	SPHERES	CUBES	DOLOSSE	FRESH		VERY ROUNDED	
						Tight	Loose	Tight	Loose
Grading	W_{85}/W_{15}					1.26	1.26	1.22	1.22
Fourier shape factor	P_C					1.87	1.87	1.62	1.62
Fourier asperity roughness	P_R					0.0128	0.0128	0.0039	0.0039
Nominal diameter	D_{n50}	mm	14.3	18.0	18.5	21.5	21.5	22.2	22.2
Layer thickness n=1	t_1	mm		16.06	14.61	22.95		25.83	
Layer thickness n=2	t_2	mm	27.80	36.62	29.68	47.53	34.70	52.45	37.43
Normalized thickness n=2	t_2/D_{n50}		1.94	2.03	1.60	2.21	1.61	2.36	1.69
Unit volume	V	cm	2.901	5.832	6.318	9.962	9.962	10.963	10.963
Bulk factor	ρ_L/ρ_a		0.586	0.601	0.430	0.536	0.536	0.621	0.621
As laid bulk factor	ρ_b/ρ_a		0.623	0.643	0.507	0.599	0.600	0.661	0.665
Packing density n=2	N	cm^{-2}	0.60	0.40	0.24	0.29	0.21	0.32	0.23
Fictitious porosity	P_f	%	37.7	35.7	49.3	40.1	40.0	34.0	33.5
Roughness n=1	σ_1	mm		7.68	8.90	7.13		8.86	
Roughness n=2	σ_2	mm	7.45	5.75	10.28	7.41	6.96	7.43	6.46
Normalized roughness n=2	σ_2/D_{n50}		0.521	0.319	0.556	0.344	0.324	0.335	0.291
Layer coefficient	k_Δ		0.97	1.02	0.80	1.10	0.81	1.18	0.84
Fictitious porosity (SPM)	P_f			47	56		37		38
Layer coefficient (SPM)	k_Δ			1.10	0.94		1.00		1.02

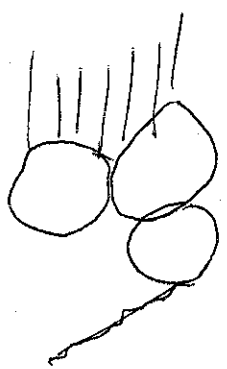

Note : SPM = Shore Protection Manual

Table 5.5 : Topographic roughness and damage from downslope profiles in flume tests

SHAPE	Parameter	0 Waves	1000 Waves	3000 Waves
EQUANT	R_a	0.301	0.305	0.301
	S	0	1.468	1.816
VERY ROUND	R_a	0.201	0.397	0.444
	S	0	5.634	7.153
TABULAR	R_a	0.232	0.284	0.376
	S	0	2.547	5.029
FRESH	R_a	0.273	0.501	0.498
	S	0	2.670	3.666
SEMIROUND	R_a	0.328	0.316	0.328
	S	0	6.121	7.480

Note : For flume profiles, probe width $w_p < 0.5D_{n50}$ and separation $\Delta y = 0.6D_{n50}$

Table 5.6 : Summary of Fourier and Fractal shape descriptors and size estimates from image analysis of Delft Hydraulics samples

	Gross shape				Roughness/Surface texture						Size		
	Mean	P_C(50%)	P_C(85%)	P_C(15%)	P_R*	P_R(50%)	P_R(85%)	P_R(15%)	F **	F ***	S_i	D_i	D_{ef} (mm)
DH1	1.51	1.59	1.12	2.24	0.0115	0.0123	0.0092	0.0163	0.0138	0.0177	61.30	133.40	48.02
DH2	1.52	1.77	1.12	2.25	0.0107	0.0114	0.0081	0.0167	0.0115	0.0148	66.30	145.80	52.49
DH3	1.43	1.45	1.05	2.14	0.0093	0.0103	0.0075	0.0142	0.0104	0.0131	66.40	145.60	52.42
DH4	1.46	1.55	1.08	2.30	0.0085	0.0101	0.0063	0.0132	0.0119	0.0140	53.10	115.90	41.72

Note 1 : P_R^* = log mean P_R

Note 2 : ** f = 0.36mm so that F refers to roughness on a scale of 1.1 to 3.6mm.

Note 3 : *** F_{40} refers to roughness on a scale normalized relative to the average block diameter and assuming S_i = 40.

Table 5.7 : Shape characteristics of armour layers - a summary

Shape	Layer thickness t(armour)	Porosity P_f	Layer coefficient k_Δ	Nominal diameter D_{n50}	P_C	P_R	X/Z (50% valu
TABULAR	75.4	38.1	0.761	49.4	2.67	0.0182	3.25
EQUANT	83.2	36.3	0.845	49.1	1.43	0.0121	1.7
FRESH	79.0	38.4	0.799	48.8	1.88	0.0147	2.2
SEMIROUND	71.4	35.3	0.729	48.8	1.89	0.0109	2.16
VERYROUND	74.0	27.6	0.757	49.3	1.55	0.0055	2.0
Average	76.6	35.1	0.778	49.1			

Table 6.1 : Damage analysis

Test	$H_s / \Delta D_{n50}$	ξ_m Surf similarity (S=surging) (P=plunging)		Damage S at 1000 waves	Damage S at 3000 waves	Dimensionless damage $S/\sqrt{N}$ at 1000 waves	Dimensionless damage $S/\sqrt{N}$ at 3000 waves
FRESH :							
FA	0.588	3.91	S	1.965	-	0.0621	-
FA2R	0.588	3.91	S	1.104	-	0.0349	-
ZA	0.588	3.91	S	0.113	0.257	0.0036	0.0047
FB	1.058	2.92	P	1.338	-	0.0423	-
FBR	1.058	2.92	P	2.394	3.441	0.0757	0.0628
ZB	1.058	2.92	P	2.840	4.877	0.0898	0.0890
ZBR	1.058	2.92	P	0.588	0.978	0.0186	0.0179
ZC	1.410	2.52	P	3.635	8.419	0.1064	0.1537
ZCR	1.410	2.52	P	1.861	2.665	0.0588	0.0487
FD	1.880	2.19	P	2.960	15.332	0.0936	0.2799
FDR	1.880	2.19	P	5.904	17.049	0.1867	0.3113
ZD	1.880	2.19	P	3.114	4.729	0.0985	0.0863
FE	2.115	2.06	P	15.522	31.557	0.4908	0.5761
FF	1.058	4.17	S	2.761	5.650	0.0873	0.1032
FFR	1.058	4.17	S	4.107	8.960	0.1299	0.1636
EQUANT :							
CA	0.588	3.91	S	1.372	0.173	0.0434	0.0032
CAR	0.588	3.91	S	1.090	1.431	0.0345	0.0261
CB	1.058	2.92	P	2.946	3.387	0.0932	0.0618
CBR	1.058	2.92	P	0.917	1.511	0.0290	0.0276
CC	1.410	2.52	P	2.488	9.221	0.0787	0.1684
CCR	1.410	2.52	P	1.468	0.666	0.0464	0.0122
CD	1.880	2.19	P	12.676	15.049	0.4009	0.3378
CDR	1.880	2.19	P	3.017	11.100	0.0954	0.2027
CE	1.058	4.17	P	0.500	0.756	0.0158	0.0138
CER	1.058	4.17	P	0.921	0.905	0.0291	0.0165
SEMIROUND :							
SA	0.588	3.91	S	0.278	0.348	0.0088	0.0064
SAR	0.588	3.91	S	0.367	0.829	0.0116	0.0151
SB	1.058	2.92	P	1.590	2.805	0.0503	0.0512
SBR	1.058	2.92	P	1.216	1.147	0.0385	0.0209
SC	1.410	2.52	P	4.888	11.355	0.1546	0.2073
SCR	1.410	2.52	P	4.662	6.019	0.1474	0.1099
SD	1.880	2.19	P	5.990	12.021	0.1894	0.2195
SDR	1.880	2.19	P	7.464	9.703	0.2360	0.1772
SE	1.058	4.17	S	2.175	2.612	0.0688	0.0477
SER	1.058	4.17	S	1.624	1.257	0.0514	0.0229

Table 6.1 continued : Damage analysis

VERY ROUND :

VA	0.588	3.91	S	0.145	0.091	0.0046	0.0017
VAR	0.588	3.91	S	0.565	1.404	0.0179	0.0256
VB	1.058	2.92	P	0.594	1.056	0.0188	0.0193
VBR	1.058	2.92	P	4.220	10.001	0.1334	0.1826
XB	1.058	2.92	P	0.527	0.502	0.0167	0.0092
VC	1.410	2.52	P	11.734	5.742	0.0548	0.1048
VCR	1.410	2.52	P	3.666	5.749	0.1159	0.1050
XC	1.410	2.52	P	3.764	5.849	0.1190	0.1068
XCR	1.410	2.52	P	2.254	4.220	0.0713	0.0770
VD	1.880	2.19	P	7.414	13.178	0.2345	0.2406
VDR	1.880	2.19	P	17.154	-	0.5425	-
XD	1.880	2.19	P	8.205	-	0.2595	-
VE	1.058	4.17	S	1.521	4.049	0.0481	0.0739
VER	1.058	4.17	S	7.157	15.624	0.2263	0.3189

TABULAR :

TA	0.588	3.91	S	0.413	0.550	0.0131	0.01
TAR	0.588	3.91	S	0.424	1.129	0.0134	0.0206
TB	1.058	2.92	P	0.785	0.789	0.0248	0.0144
TBR	1.058	2.92	P	1.052	1.351	0.0333	0.0247
TC	1.410	2.52	P	2.029	3.723	0.0642	0.0680
TCR	1.410	2.52	P	1.680	4.529	0.0531	0.0827
TD	1.880	2.19	P	6.341	11.281	0.2005	0.2060
TDR	1.880	2.19	P	3.602	7.900	0.1139	0.1442
TE	1.058	4.17	S	0.222	0.306	0.0070	0.0056
TER	1.058	4.17	S	-	0.395	-	0.0072

Table 8.1 : Correlation of Portland limestone wear from mill abrasion test with prototype wear near block A at West Bay

Fractional weight remaining W/W_o	Fourier asperity roughness P_R	Revolutions in abrasion mill (thousands)	Time (years) exposed to conditions near block A at West Bay			
			W_o = 15 tonnes	8 tonnes	2.5 tonnes	1.0 tonne
			D_n = 1.82m	1.47m	1.0m	0.74m
			x = 1.0	0.81	0.55	0.41
1.000	0.0135	0	0	0	0	0
0.981	0.0112	1	1	0.81	0.55	0.41
0.965	0.0094	2	2	1.62	1.10	0.81
0.930	0.0065	5	5	4.06	2.75	2.03
0.891	0.0049	10	10	8.11	5.49	4.06

Note : P_R values are based on the abrasion mill theory given in Latham & Poole, 1988 with experimentally determined coefficients b = 0.95, k_f = -0.30, k_s = -0.0067 and estimated P_L and P_O values

Table 8.2 : Equivalent wear factors for different block sizes and environmental site conditions in the intertidal zone of a breakwater

Armourstone size		EQUIVALENT WEAR FACTOR x			
W_o (tonnes)	D_{n50} (m)	Mild environment static design	Average	Aggressive environment static design shingle attack	Aggressive environment dynamically adjusting design
15	1.82	6.2	2.5	1.2	0.62
10	1.59	5.4	2.2	1.1	0.54
8	1.47	5.0	2.0	1.0	0.50
5	1.26	4.3	1.6	0.8	0.43
2.5	1.00	3.4	1.4	0.7	0.34
1	0.74	2.5	1.0	0.5	0.25

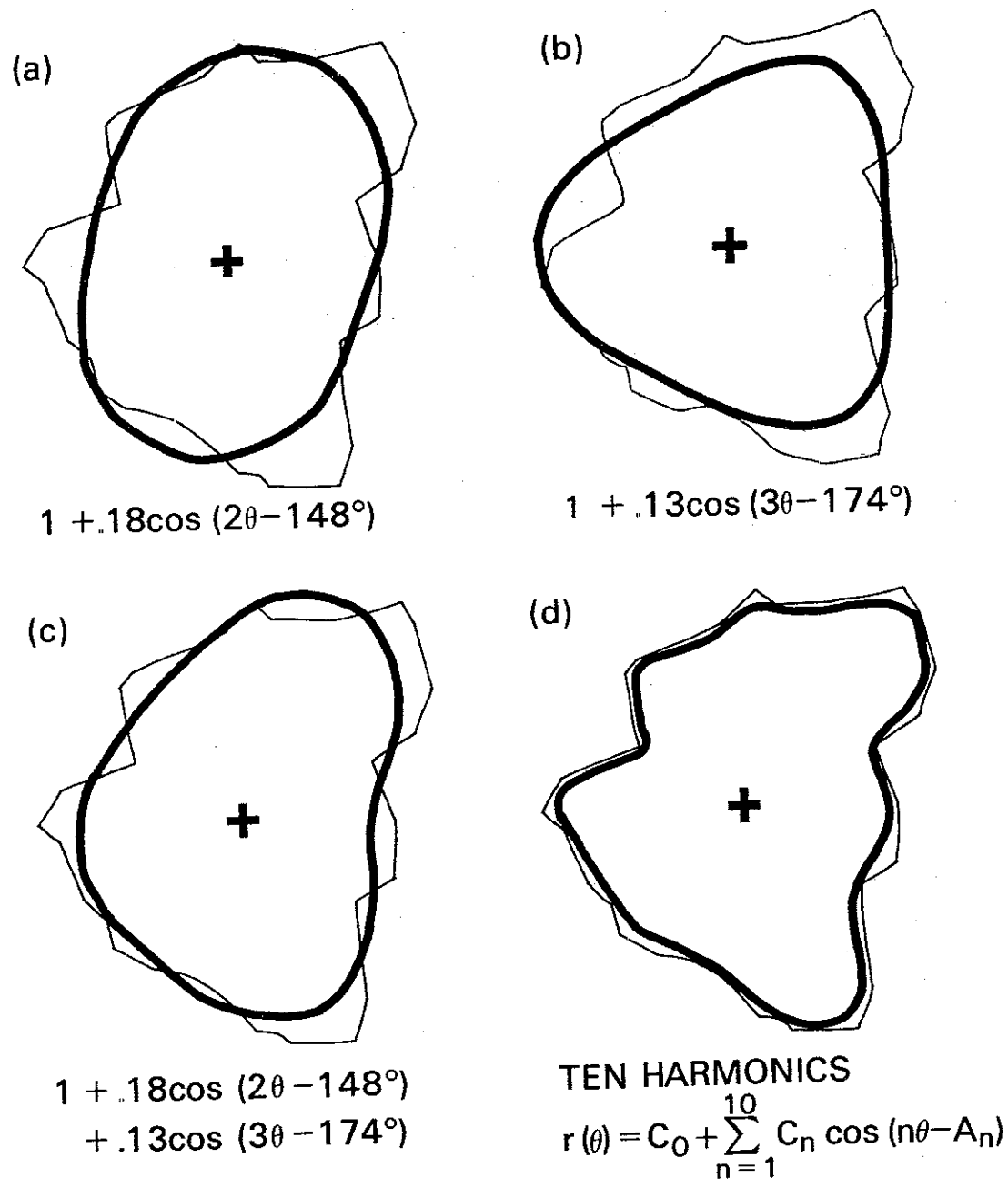

Figure 2.1 Harmonic contributions to shape, after Ehrlich & Weinberg (1970). The thin line represents the digitized coordinates; (a) and (b) show the contribution of the second and third harmonics respectively. In (c), their combined contributions are shown and (d) which includes the first 10 harmonics gives quite a good approximation.

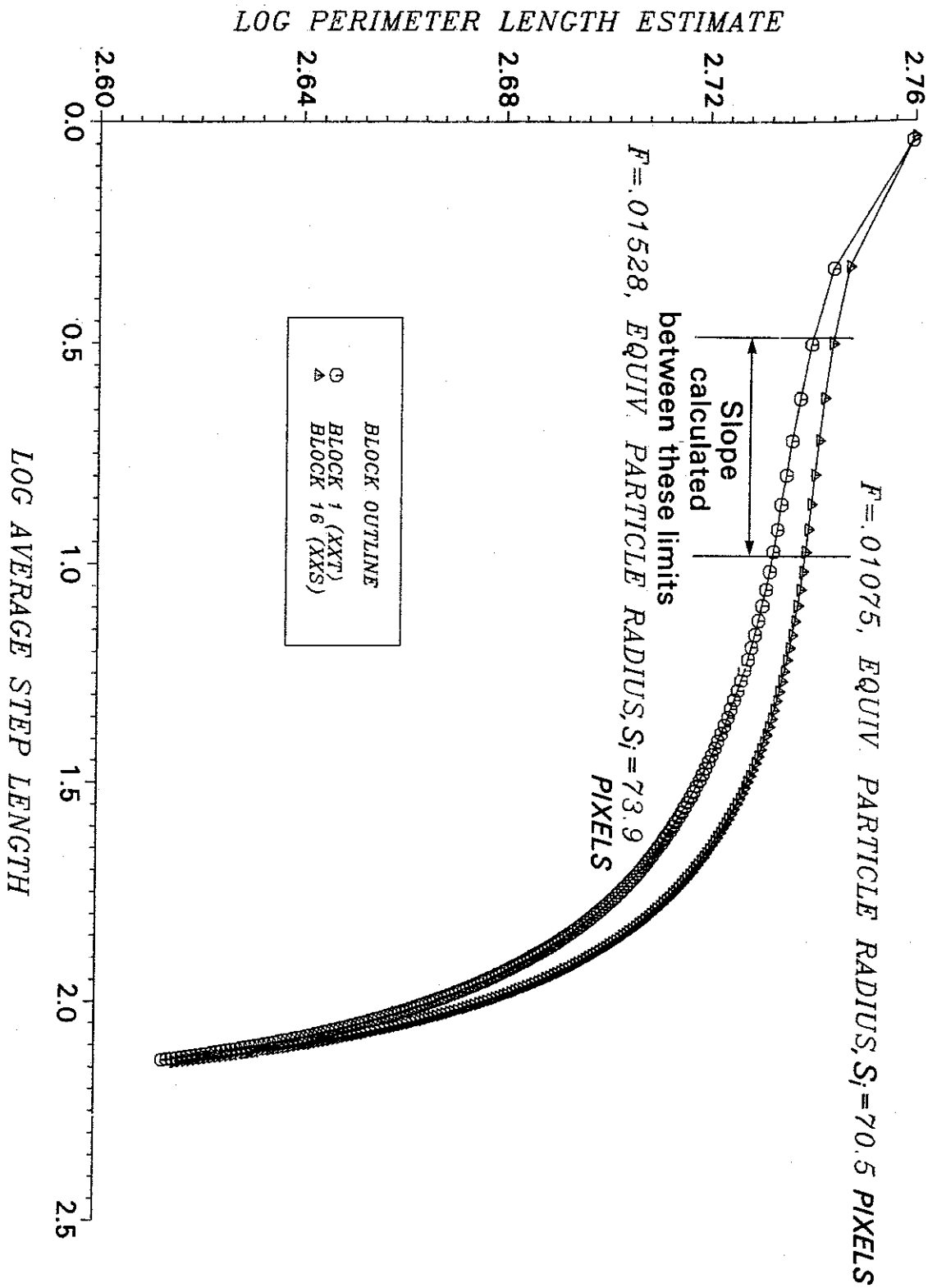

Figure 2.2 Mendelbrot-Richardson plot for two block outlines from Herne Bay. The Fractal coefficient F is calculated using the Schwarz & Exner (1980) algorithm for step lengths between 3 and 10 pixels.

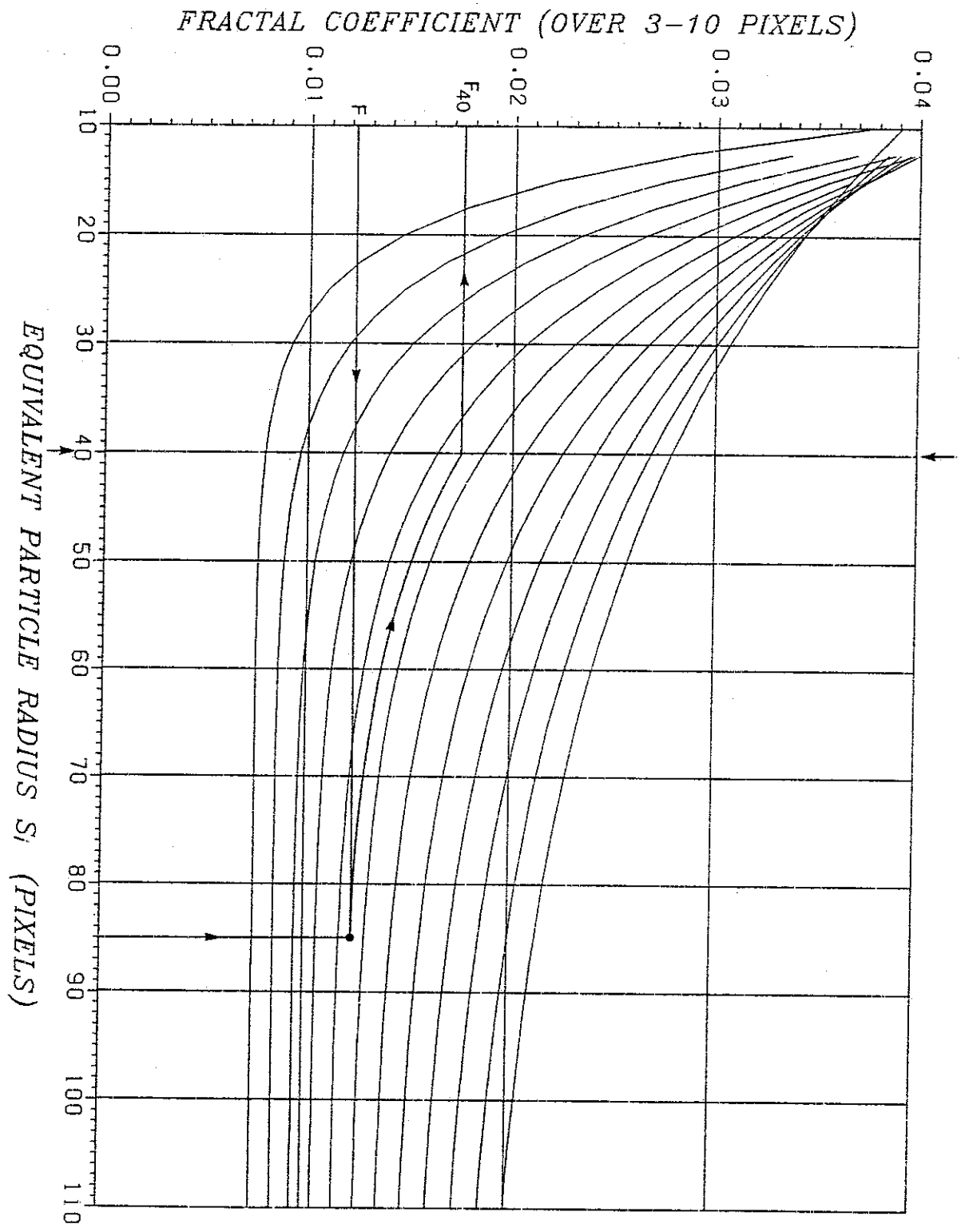

Figure 2.3 Calculation of the corrected Fractal coefficient F_{40} for a video image equivalent particle radius S_i of about 40 pixels. (The correction curves were developed in Latham, 1987).

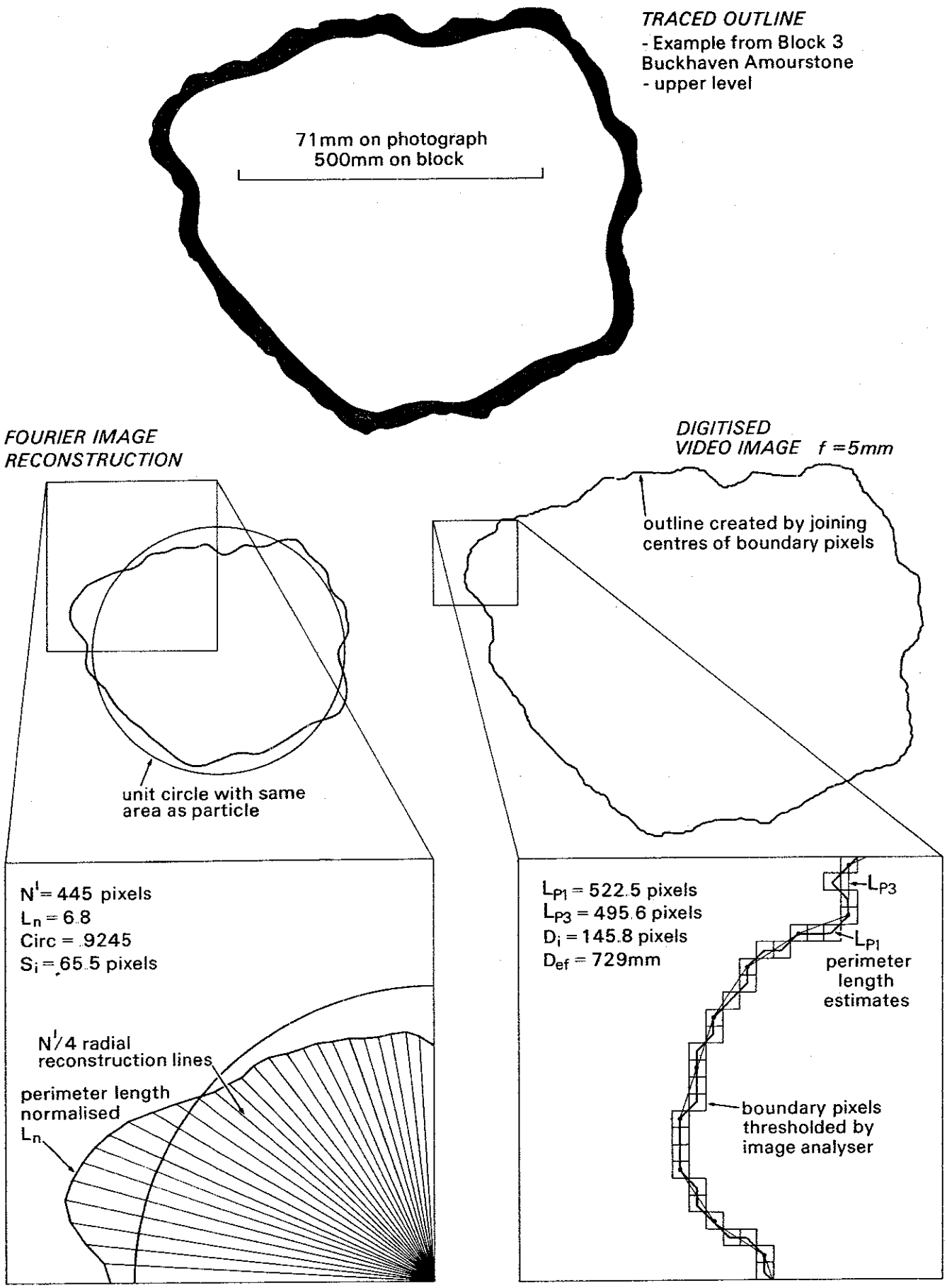

Figure 2.4 Digitization and Fourier reconstructed normalised outline with explanation of size parameters. See also **Appendix C.**

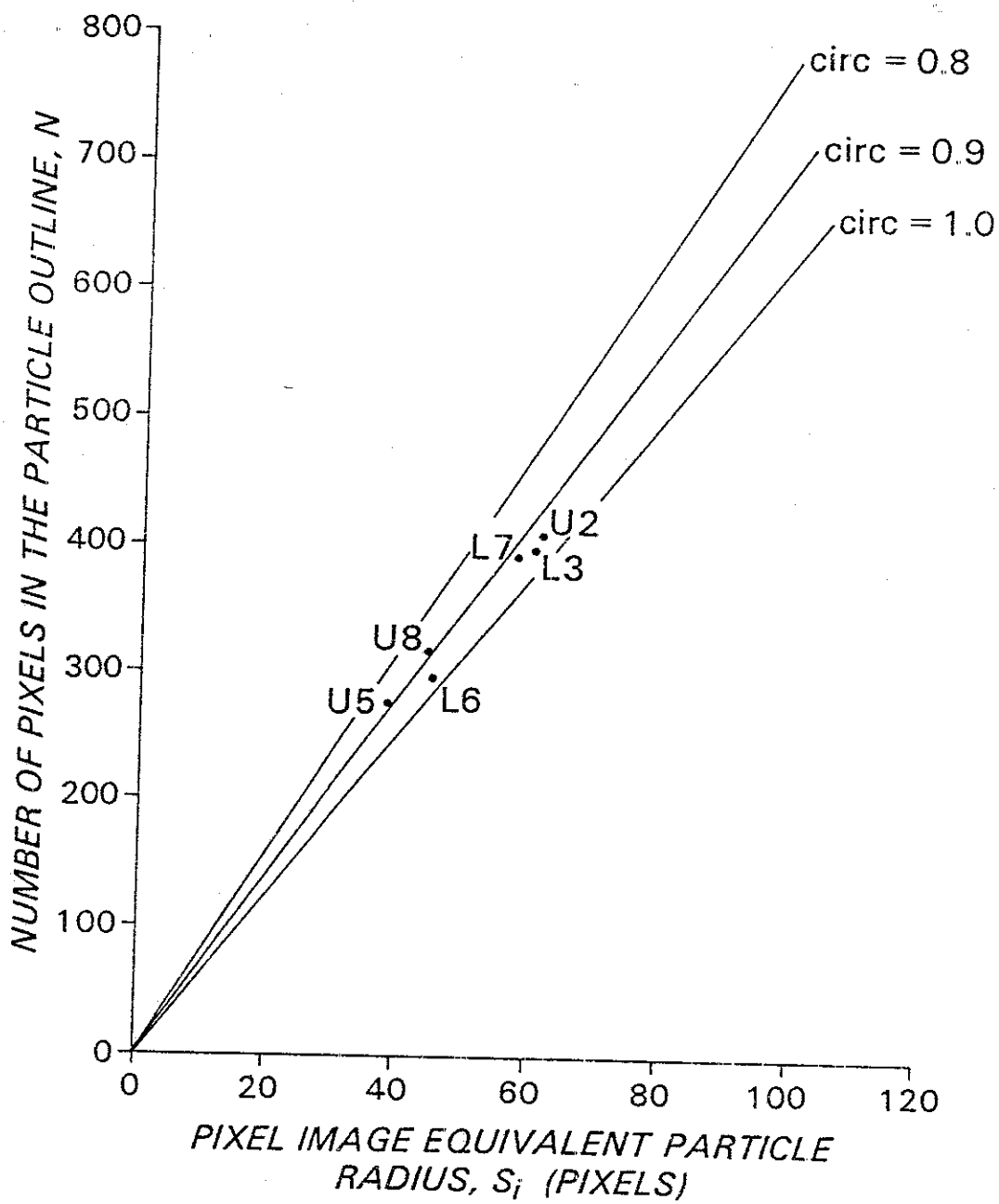

Figure 2.5 Relationship between the number of pixels in the outline, N' and the video image equivalent particle radius, Si. Example data from Buckhaven (U - upper, L - lower), see Appendix C.

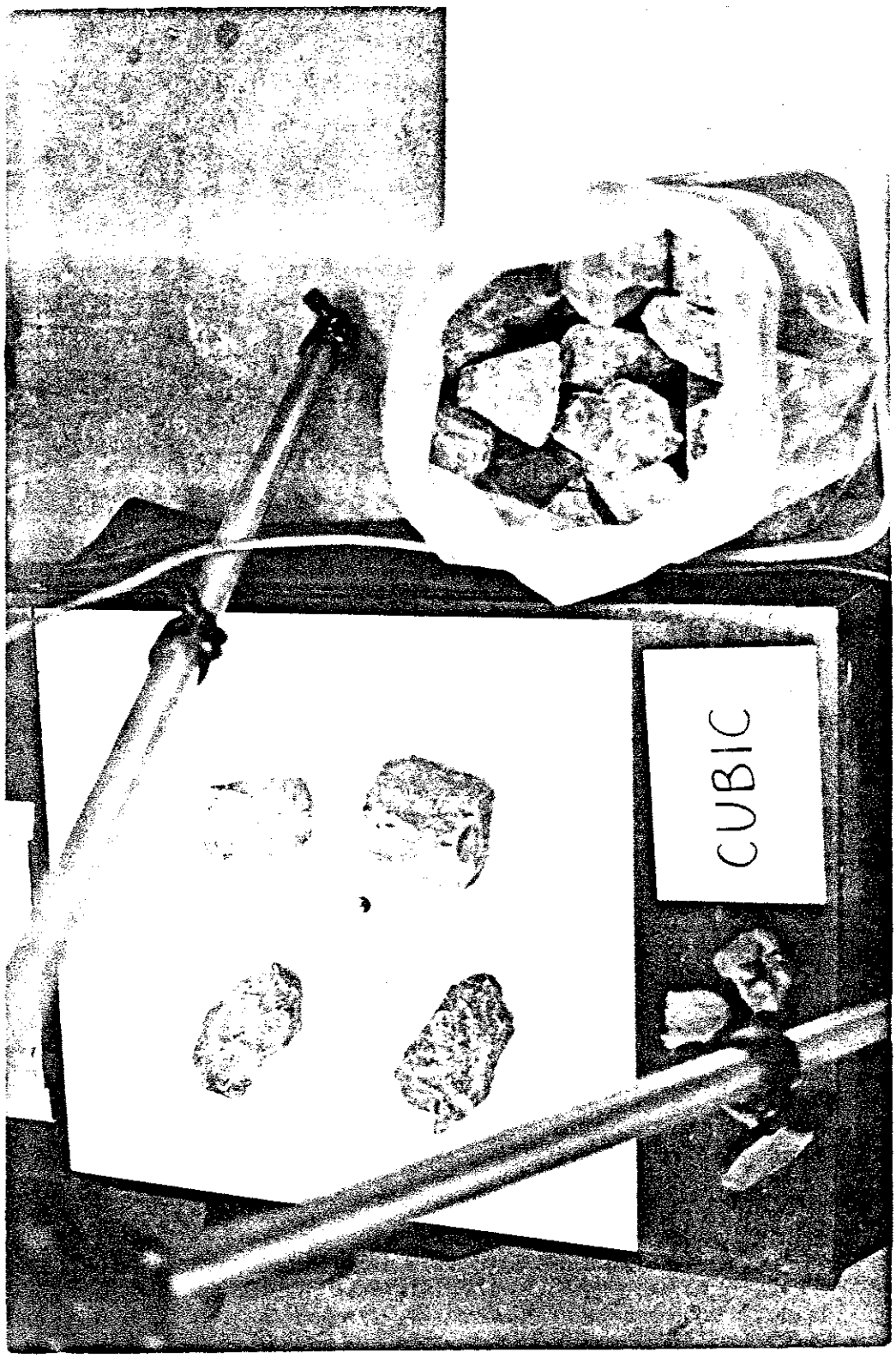

Figure 2.6 Illustration of procedure for obtaining random projections of blocks on light table using plasticene to obtain random orientations from inside plastic bag.

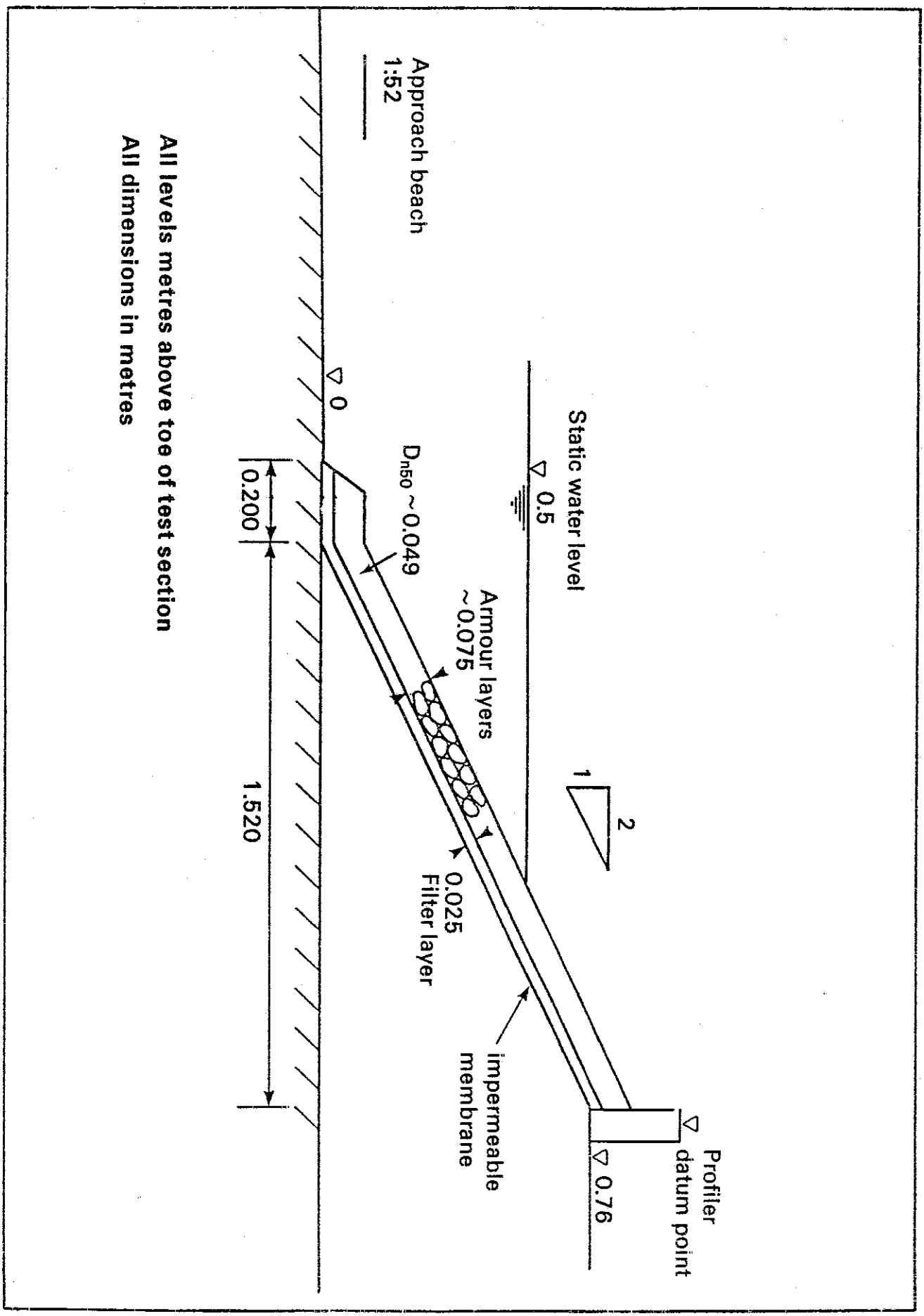

Figure 4.1 Cross-section through the model test section.

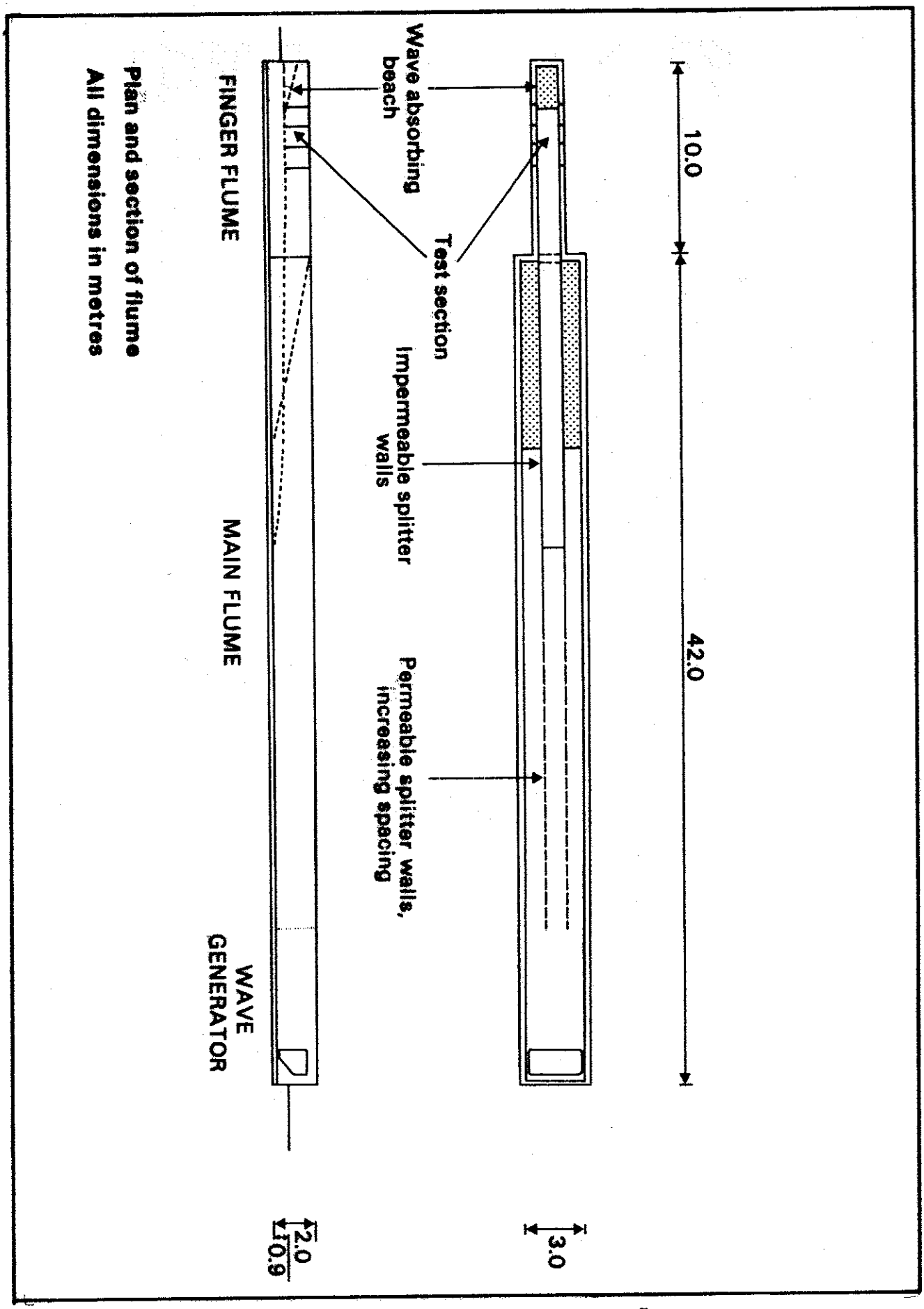

Figure 4.2 Plan of deep random wave flume

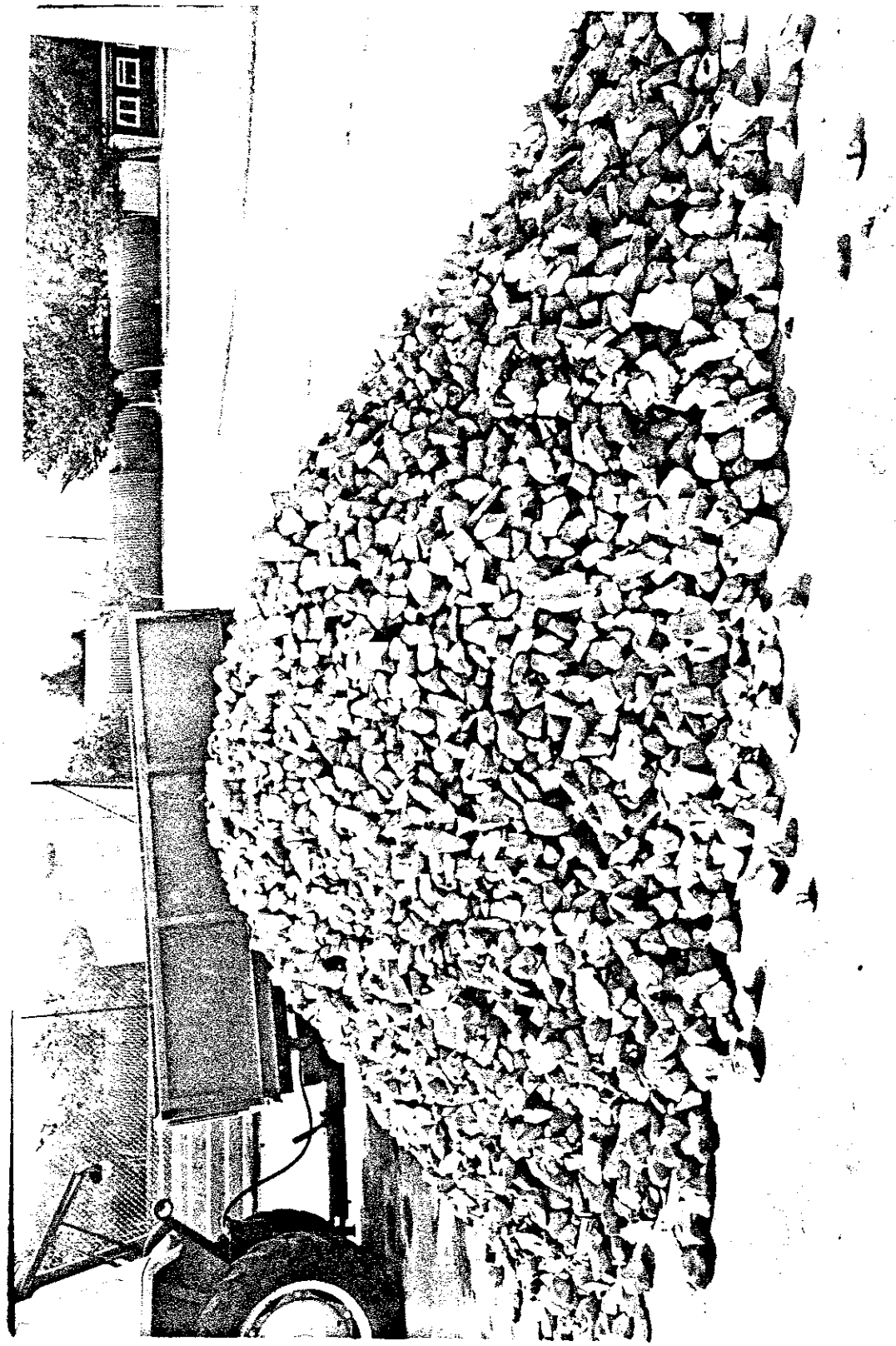

Figure 5.1 The 10 tonne pile of 40 to 75mm sized aggregate from which the five armourstone batches were prepared.

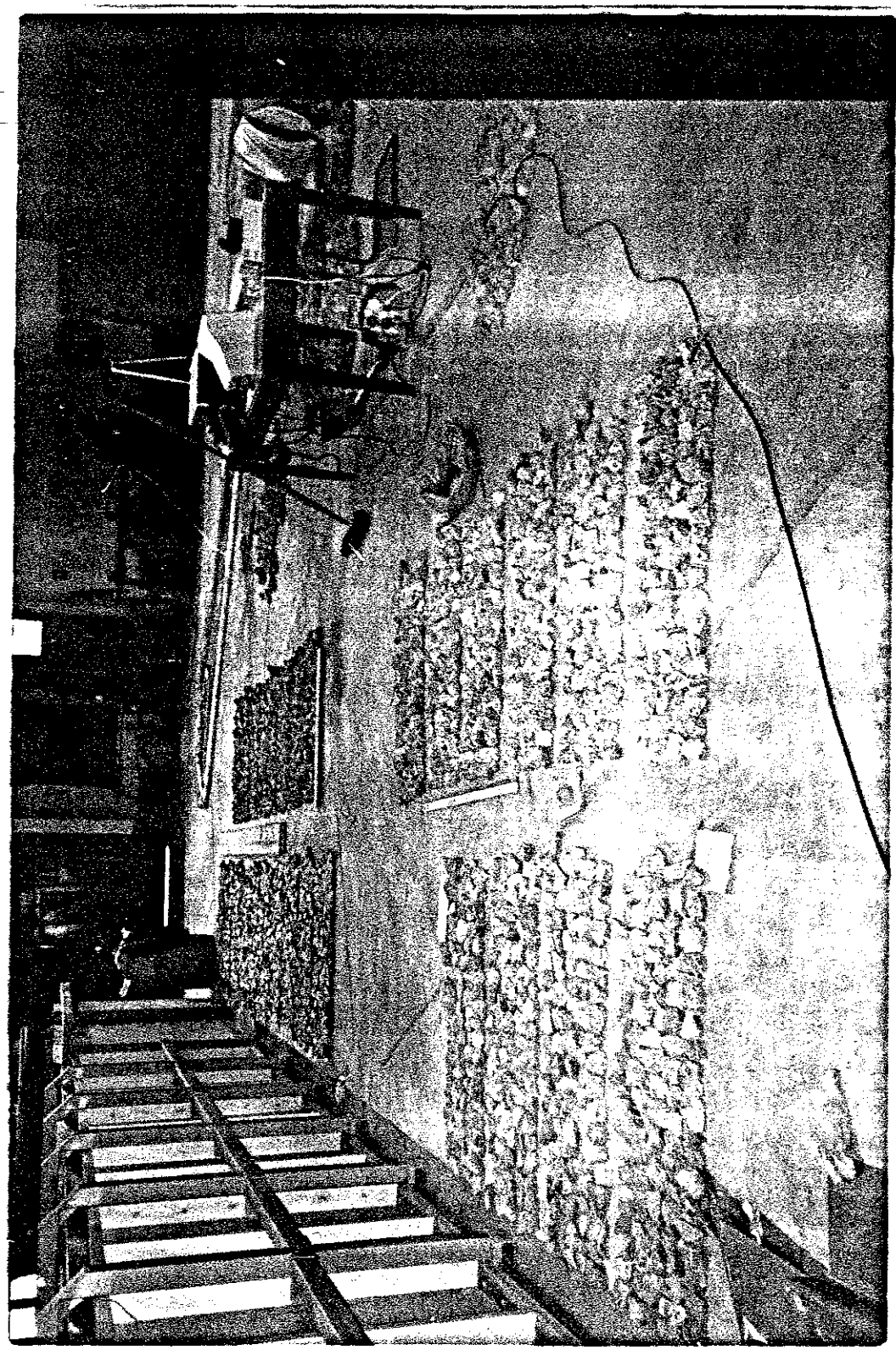

Figure 5.2 Material preparation and sizing of armourstone batches.

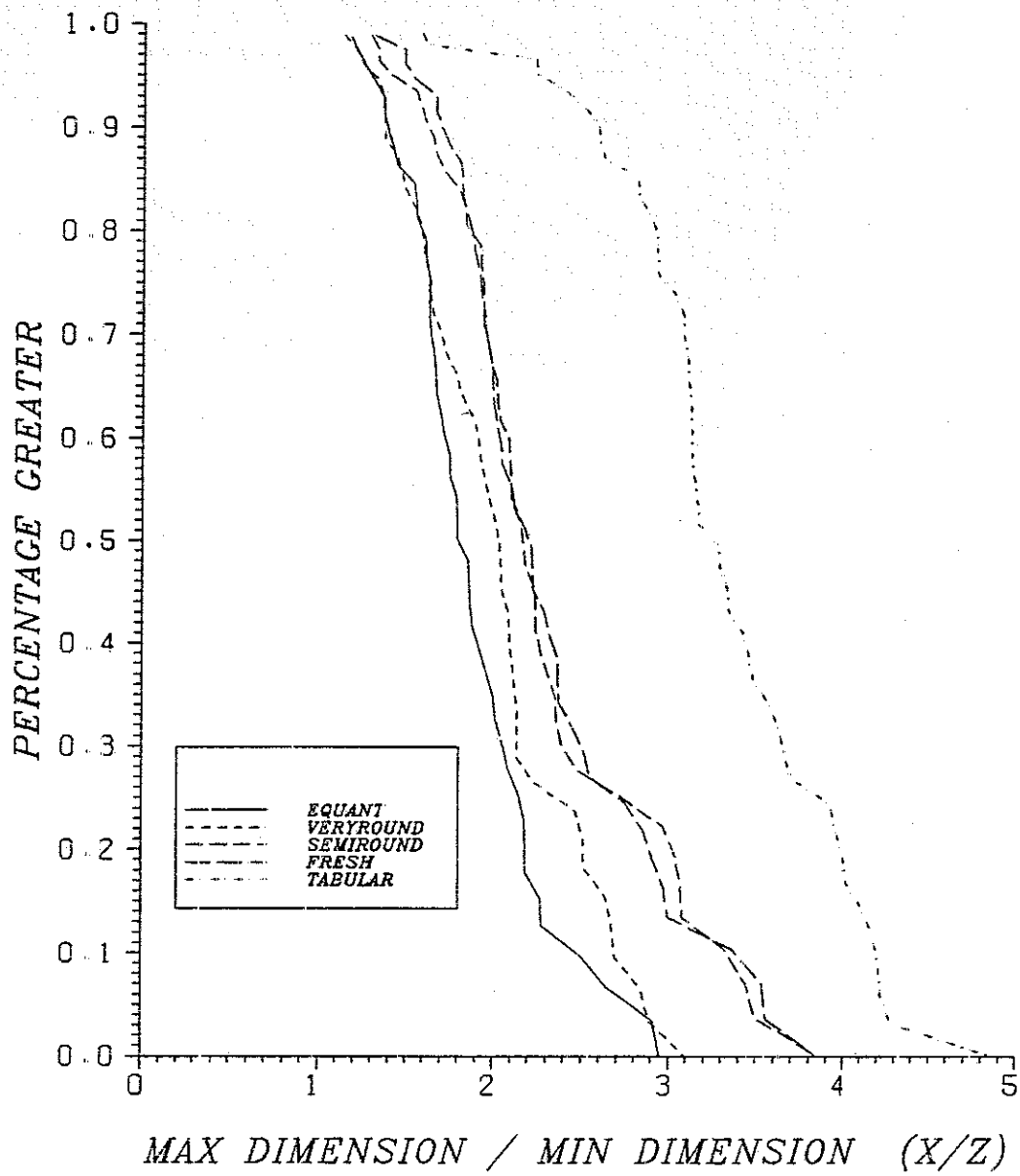

Figure 5.3 X/Z ratio percentage exceedance curves for the subsamples representing the five shape classes.

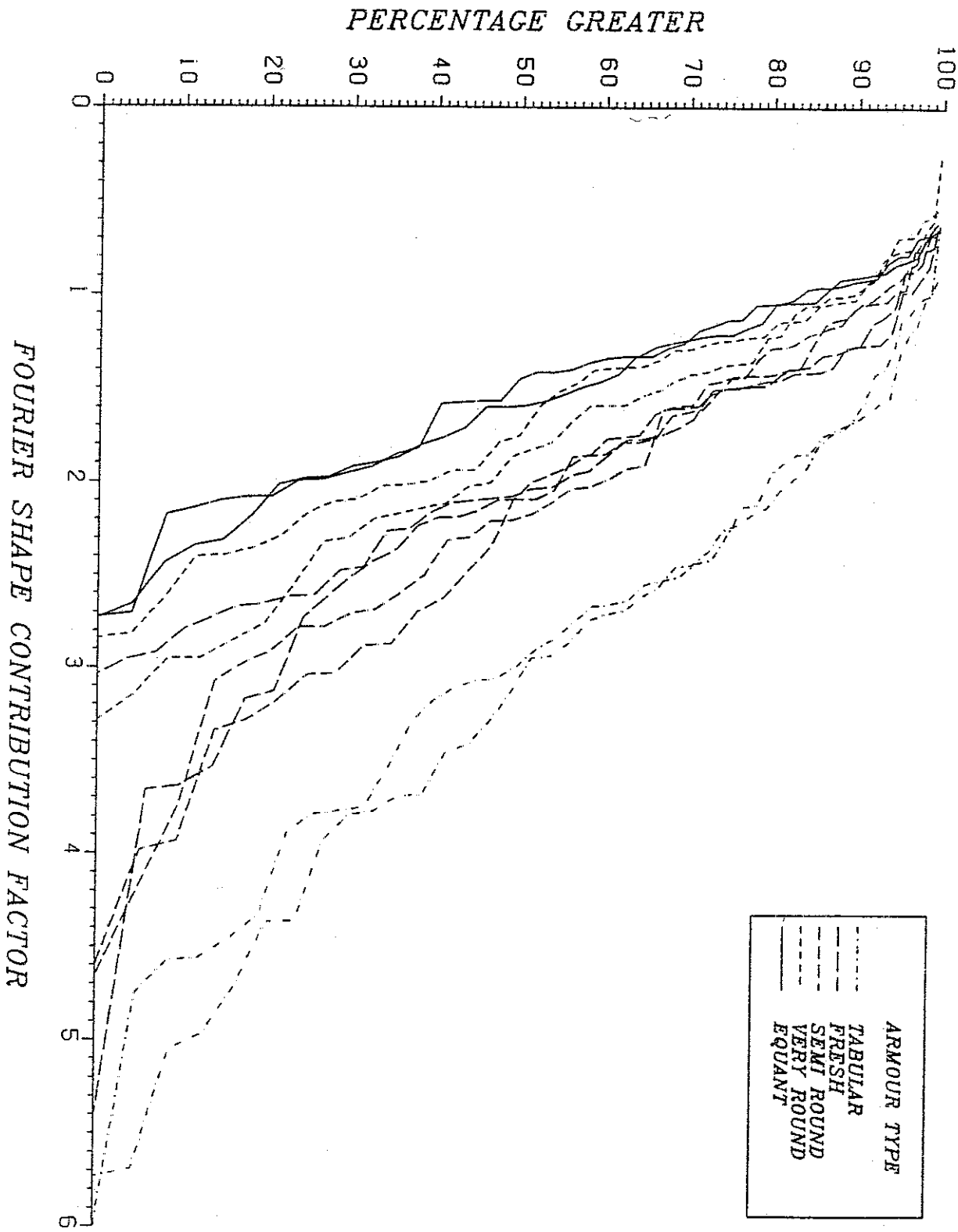

Figure 5.4 The Fourier shape contribution factor P_C percentage exceedance curves for both the random projections of the five shape classes.

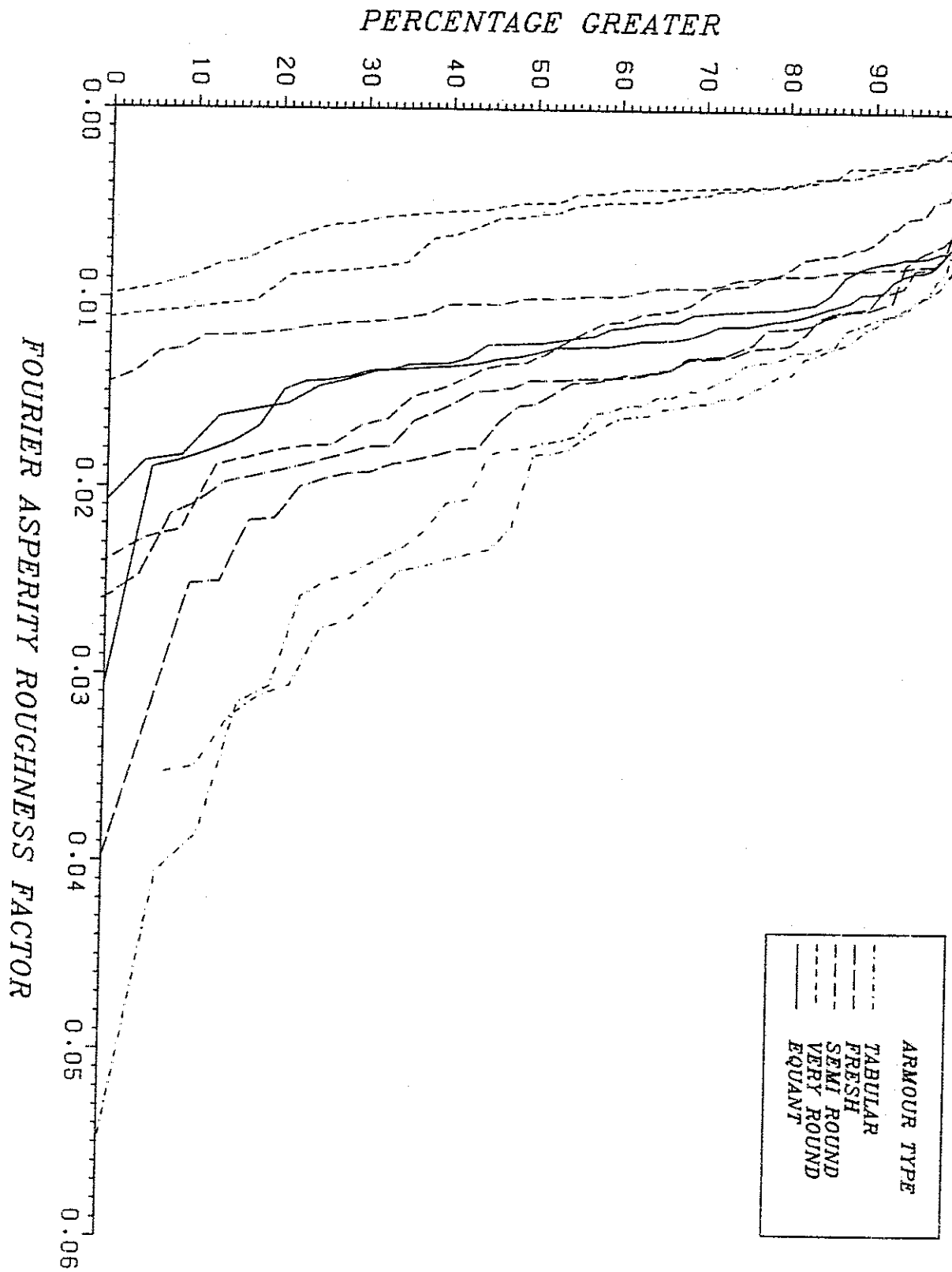

Figure 5.5 The Fourier asperity roughness factor P_R percentage exceedance curves for both the random projections of the five shape classes.

Figure 7.1 : Plunging wave equation - TABULAR @ P = 0.1; C_{pl} = 5.93

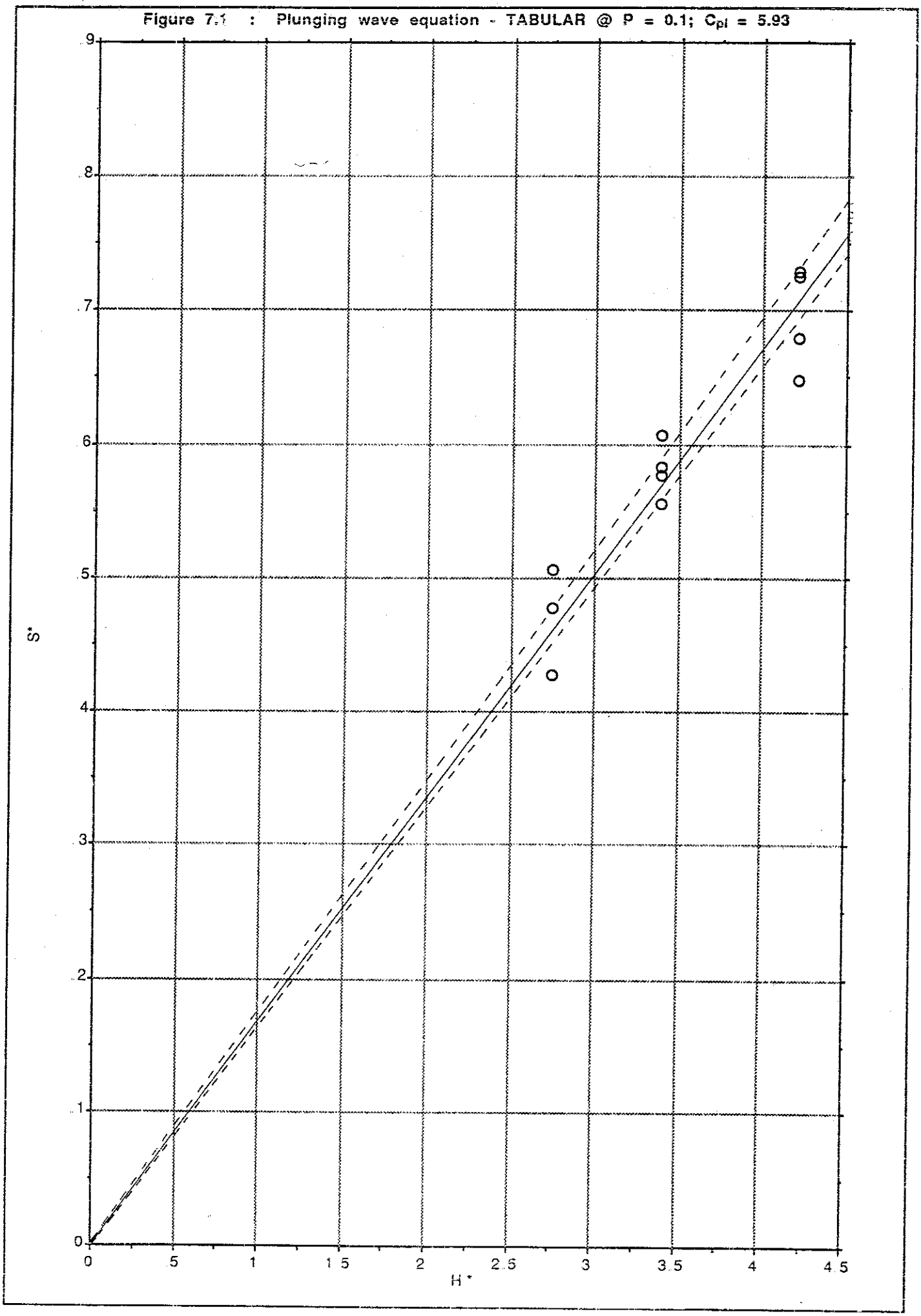

Figure 7.2 : Plunging wave equation - FRESH @ P = 0.1; C_{pl} = 5.39

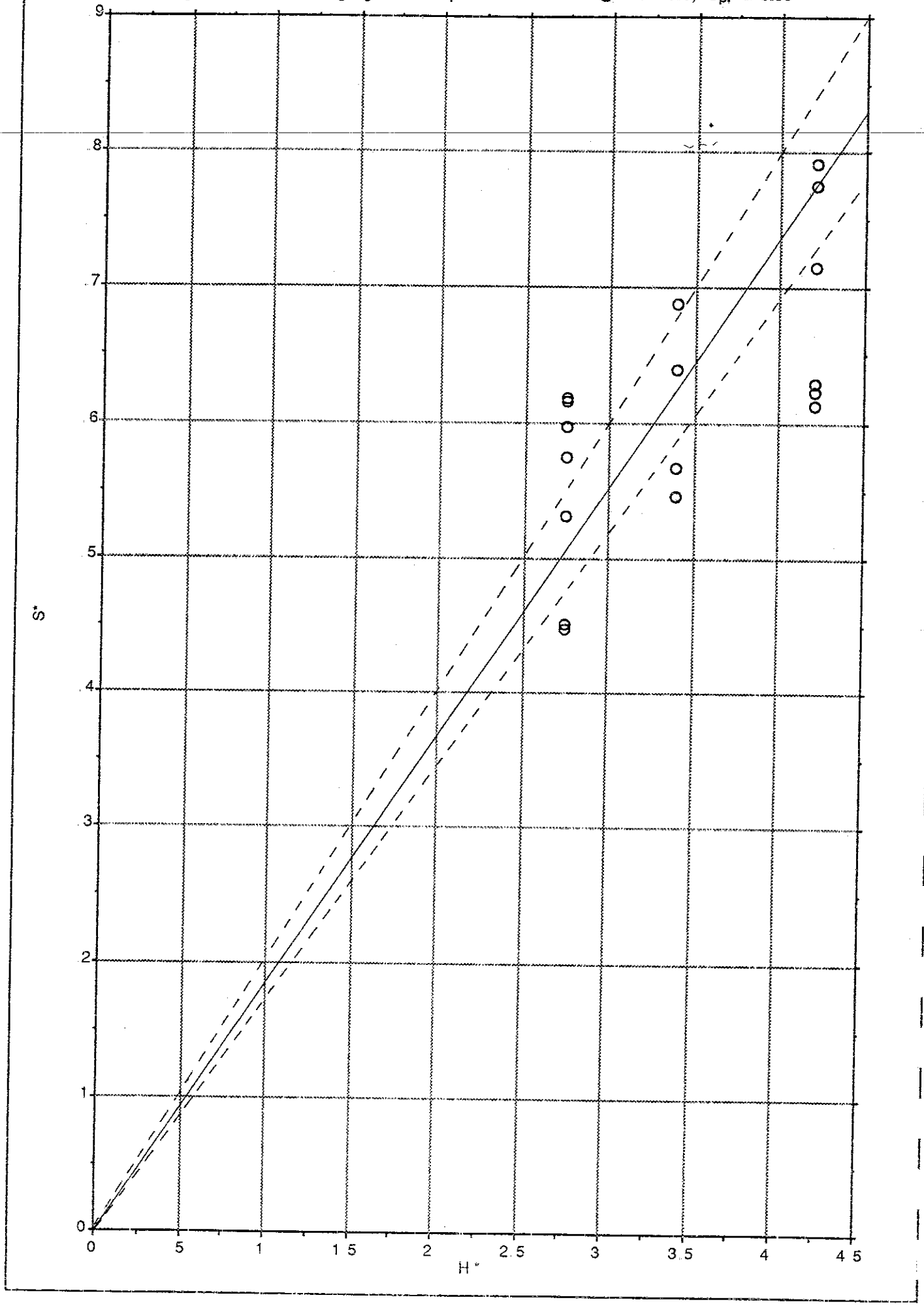

Figure 7.3 : Plunging wave equation - EQUANT @ P = 0.1; C_{pl} = 5.64

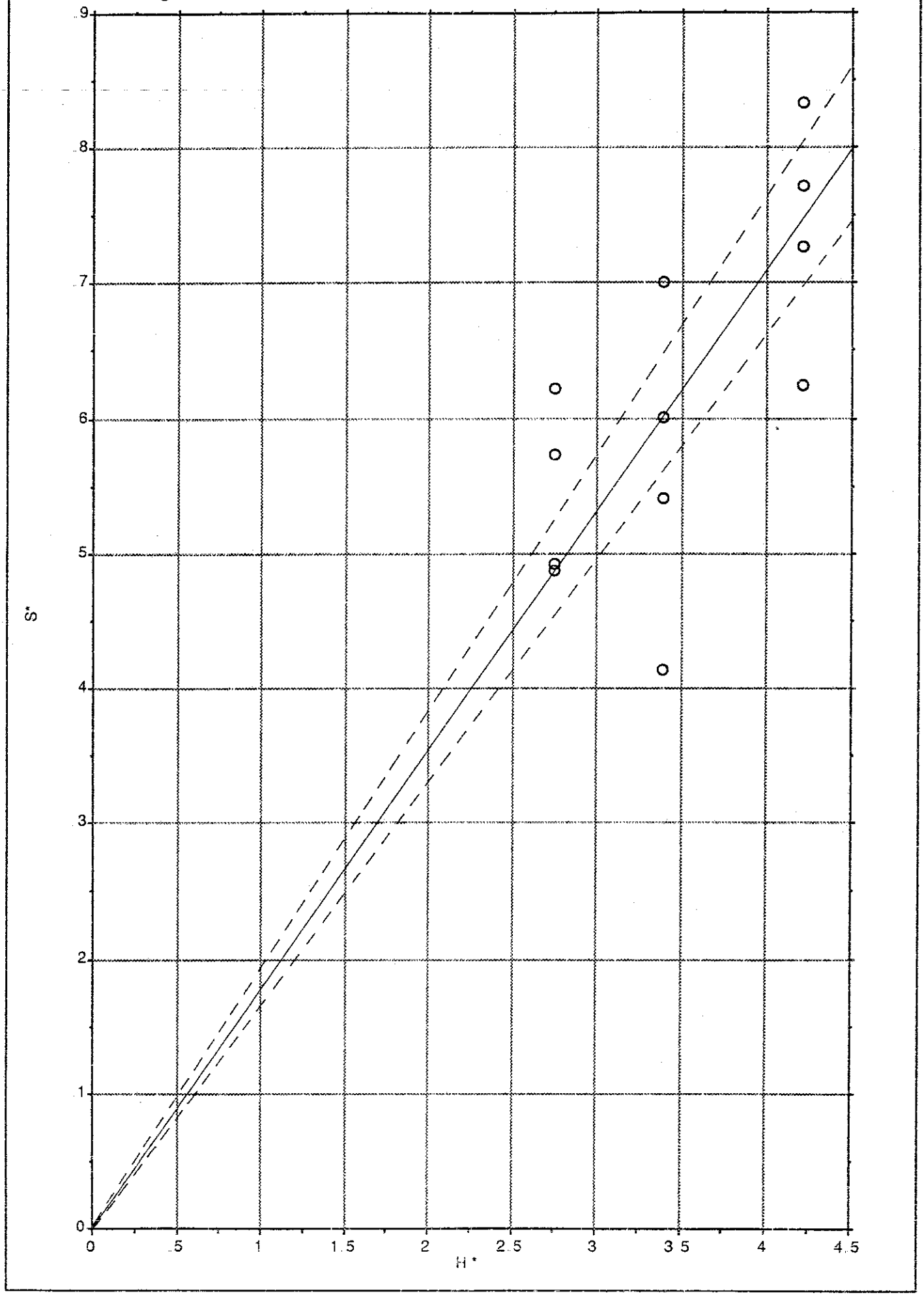

Figure 7.4 : Plunging wave equation - SEMIROUND @ P = 0.1; C_{pl} = 5.39

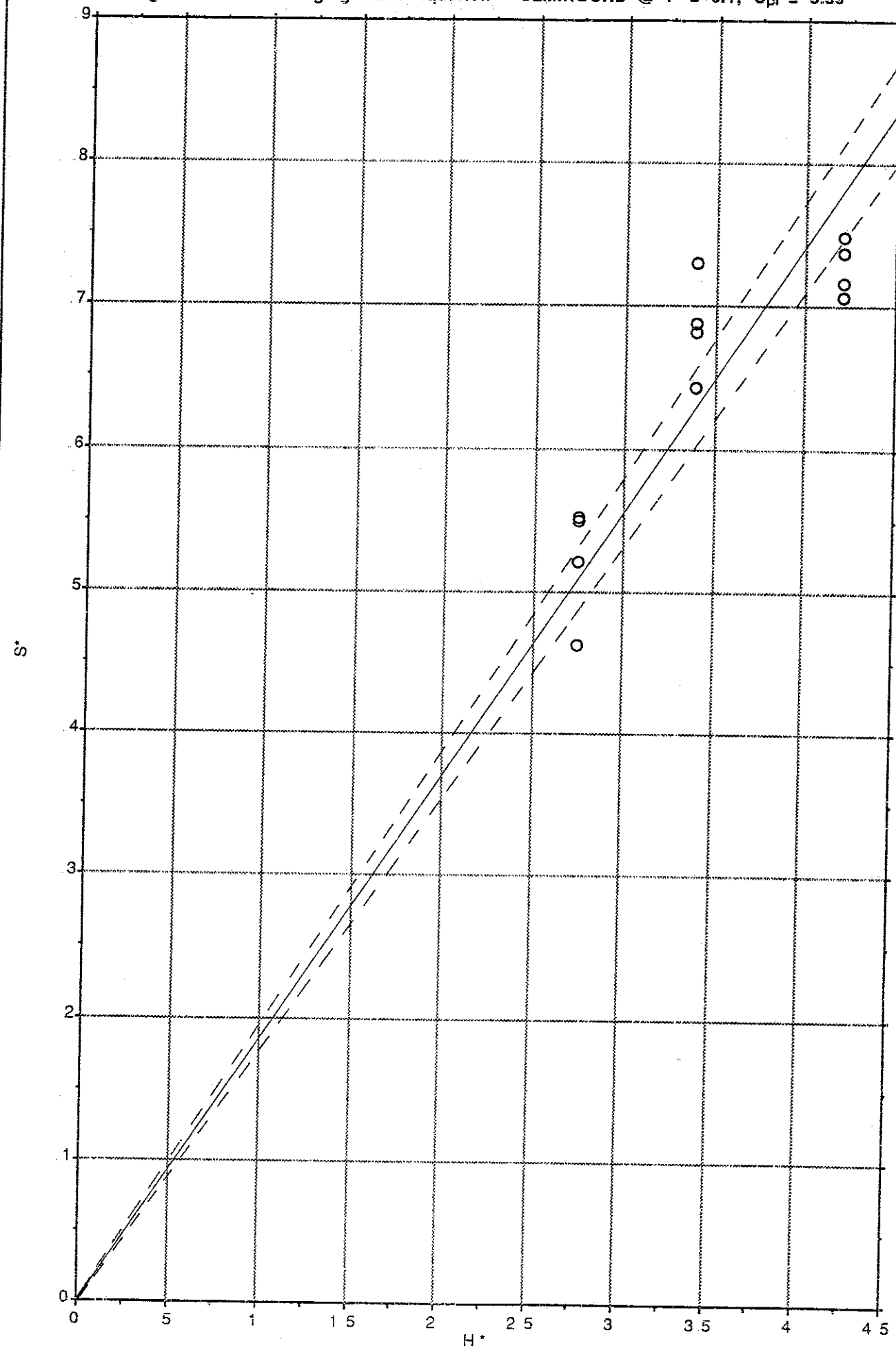

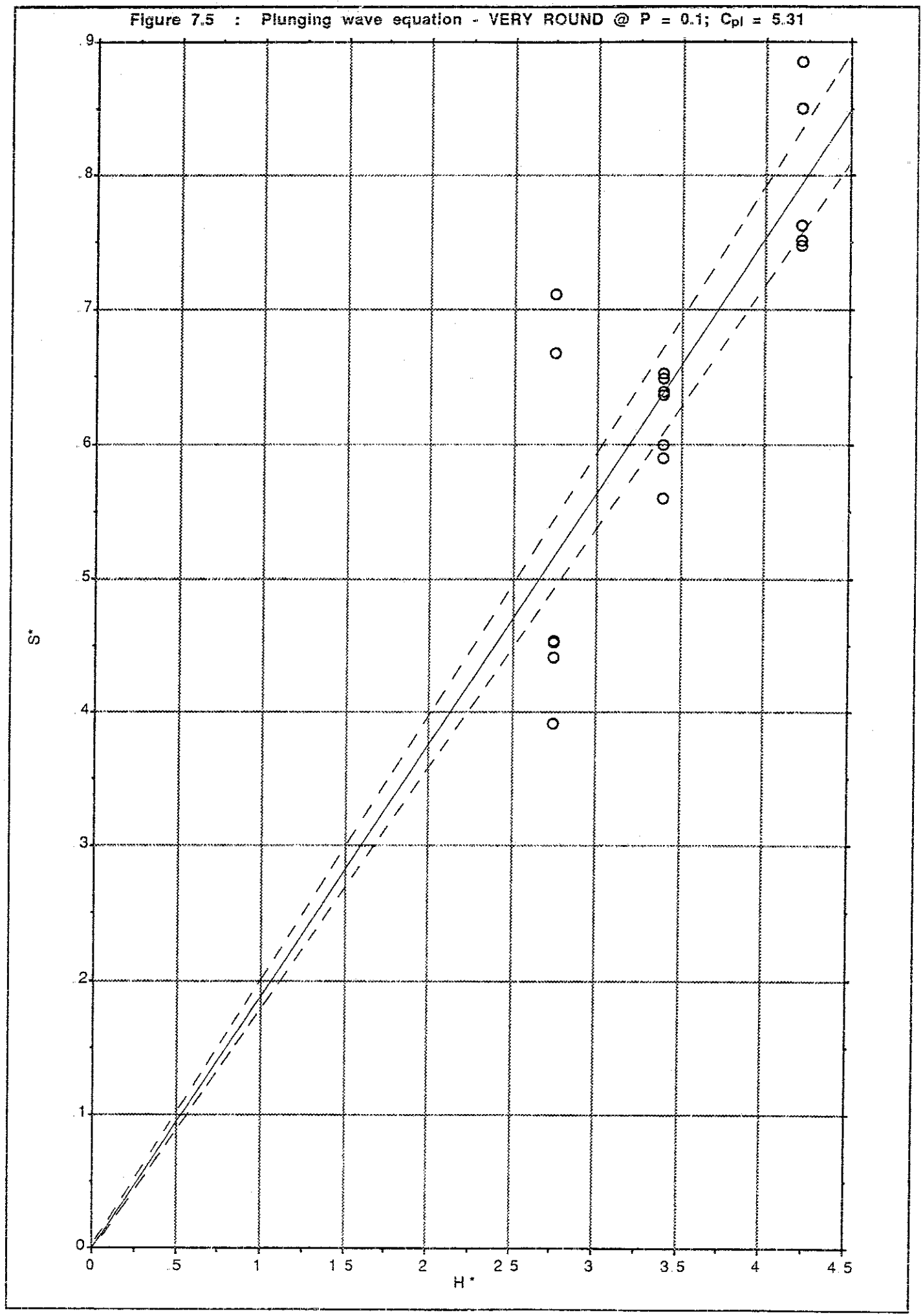
Figure 7.5 : Plunging wave equation - VERY ROUND @ P = 0.1; C_{pl} = 5.31
S*
H*
0
.5
1
1 5
2
2 5
3
3 5
4
4 5
0
1
2
3
4
5
6
7
8
9

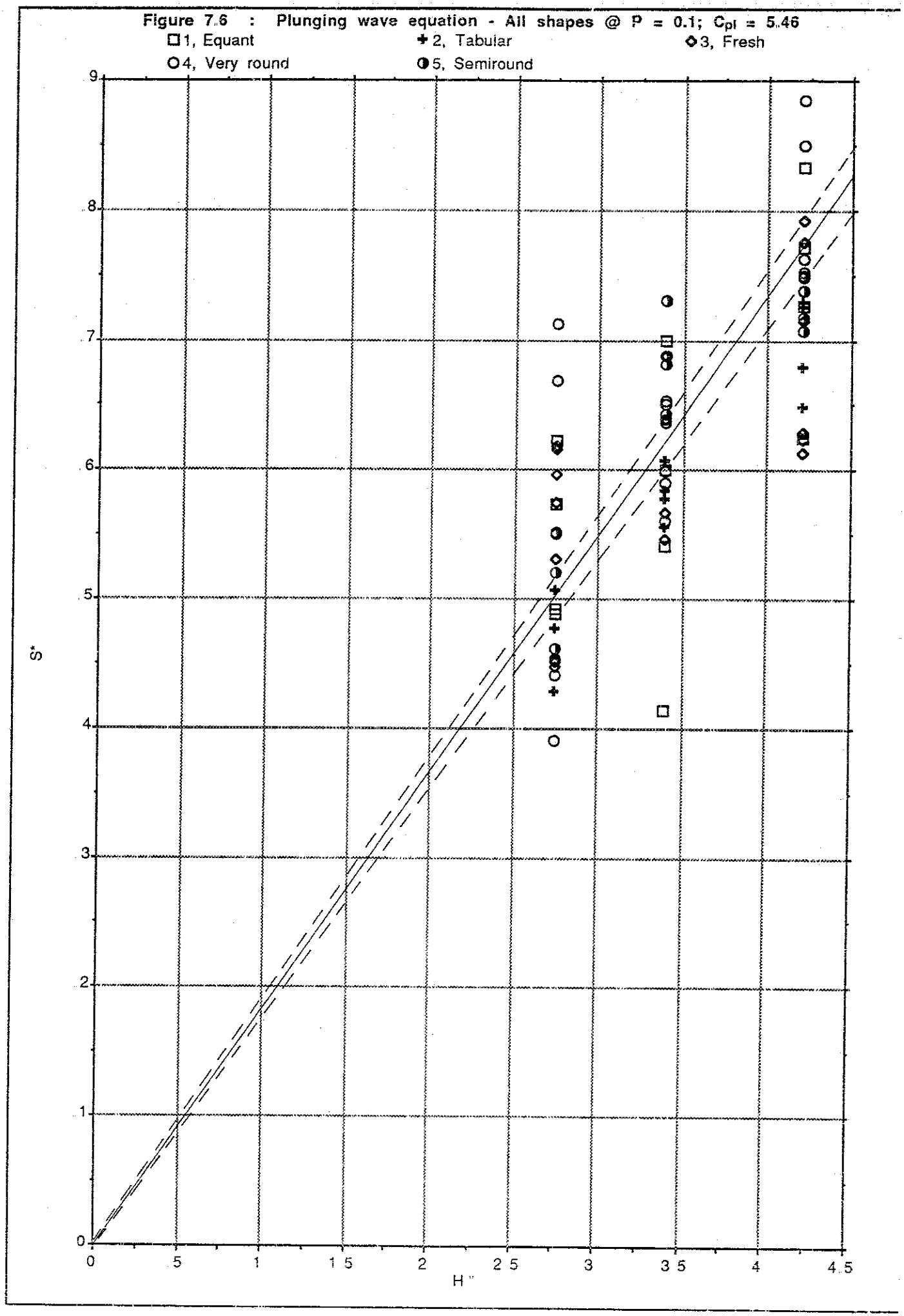
Figure 7.6 : Plunging wave equation - All shapes @ P = 0.1; Cpl = 5.46
1, Equant
2, Tabular
3, Fresh
4, Very round
5, Semiround
S*
H''
0
1
2
3
4
5
6
7
8
9
0
.5
1
1.5
2
2.5
3
3.5
4
4.5

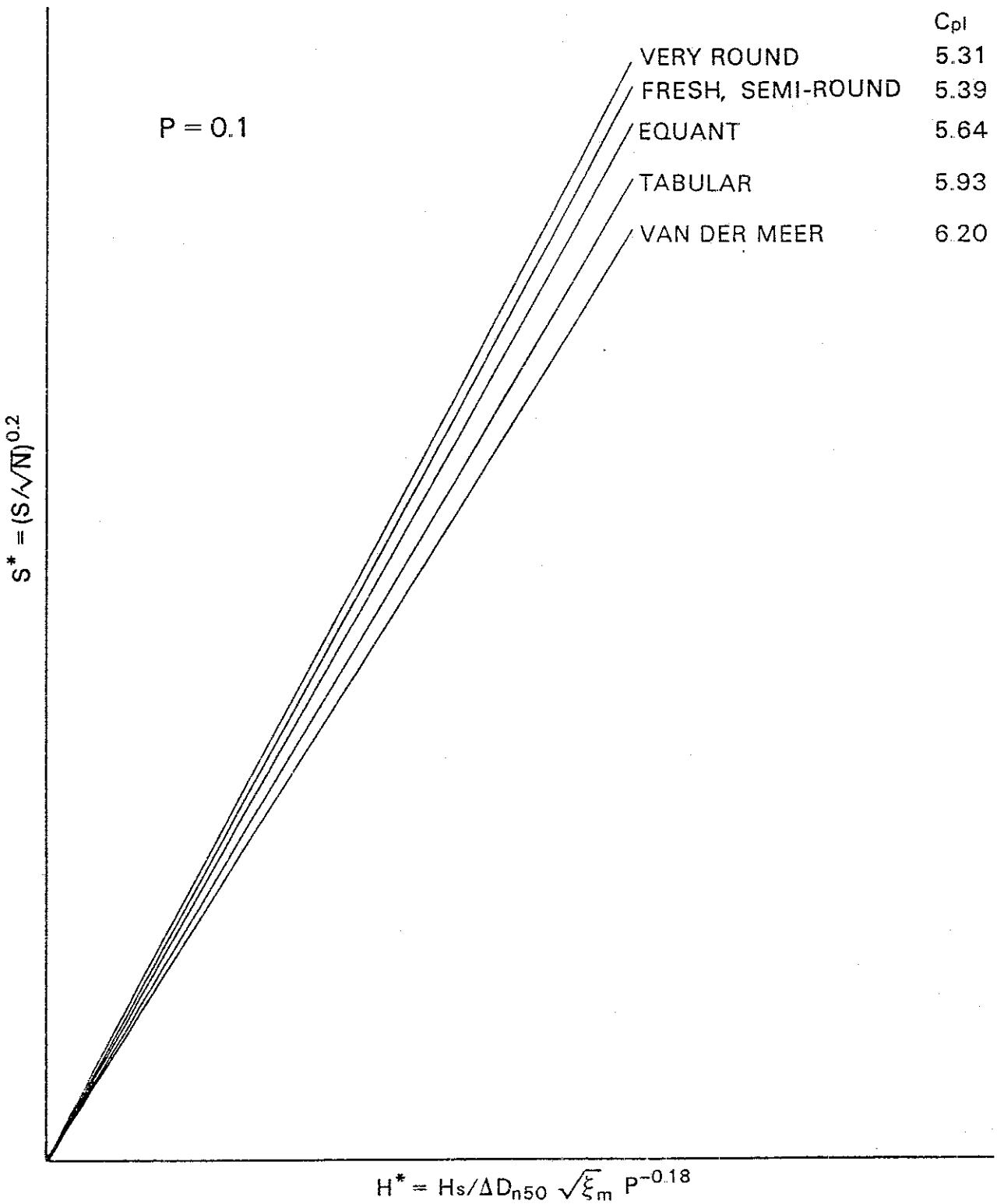

Figure 7.7 Summary of regression analysis results for plunging wave equation with P = 0.1.

Figure 7.8 : Surging wave equation - TABULAR @ P = 0.1; C_{su} = 1.32

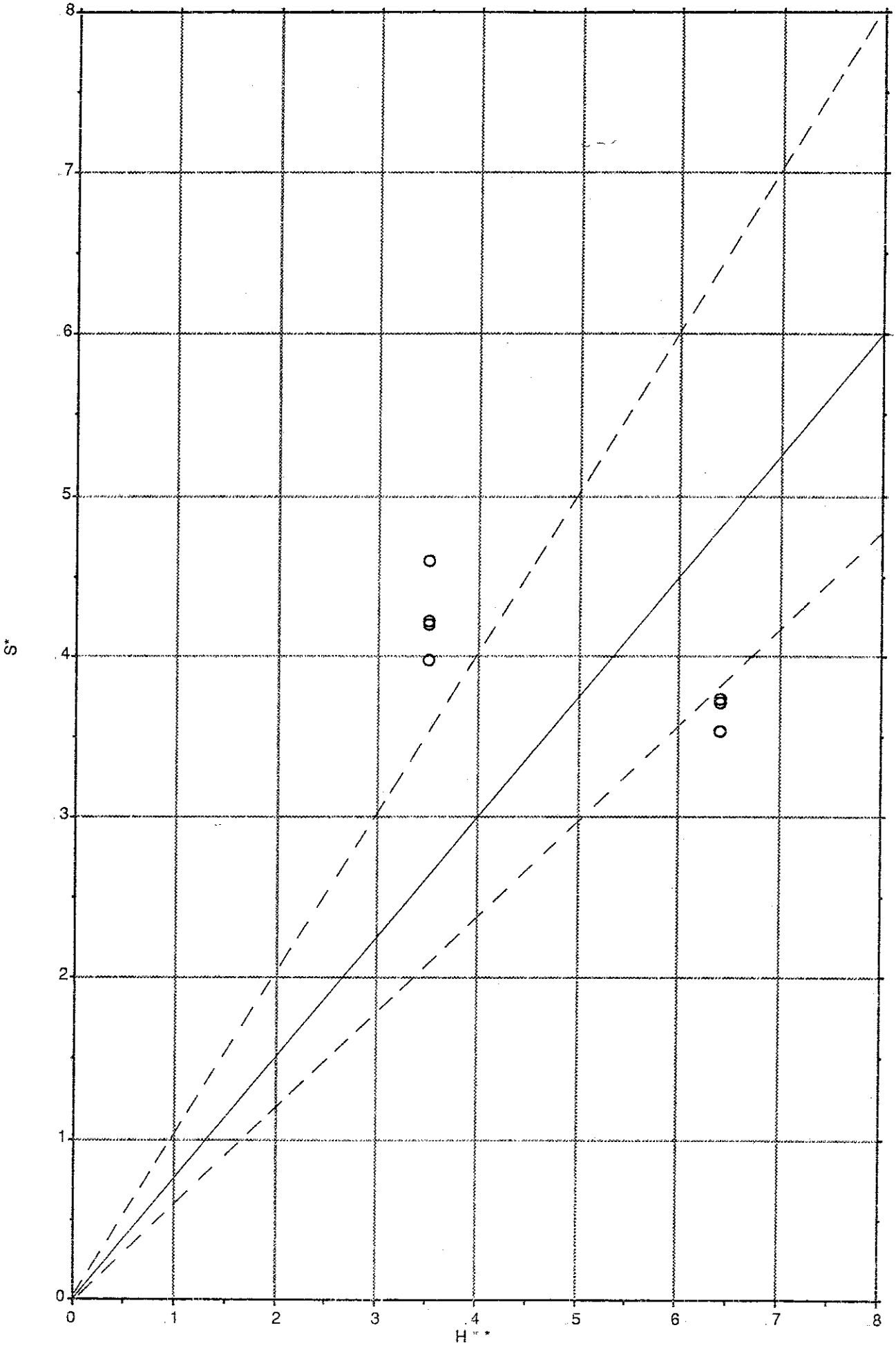

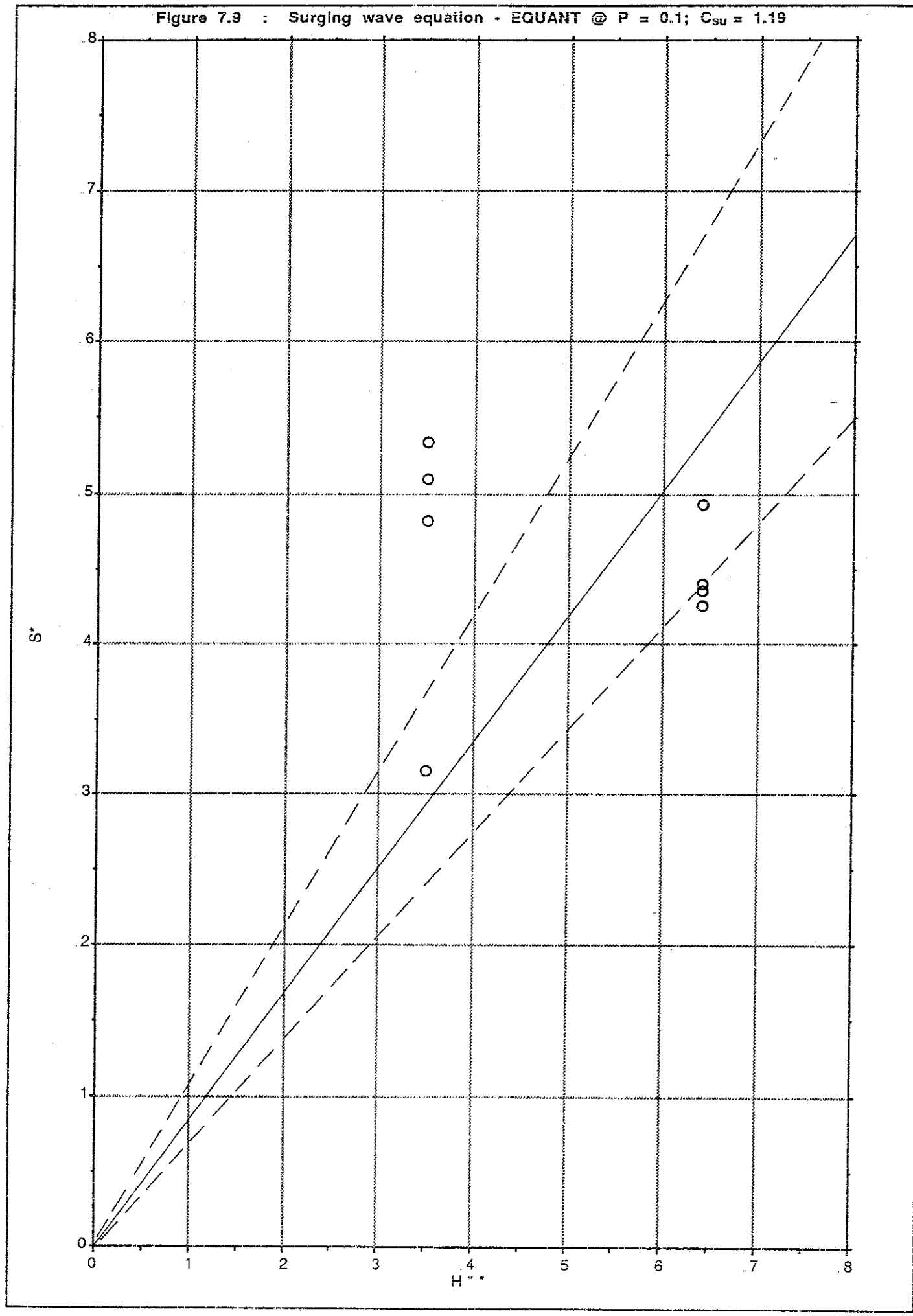
Figure 7.9 : Surging wave equation - EQUANT @ P = 0.1; C_{su} = 1.19
S*
H* *
0
1
2
3
4
5
6
7
8

Figure 7.10 : Surging wave equation - SEMIROUND @ P = 0.1; C_{su} = 1.10

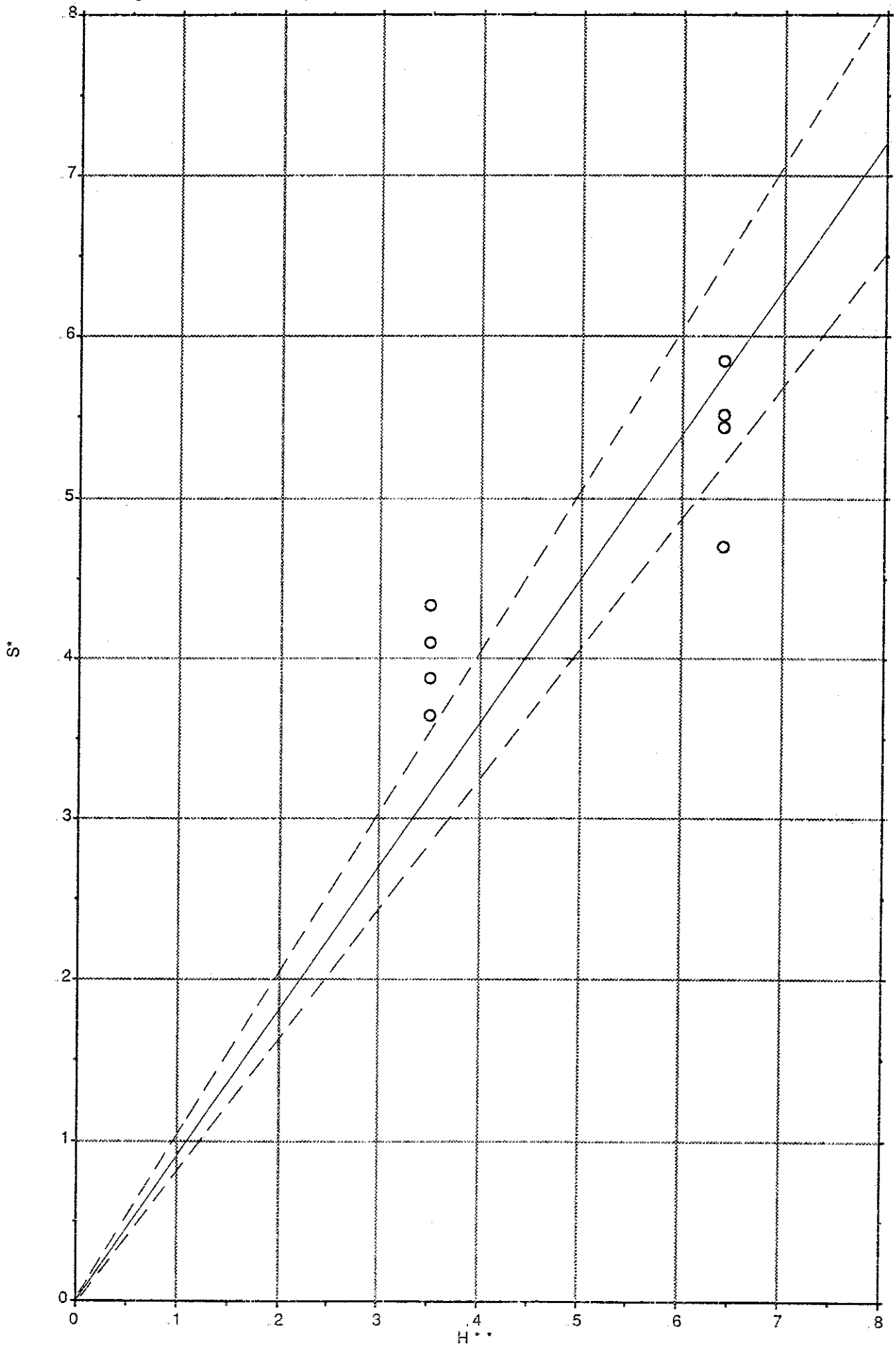

Figure 7.11 : Surging wave equation - VERY ROUND @ P = 0.1; C_{su} = 0.95

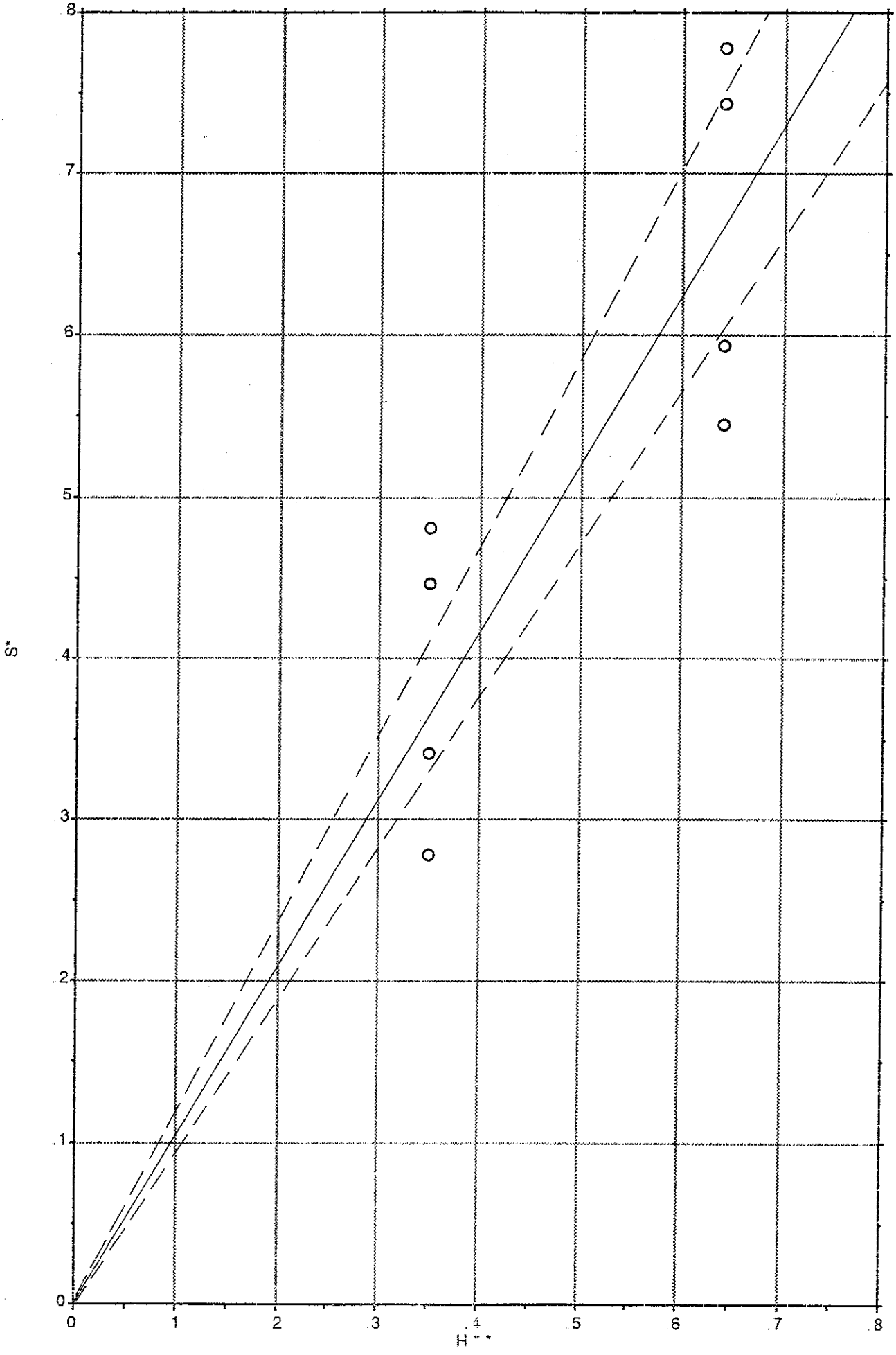

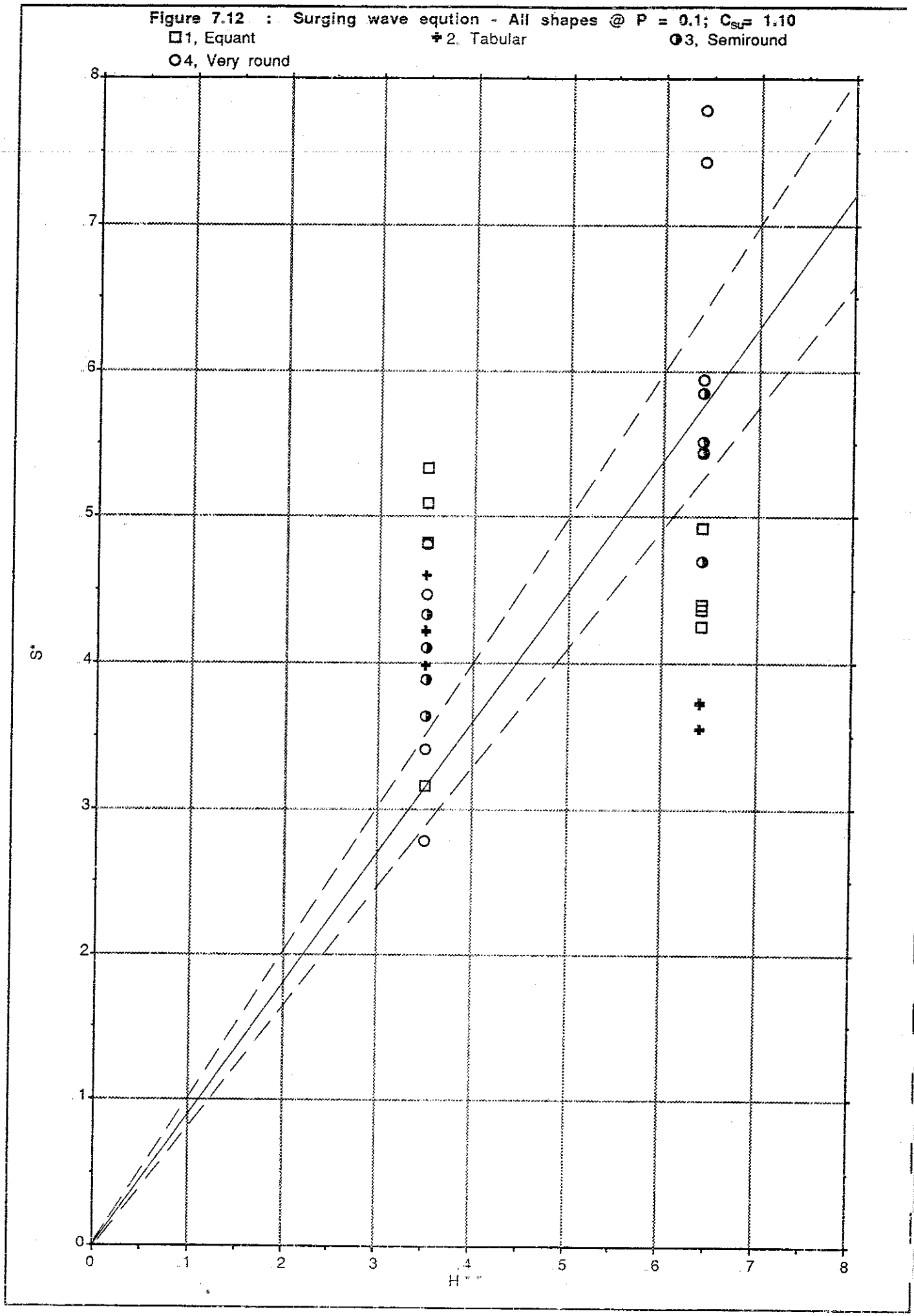
Figure 7.12 : Surging wave eqution - All shapes @ P = 0.1; C_{su}= 1.10
1, Equant
2, Tabular
3, Semiround
4, Very round
S*
H*
0
1
2
3
4
5
6
7
8

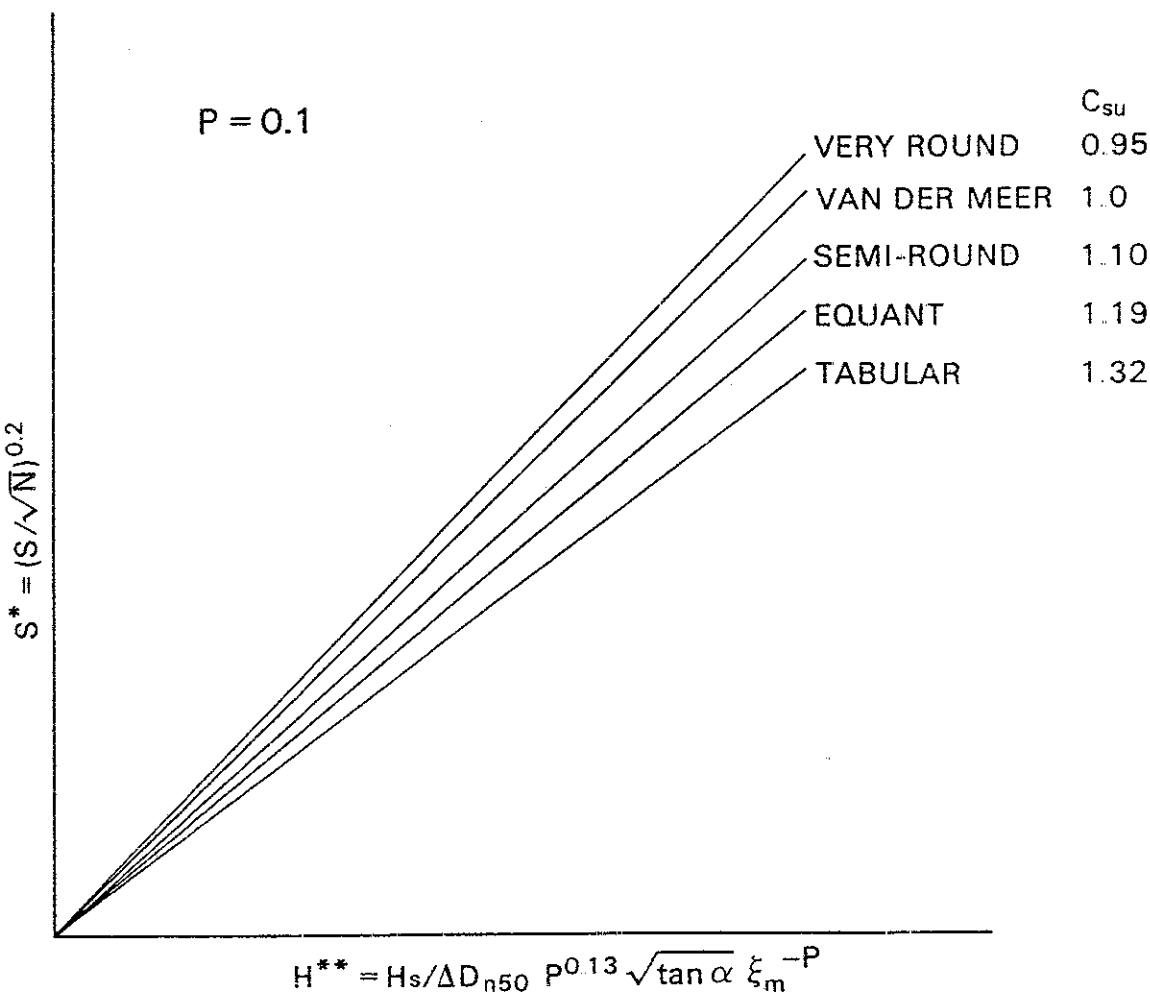

Figure 7.13 Regression analysis plot for Van der Meer's surging wave equation with P = 0.1, for all shape classes.

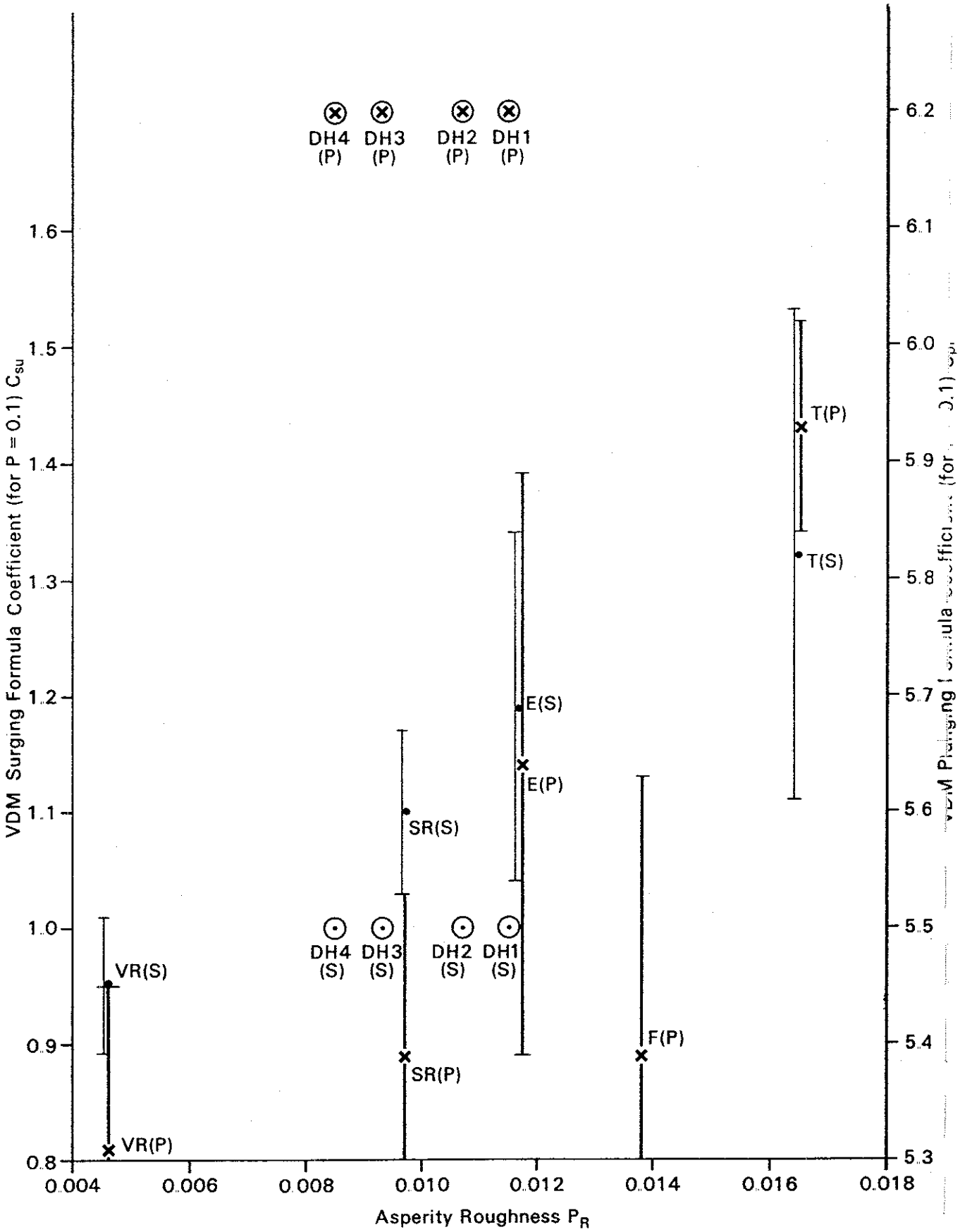

Figure 7.14 Effect of shape on stability in relation to shape analysis results of Van der Meer's flume test material (circled points). Crosses are plunging condition (P) and points are surging condition (S). Left axis is surging formula coefficient C_{su} and right axis is plunging formula coefficient C_{pl}. P = 0.1 is assumed.

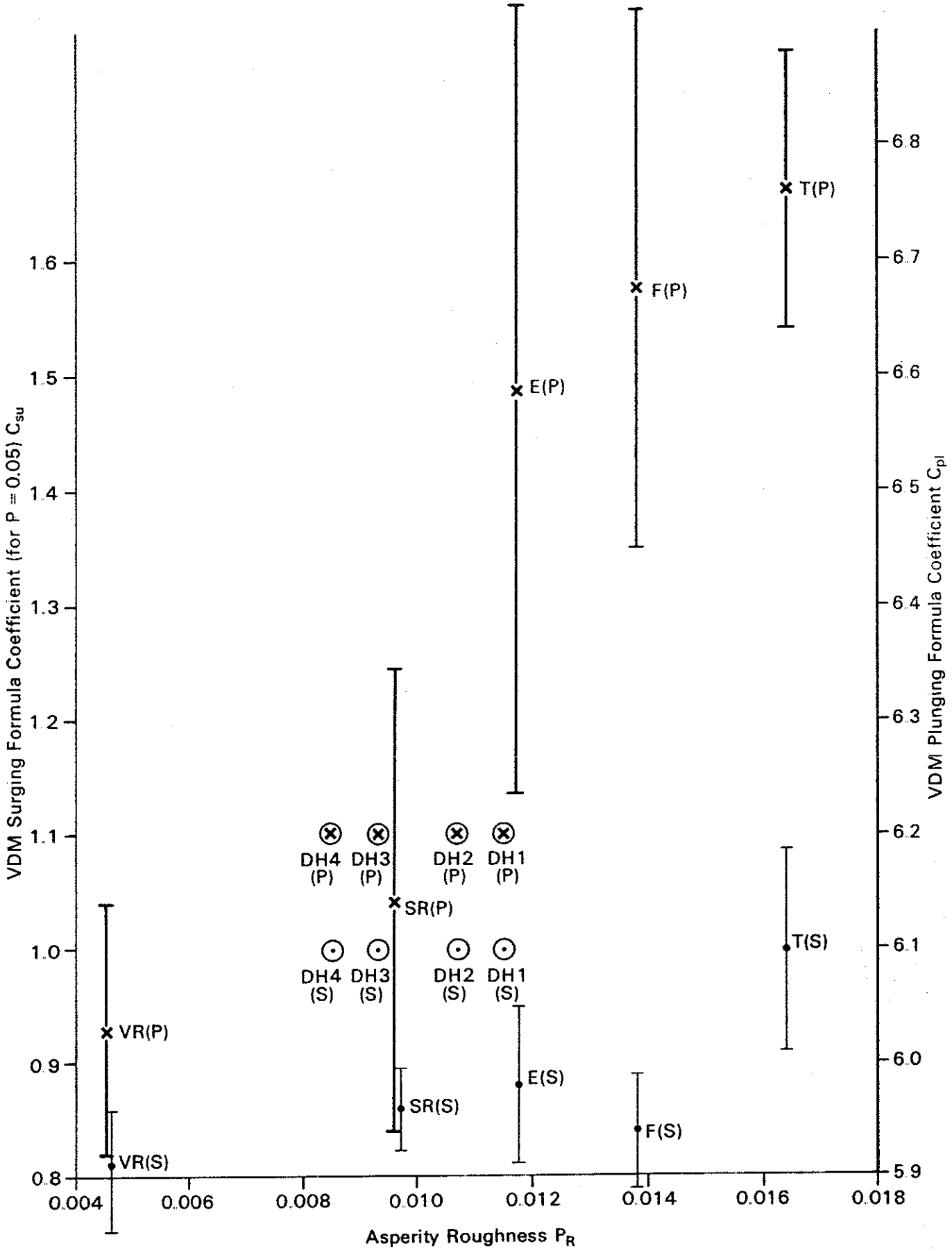

Figure 7.15 Effect of shape on stability in relation to shape analysis results of Van der Meer's flume test material (circled points). Crosses are plunging condition (P) and points are surging condition (S). Left axis is surging formula coefficient C_{su} and right axis is plunging formula coefficient C_{pl}. P = 0.05 is assumed.

Figure 7.16 : Plunging wave eqution - All shapes @ P = 0.05; C_{su} = 6.39

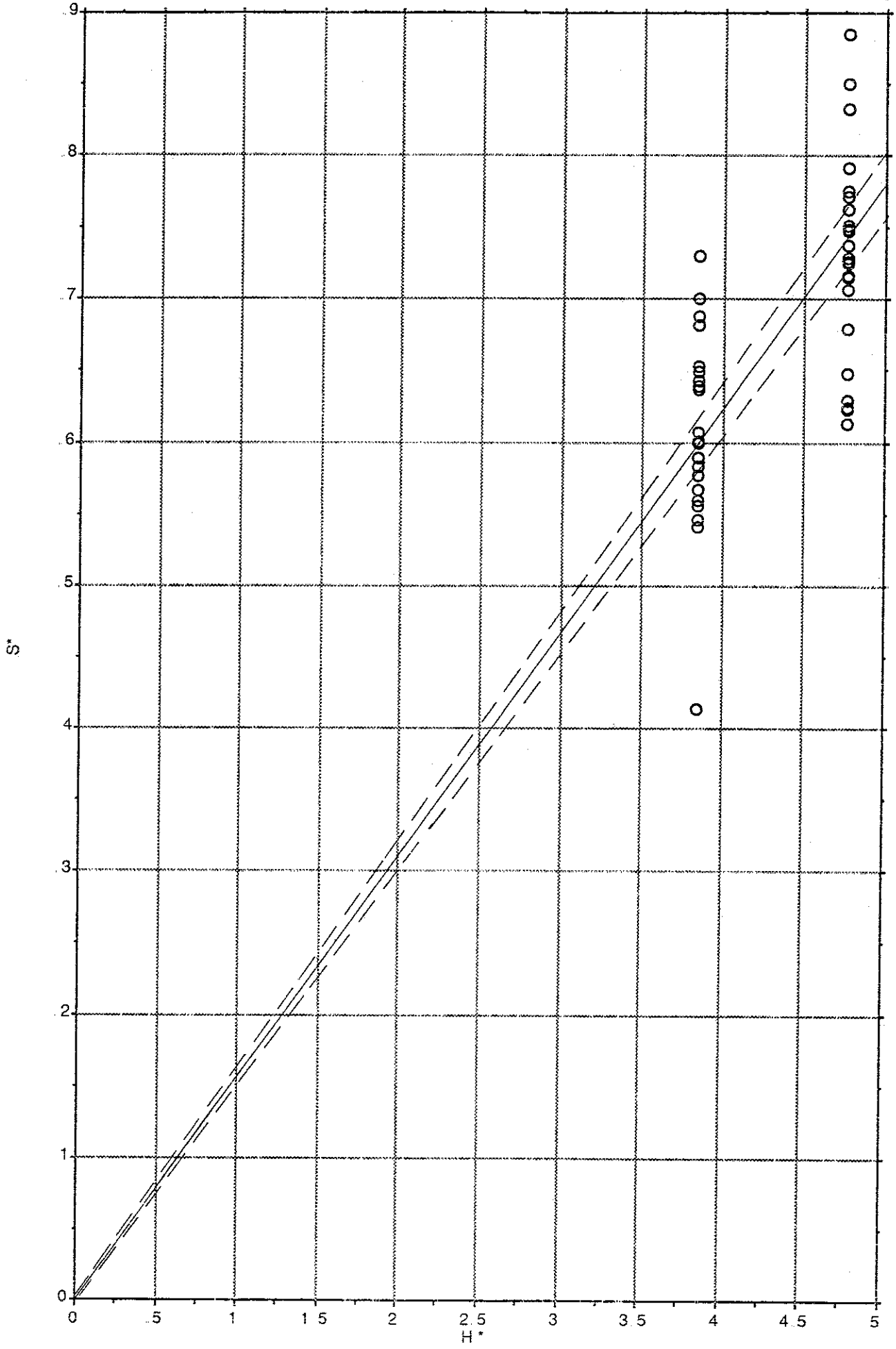

Figure 7.17 : Surging wave equation - All shapes @ P = 0.05; C_{su} = 0.93

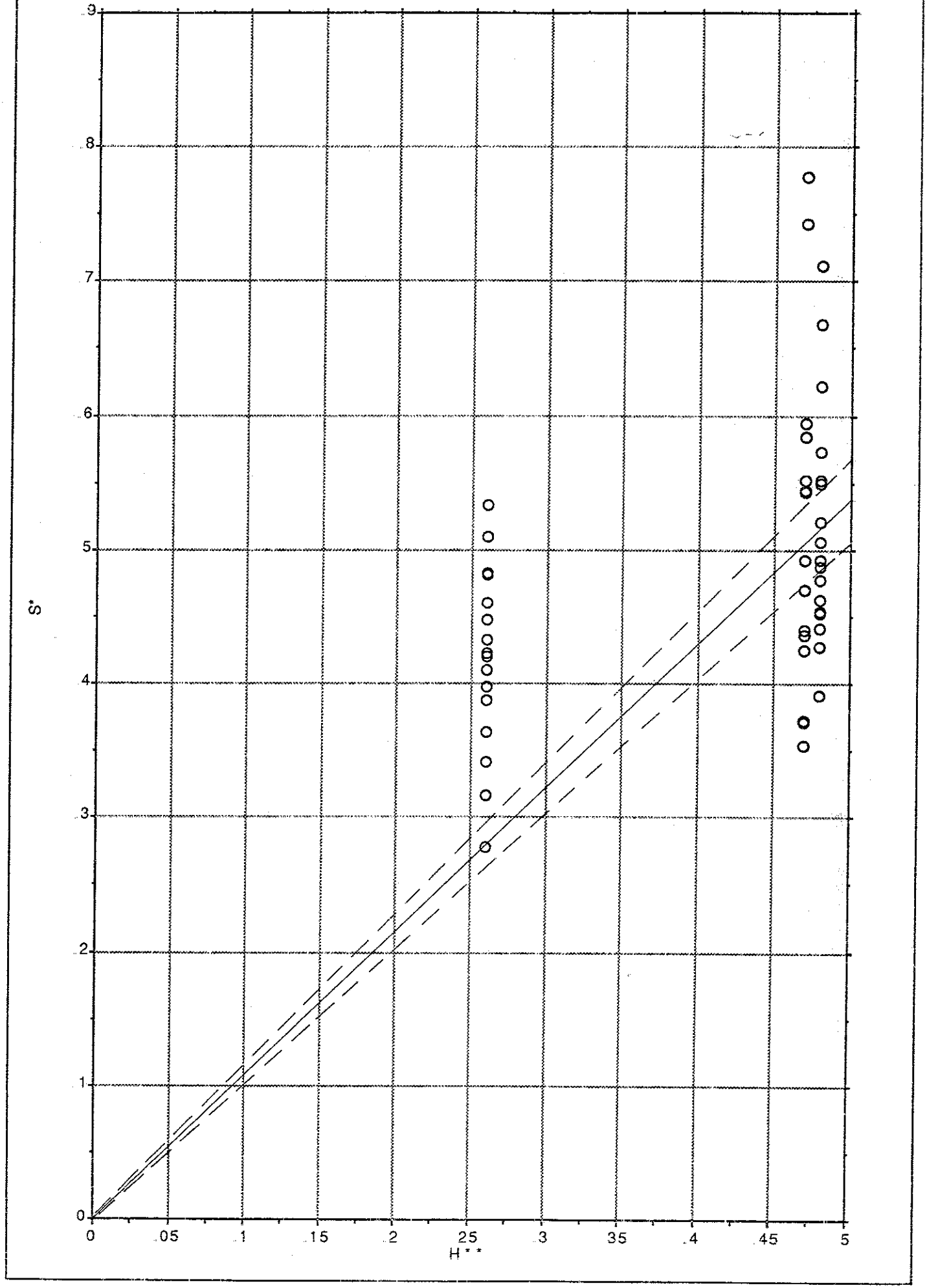

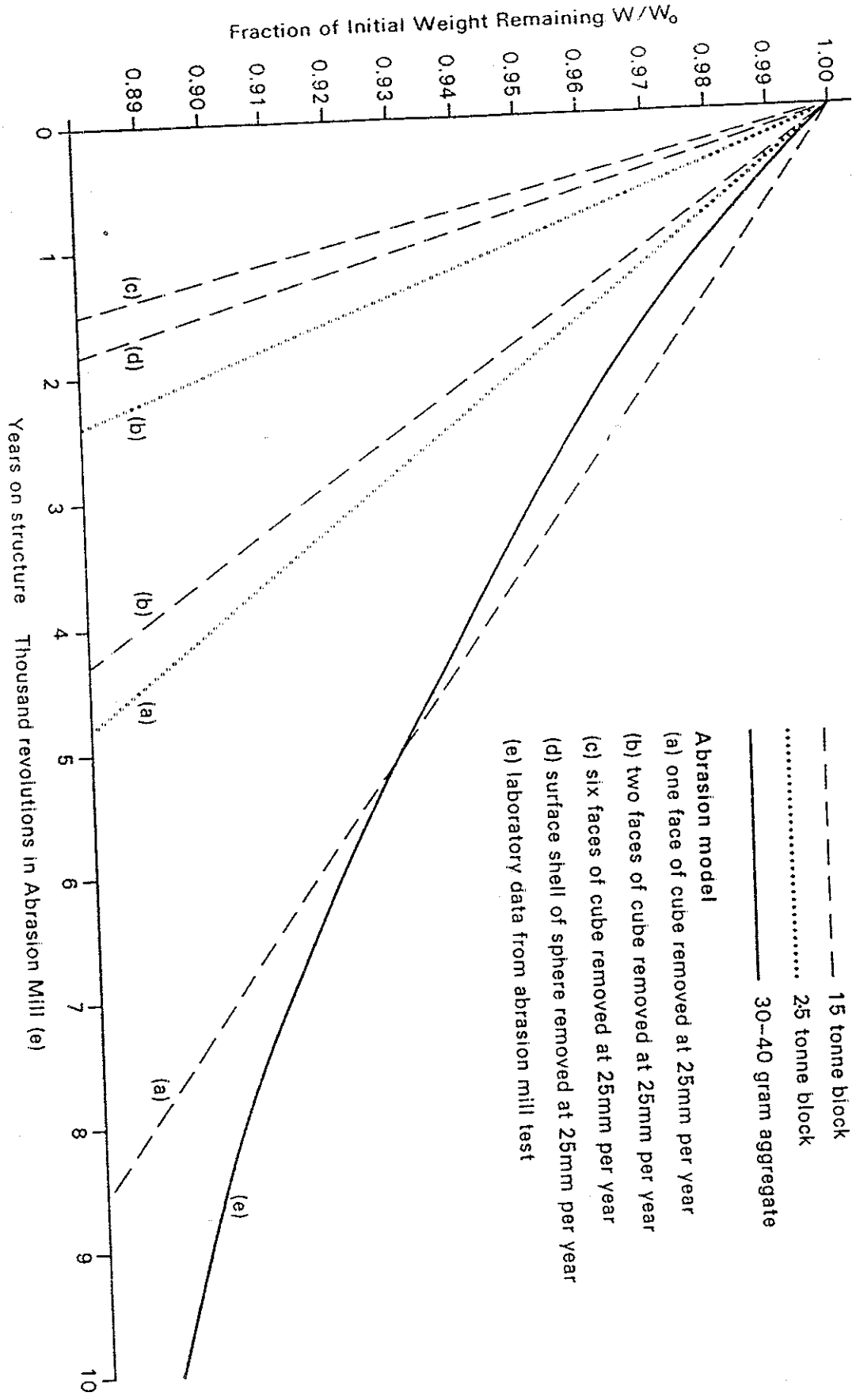

Figure 8.1 Correlation of wear in Portland limestone from laboratory mill abrasion test with wear on prototype blocks at West Bay near 'block A' (see Clark, 1988) assuming various prototype abrasion models and initial block sizes.

Figure 8.2 Abraded 15 tonne blocks of Portland limestone near 'block A' at West Bay, Dorset.

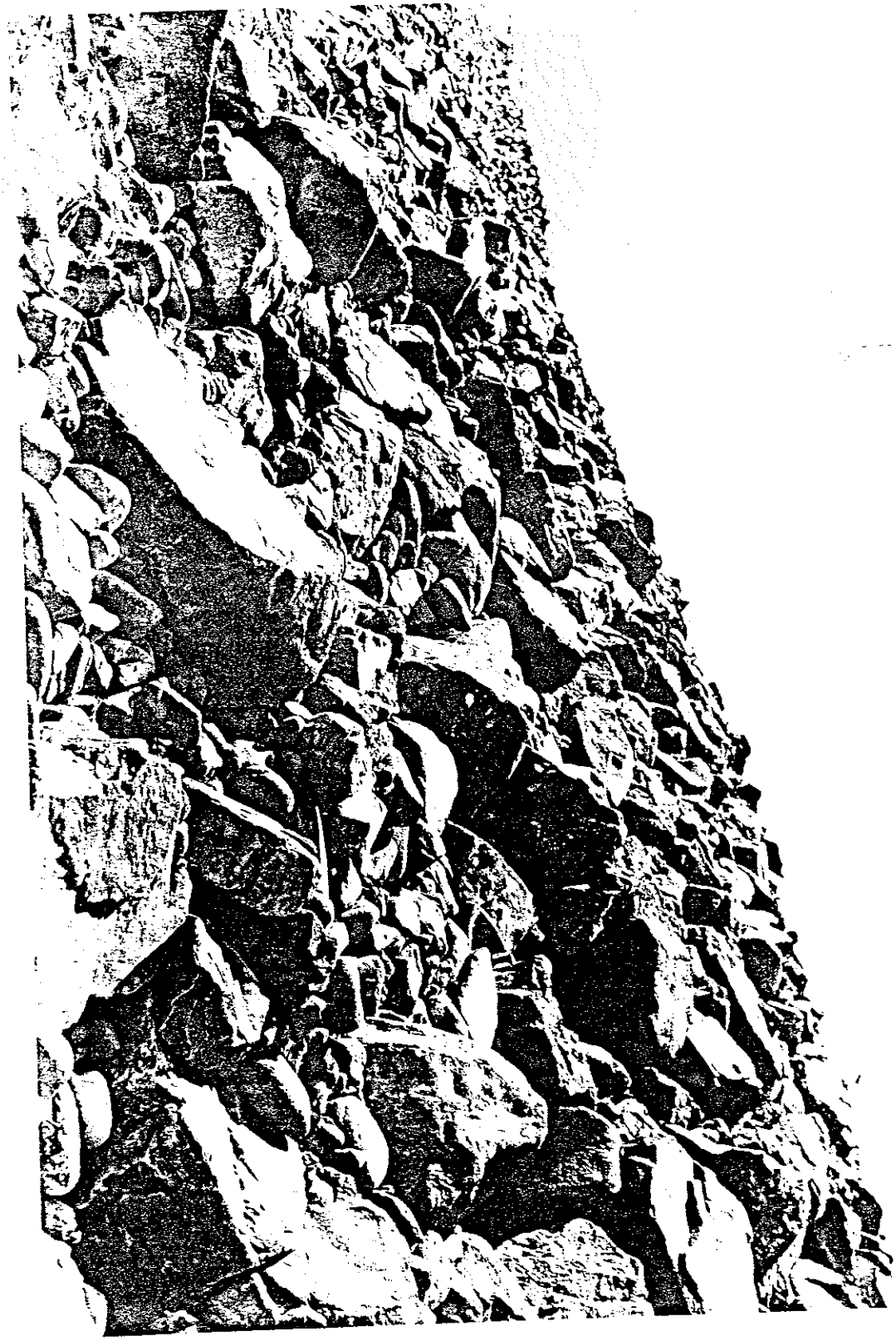

Figure 8.3 The slope protection works at Buckhaven, Scotland.